Republic of Iraq
Ministry of Higher Education and Scientific Research
University of Misan /College of Engineering
Department of Civil Engineering

STRUCTURAL PERFORMANCE OF HIGH- STRENGTH SELF-COMPACTED CONCRETE COMPOSITE ELEMENTS

By

Zaineb Ibraheem Saeed

A thesis submitted in partial fulfillment
of the requirements for the Master of Science
degree in Civil Engineering
University of Misan
December 2025

Thesis Supervisor: Assist. Prof. Dr. Murtada Abbas Abd Ali

بسم الله الرحمن الرحيم

ويَرَى الَّذِينَ أُوتُوا الْعِلْمَ الَّذِي أُنْزِلَ إِلَيْكَ مِنْ رَبِّكَ هُوَ
الْحَقَّ وَ يَهْدِي إِلى صِراطِ الْعَزِيزِ الْحَمِيدِ۞

صدق الله العلي العظيم

سورة سبأ –الاية (6)

DEDICATION

And what compromise but God?

I would like to dedicate my humble work to my kind GOD, who enabled me to complete this work and fulfill the trust.

and to the fortified cave and the light between heaven and the earth, to the great teacher (Imam Al-Hujjahu Ibn Al-Hassan)

" Aajal Allah Farajah Al-Sharif ".

ACKNOWLEDGEMENTS

First and foremost, all thanks and gratitude to the Generous Lord for the completion of this work. I would like to express my special thanks to my supervisors, Assist. Prof. Dr. Murtada Abbas Abd Ali.

I would like to extend my thanks to Prof. Dr. Abbas O. Dawood Dean of the college of engineering, and to all my teachers Prof. Dr. Sa'ad Fahad, Prof. Dr. Ahmad Al-Shara, Prof. Dr. Abdulkhaliq A. Jaafer ,Assist. Prof. Dr. Nasser Hakim ,Assist. Prof. Dr. Samir Mohammed chassib, Dr. Faten I. Mussa, and Dr. Hayder AL-Khazraji.

To my loving and supportive family, my father, mother and sisters. To those who made an effort to help me and were the best support for my friends and colleagues.

To everyone who has enlightened the minds of others with his knowledge or guided the confusion of those who ask for the correct answer, he has demonstrated the humility of scholars and the tolerance of those who know.

Thank you

Zaineb Ibraheem Saeed

CERTIFICATION

I certify that this thesis entitled (**STRUCTURAL PERFORMANCE OF HIGH-STRENGTH SELF-COMPACTED CONCRETE COMPOSITE ELEMENTS**), which is being submitted by (**Zaineb Ibraheem Saeed**), was made under my supervision at the University of Misan/College of Engineering, in partial fulfillment of the requirements for the Degree of Master of Science in Civil Engineering. In view of the available recommendations, I forward this thesis for debate by the examining committee.

Signature:

Name: Assist. Prof. Dr. Murtada Abbas Abd Ali

Date : / /202

(Supervisor)

Signature:

Name: Assist. Prof. Dr. Murtada Abbas Abd Ali

Head of the Civil Engineering Department /University of Misan

Date : / /202

Report Of The Examining Committee

We certify that we are the examining committee and have read the thesis, which is titled **(STRUCTURAL PERFORMANCE OF HIGH-STRENGTH SELF-COMPACTED CONCRETE COMPOSITE ELEMENTS)** ,which is being submitted by **Zaineb Ibraheem Saeed**. In our opinion, it satisfies the requirements for a thesis for the Master of Science in Civil Engineering (Structures) degree after the student's work was reviewed for content and concerns.

Signature:
Name: Assist.Prof.Dr.Murtada A.Abd Ali
(Supervisor)
Date: / /202

Signature:
Name: Assist. Prof. Dr. Hajer S. Abbas
(Member)
Date: / /202

Signature:
Name: Assist. Prof. Dr. Nasser H.Ta'ma
(Member)
Date: / /202

Signature:
Name: Prof. Dr. Sa'ad F. Resan
(Chairman)
Date: / /202

Approval of the College of Engineering

Signature:
Name: Prof. Dr. Abbas O. Dawood
Dean, College of Engineering
Date : / /202

ABSTRACT

Two concrete layers with expanded polystyrene (EPS) core panels are the best composite construction method that combines lightweight and efficient performance. Composite concrete structural panels are affected by their weight-to-strength ratio and the shear connector's ability to transfer loads and achieve the composite action. This study aims to develop high-strength self-compacting composite elements with shear connectors made of expanded metal mesh. The experimental program consisted of three phases and two parameters: shear connectors and pouring concrete layers in one stage and two stages. The initial phase focuses on identifying and achieving the characteristics of the high-strength self-compacting concrete required. In the second phase, four distinct shear connector configurations were examined under flexural bending load: (1) rectangular-shaped connector, (2) I-shaped connector, (3) Z-shaped connector, and (4) truss-shaped connector. 24 simply supported beams with dimensions of 1200x200x200 mm, are proposed to be applied in 4 groups, consisting of six beams in each group. 12 beams are cast in one stage. Twelve more beam specimens are cast in two stages, with a 24-hour difference between each stage. The third experimental phase is conducted to investigate the flexural behavior of six one-way expanded polystyrene concrete panels of dimensions (1220x610x180) mm with rectangular shear connectors, divided into two groups of three specimens, cast in the same manner as in the second phase after a one-day delay. The first crack load, ultimate load, deflection, ductility index, strain characteristics, and failure mode are investigated for beams and panels. For the first stage, the concrete mixture exhibited high early compressive strength, in addition to high strength, reaching 72.3MPa at 28 days. Due to its homogeneity and cohesion, the fresh concrete achieved high flow under its own weight, which facilitated easy transport and pouring, allowing it to reach inside the shear connector sections and reinforcement used in specimens of the second and third stages. n the second phase, beams with shear connectors in a rectangular shape, cast in one stage, yield high results in terms of the averages of ultimate load and maximum deflection, in addition to energy absorption (246.66 kN, 15.41 mm, and 2124.48 kN•mm, respectively), compared to other types of shear connectors. Beams with an I-shaped connector cast in one stage proved a high result in the averages of initial stiffness and ductility index (26.83 kN/mm and 2.4%). All beams failed in shear failure, whereas those with truss connectors exhibited flexural failure. Depending on the maximum

stresses, the types of connectors can be arranged in descending order from rectangle, I, Z, and truss shape. In the third phase, all panels with rectangle shear connectors failed in shear with a high ultimate load of an average of 415 kN for the panels cast in one stage and 398 kN for the second group, which was cast in two stages. Panels cast completely exhibited increased average initial cracking load, ultimate load, ductility index, and energy absorption by 3.6%, 4.09%, 14%, and 34%, respectively. Panels cast in two stages achieved high initial stiffness, 27% greater than that cast in one stage. The calculated composite action value of all panels decreased due to the decrease in section stiffness, which ranged between 19% and 38%, while high values exceeding 100% were achieved based on the failure load.

LIST OF CONTENTS

LIST OF TABLES

Appendix C

Appendix E

LIST OF FIGUREES

Appendix C

Appendix D

Appendix E

LIST OF SYMBOLS

f_t	Splitting tensile strength (MPa)
f_r	Modulus of rupture (MPa)
P_y	Yield Load (kN)
P_u	Ultimate load (kN)
P_{cr}	First crack load (kN)
Δ_y	Yield displacement (mm)
Δ_{umax}	Maximum deflection (mm)
Δ_{cr}	Deflection at first crack load (mm)
μ	Ductility index
σ	Maximum bending stress
fy	Yield stress of steel (MPa)
F_u	Ultimate Stress (MPa)
F_{cu}	Cube Compressive Strength (MPa)
As_{min}	Minimum reinforcement

ABBREVIATIONS

EPS	Expanded polystyrene sandwich (insulation material)
GFRP	Glass Fiber Reinforced Plastic
CFRP	Carbon Fiber-Reinforced Polymer
PCSP	Precast Concrete Sandwich Panels
SCC	Self-compacting concrete
DCA	Degree of Composite Action
ACI	American Concrete Institute
HSSCC	High-strength self-compacting concrete
CLT	Cross-laminated timber
XPS	Extruded polystyrene sandwich (insulation material)
RC	Reinforced concrete
W/C	Water to cement ratio
SP	Superplasticizer
BS	British Standard
FA	Fly ash
SF	Silica fume
CA	Coarse aggregates
EFNARC	European Federation of Specialist Construction Chemicals and Concrete Systems
ASTM	American Society for Testing and Materials
ACI	American Concrete Institute
IQS	Iraqi standard
MF	Fineness modulus of sand
IS	Indian standard
ANSI/AISC	American National Standard Institute/American Institute of Steel Construction

CHAPTER ONE: INTRODUCTION

1.1 General

Slabs of reinforced concrete are essential to building. They give the structure the stiffness and strength that it needs to support and disperse loads, which promotes stability, particularly in multi-story buildings. They provide fire and weather resistance as well.

Between 40% and 60% of the overall dead load of buildings is contributed by the weight of slabs [1]. A large foundation and higher construction costs can result from a hefty slab, increasing the self-weight of the building. Slab weight, depending on its type, the materials used, the number of layers, and its integrity (free from cracks and collapse) determines the roof's load-bearing capacity, which is important for ensuring the safety of the structure. There is increasing interest in affordable and easy-to-assemble building methods that are lightweight. Some modern systems for reducing roof weight include beamless slabs that transfer loads directly to the columns [2], precast [3], weight-saving hollow core [4], the use of lightweight concrete [5, 6], and insulated concrete sandwich panels, which have been increasing in popularity in the last decades due to advantages such as fire retardancy, enhanced thermal and sound insulation, robustness, and suitability for precast.

1.2 Precast Construction Technology

Precast concrete technology is an innovative process that enables the production of high-quality concrete elements in factories, which are then transported to the construction site for assembly and installation. Many structural members, such as columns, beams, wall panels, hollow-core slabs, and floor units, are with the most frequently used types. Using precast products has several benefits, such as

1- Control of quality: Precast concrete is made in specialized factories where every step of the procedure, including curing, mixing ratios, and material quality, is regulated, resulting in consistent and reliable concrete elements.
2- Controllable cost: In standardized element mass production, precast increases its durability and requires less maintenance, which leads to cutting the amount of workforce on the construction site, which lowers expenses.
3- Control of time: The use of precast concrete reduces construction time because the elements are produced in the factory and assembled at the construction site more quickly than on-site elements.

1.3 Expanded Polystyrene (EPS) Core Panel System

The EPS core panel system is a precast, insulated concrete sandwich panel that serves as an alternative to conventional load-bearing structural units. They can be used as wall (vertical) and roof/floor (horizontal) panels. These panels are constituted of two concrete reinforced layers known as wythes, which are separated by a less dense core (Figure 1.1). The core could be made of expanded polystyrene or extruded polystyrene [7]. It is made by expanding polystyrene granules using steam inside a mold, resulting in sheets made up of small, tightly packed spheres (like traditional white cork). Expanded Polystyrene, often referred to as EPS, is a kind of rigid, closed-cell foam plastic. EPS properties include low thermal conductivity, high compressive strength, lightweight, and the best eco-efficiency [8]. It can be used as a building material or a design element. The outer layers of concrete sandwich panels can be classified as either non-structural or structural; if a wythe makes a substantial contribution to the panel's load resistance, it is regarded as structural [9]. The two wythes are connected using shear connectors through the core for transferring shear forces between them. Shear connectors are either concentrated or continuous. Continuous shear connectors improve the composite action over the length of the panel. Various types of shear connectors were used: steel bar [10], steel truss [11] (Figure 1.10, GFRP shear connector [7], and other types that differ in terms of shape and material [9]. Precast concrete sandwich panels (PCSP) can be divided into three major categories: fully composite, partially composite, and non-composite panels, as shown in Figure 1.2.

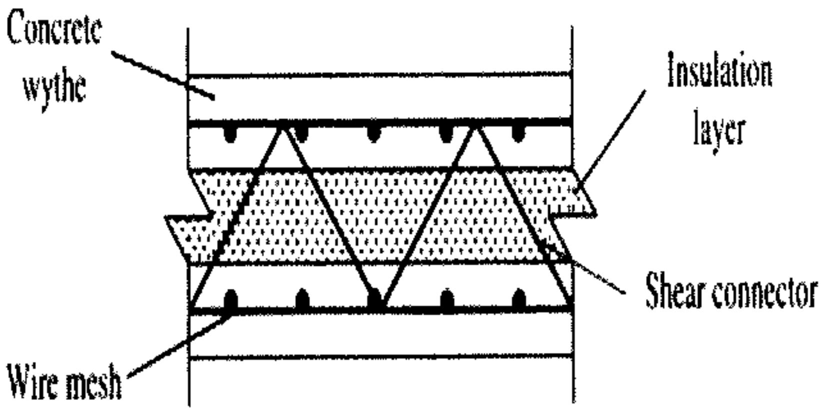

Figure 1.1 Components of Precast Concrete Sandwich Panel with Truss-Shear Connector [12].

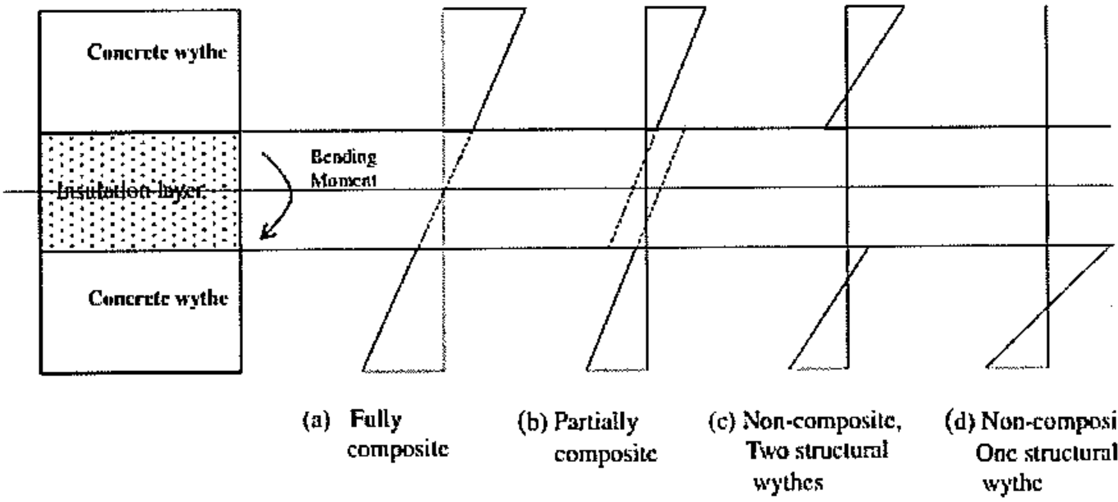

(a) Fully composite (b) Partially composite (c) Non-composite, Two structural wythes (d) Non-composite, One structural wythe

Figure 1.2 Bending Stress Distribution [12].

1.3.1 Behavior of Concrete Sandwich Panel

Almost all precast concrete panels currently in use include a composite material. The behavior of the PCSP is complex due to the interaction of its components and the percentage of composite action. With the use of shear connectors, composite panels are made to ensure that the two concrete wythes are completely attached and capable of supporting the imposed load. The behavior of most PCSPs lies somewhere between fully composite and non-composite [13]. Fully composite panels whose wythes are connected in such a way that both wythes resist applied flexural loads as if they were an integral section. In this case, connectors must transfer the required longitudinal shear so that the bending stress distribution on the cross-section of the panel. Non-composite panels with two concrete wythes joined by components (connectors) incapable of transferring longitudinal shear. If the two concrete wythes are of equal stiffness and reinforcement, each wythe resists 50 percent of the load. The panels were tested in 3-point and 4-point flexure bending tests [14] [15], and push-off shear loading tests [11, 16], which are most common, as these tests can be done with standard laboratory equipment (displacement sensors, load cells, hydraulic jacks, and test frames. The failure behavior of composite panels is the crushing of concrete, or the yielding of steel reinforcement, or the slipping between wythe-to-EPS core interfaces.

1.3.2 Structural Wythe of Concrete Sandwich Panel

In fully or partially composite panels, both concrete wythes are structural. In non-composite panels, either one of the wythes is structural and the other is non-structural, or both wythes are structural and independently resist the applied loads. Reducing the panel's thickness is crucial for reducing its weight. A concrete wythe's thickness varies according to its structural purpose, concrete cover, connecting anchorage, and finish, with a minimum thickness of 50 mm [13]. Traditional steel reinforcement, welded wire mesh, can be used as reinforcement [9]. Usually, each of the two wythes uses the same type of concrete. The compressive strength of concrete shall not be less than 20 MPa. Lightweight concrete, normal concrete [12], high-performance concrete, and self-compacting concrete [14] are among the concrete types used in EPS concrete layers.

Self-compacting concrete (SCC) has been utilized in building and civil engineering projects for more than 35 years. The SCC addresses many problems associated with the skill of workers, complexity of reinforcement, type and shape of structural section, pumpability, and segregation resistance. Self-compacting concrete can achieve high strengths and is preferred for use in construction due to its workability and enhanced durability, as well as enhanced tensile and compressive strengths in contrast to traditional SCC [17, 18]. SCC does not have a specific standard mix procedure. A few principles were established for SCC mixes: lowering the water-to-powder ratio, regulating the overall amounts of coarse aggregate, incorporating fine materials instead of a portion of the cement, and utilizing a superplasticizer [19].

1.3.3 Degree of Composite Action (DCA)

The slip occurring in the sandwich panels can be defined using the concept of the degree of composite action. A degree of composite action determines the structural efficiency of precast concrete sandwich panels. The percentage of composite action that a sandwich panel can exhibit is an important engineering design parameter. In some cases, the panel can be conservatively considered as non-composite, and only one of the outer wythes is used to take the axial or flexural load. However, in many cases, the sandwich panel, which contains concrete wythes at each side connected with some form of shear tie, will exhibit a percentage of composite action.

The degree of composite action is influenced by the interface between the old and new concrete layers. It's known that sandwich panels combine the advantages of precast elements and specific features of cast-in-situ concrete. These composite units have an interface between the parts; the interface may be the weakest zone, given the occurring discontinuity of the construction material. The degree of composite action depends on the resistance to flexure and shear in the interface of concrete units, resulting from the adhesion, the work of the transverse reinforcement, and the height of concrete layers [20, 21]. Different methods have been introduced to define a degree of composite action based on strength, deflection, and moment of inertia [14, 15, 22].

1.4. Expanded Metal Mesh

A metal grid created by punching slits into a metal sheet and then extending (expanding) it is known as expanded metal, or expanded mesh (Figure 1.3a). The perforations open up into diamond-shaped apertures, transforming the sheet into a mesh-like structure without causing any material loss.

1.4.1 Properties of Expanded Metal Mesh

The most important features of the expanded mesh:

1-There are two types of expanded mesh: the standard type, where the mesh surface is wavy/raised, and the flattened type, which is rolled flat for smoother surfaces. The first type provides a high level of slip resistance.

2- One piece is used to create expanded metal. It has great strength and stability because there are no welds or weaving knots.

3- They can be manufactured from a variety of materials, including carbon steel, stainless steel, aluminum, and nickel.

4- High power-to-weight ratio.

5- Expanded metal is more rigid than wire mesh, particularly when composed of thicker sheets. Compared to woven mesh (Figure 1.3b), thin expanded metal is easy to cut and shape to size and can be rolled and bent.

6- Scales or hexagonal shapes are also feasible, but diamond-shaped (typical 45° staggered pattern) is the most common. The mesh is typically slightly wavy in three dimensions due to the edges at the expanded sections being slightly offset in planes.

7- Depending on the scales, open area often falls between 40 and 80 percent.

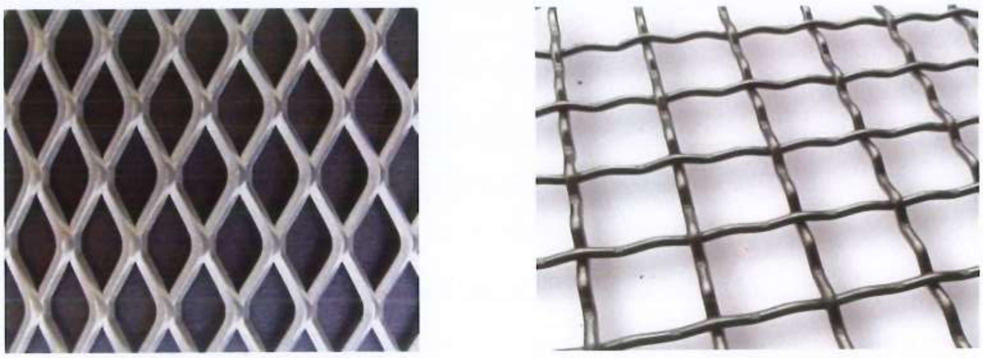

a. Expanded wire mesh b. Woven wire mesh

Figure 1.3 Types of Mesh.

1.4.2 Applications of Expanded Metal Mesh

There are several industrial, architectural, and security uses for expanded metal mesh:

1- Used to offer ventilation and create a contemporary appearance in parking lots, sports facilities, and building exteriors.

2- Offers excellent durability and security for enclosure and fencing applications.

3-Because of its variety of patterns, it is utilized in creative decorations, suspended ceilings, and internal dividers.

1.4.3 Advantages of the expanded network with concrete

Expanded metal mesh is used in concrete and construction applications due to the numerous advantages it offers, most notably:

1-Used in building joints and giving new concrete a rough surface to stick to.

2-Used to provide tensile strength and stop cracking in concrete slabs and roofs. Heavy loads can be supported by several layers.

3-Its open-cell design ensures optimum load distribution and improves structural integrity by providing outstanding bonding with the concrete.

4-Used to strengthen old or damaged structural elements in concrete buildings as part of rehabilitation processes.

5-The lightweight design makes installation and transportation simple.

6-With no loose joints or welding, the structure is more structurally sound and has fewer failure regions.

7-A more affordable option than some other reinforcement techniques.

8-Able to resist corrosion, depending on the type of metal.

1.5 Description of the Research's Problem

The primary factor influencing the structural precast sandwich panel (SPSP)'s performance is its relative light weight in relation to its high strength (Mahdi, 2022; Lee, 2018) [23, 24]. Expanded mesh has several uses, such as in the construction of new buildings as well as the maintenance and restoration of old ones (ACI 549, 2020). One of the most important things that is taken into consideration when choosing materials in buildings is strength and durability, as well as their availability, affordability, and ease of installation in any shape that serves the structural elements. Any structural designer aims to design safe structures that meet the requirements of the governing design codes. The benefits of precast technology and lightweight structural elements have been merged in sandwich composite construction to create a new system that can take the place of its traditional equivalent. Expanded is a thinner material. Also, the impossibility of nailing, screwing, or welding. The thin section would be viewed as unsafe to live in, so these could not become widely accepted. Also, sandwich construction deals with the problem of delamination of face sheets, leading to their premature failure.

To overcome these problems, one of the main objectives of this study is to develop a composite concrete panel with high compressive strength and a shear connector made of an expanded metal mesh. This could potentially address the majority of the drawbacks of precast composite constructions.

1.6 Experimental Method for the Study

The study plan consists of three phases. The first phase will be focused on testing the characteristics of the concrete mixtures by investigating cubes, .cylinders, and prisms.

In the second phase, for drawing accurate conclusions and making reliable predictions, three suitable-sized beam for each variable (24 in total) would give the study greater statistical power, meaning it would be better able to detect true differences or relationships between variables. The metrics that will be used to analyze the beam specimens' performance are the deflection and the load at the first crack, and the deflection and the load at collapse.

In the third phase, considering the aspect of time and money, a single type of shear connector (rectangle) was used to test six composite concrete panels insulated with expanded polystyrene (EPS) (three for each variable).The failure mode, load-strain responses, and the first crack and ultimate loads, along with associated deflections, will be tested

1.7 Significance of Research

This study is to test the performance of high-strength self-compacting composite elements by two parameters: the type of shear connector and the effect of the old and new concrete interfaces. The following are the particular goals of this study:

1. Designing a self-compacting concrete mix that achieves high strength and high workability.

2. Determine the flexural behavior of reinforced concrete beams with shear connectors with four different shapes of shear connectors-rectangular, I-shaped, Z-shaped, and truss-shaped.

3. Studying the effect of single-stage and two-stage casting on composite beams behavior.

3. Study of the flexural behavior and the composite action of one-way composite concrete panels.

4. Studying the effect of single-stage and two-stage casting on composite panels behavior.

1.8 Outline of Thesis

The dissertation is organized into five chapters in the manner described below:

1. Chapter One: This chapter serves as an introduction and outlines the three goals of the research.

2. Chapter Two: Examines the system's influencing elements and composite structures. Additionally, it examines previous research on ferrocement and its behavior, which gives context for determining the study's research gap.

3. Chapter Three: In this chapter, the experimental program, specimen preparation, test setup, and instruments are presented together with the material properties.

4. Chapter Four: In addition to discussing and contrasting the models' performance outcomes, this chapter includes the findings and observations from the experimental study.
5. Chapter Five: In this chapter, the study's findings and conclusions are summarized, along with suggestions for additional research in this area.

CHAPTER TWO: LITERATURE REVIEW

2.1 General

The construction industry has transformed in recent years, moving away from traditional methods and toward more efficient and organized practices. Composite concrete element production has grown into a specialty in creating concrete products that are lightweight, strong, easy to apply, and cheap, all-in-one materials. Therefore, a representative composite system largely depends on the components and materials chosen for each function. This chapter provides a review of the literature for composite systems through practical experiments and also provides the most important considerations that affect their behavior.

2.2 Composite Concrete Sandwich Panels

In 2008, Benayoune A.[12], investigated the effect of the stiffness of a continuous steel truss shear connector, on both the ultimate strength and the compositeness of the panels. The flexural behavior of one-way and two-way panels was investigated by six panels of precast concrete sandwich panels (PCSP) with dimensions shown in Table 2.1. The panel consisted of two normal-strength concrete layers of 40 mm thickness reinforced with wire mesh with 100mm x100mm openings, a 6mm diameter, a polystyrene layer of 40 mm thickness, and the steel truss shear connector was made of 6 mm diameter (Figure 2.1). The one-way panels were simply supported and subjected to two-line lateral loads while the two-way panels were also simply supported on four sides and subjected to four-point lateral loads.

Table 2.1. Details of Test Panels [12].

Panels	Size(mxm)	Aspect ratio	Number of truss connectors	
			Longitudinal	Transverse
P11and P12	2x 0.75	2.67	3	_
P21and P22	1.5x 1.5	1	6	6
P23and P24	1x 0.5	2	2	_

In this study, the shear connectors were able to transfer forces from one wythe to the another efficiently till failure to enable the two concrete layers to prolong the composite behavior. The result confirmed that the one-way precast concrete sandwich panels (PCSP) had a similar behavior to that of a one-way solid slab. They developed flexural cracks in the bottom wythe along the width of the panel. The first crack occurred approximately at a load of 55% of the ultimate load. Also for the two- way panels, the crack patterns in the tension zone were found to be similar to those of the two-way solid slabs. The first cracks occurred approximately at a load of 60% of the ultimate load in each case in the bottom layer. All PCSP failed due to the tension steel failure with excessive cracks in the tension zone of the bottom wythe. All panels proved to be very ductile, exhibiting large deformation before failure. The number of connectors represents the areas of shear connectors that were added so that axial stiffness increases the loads until failure, which are 20 kN, 25.16 kN, and 29.75 kN for connector numbers 2, 3, and 6, respectively.

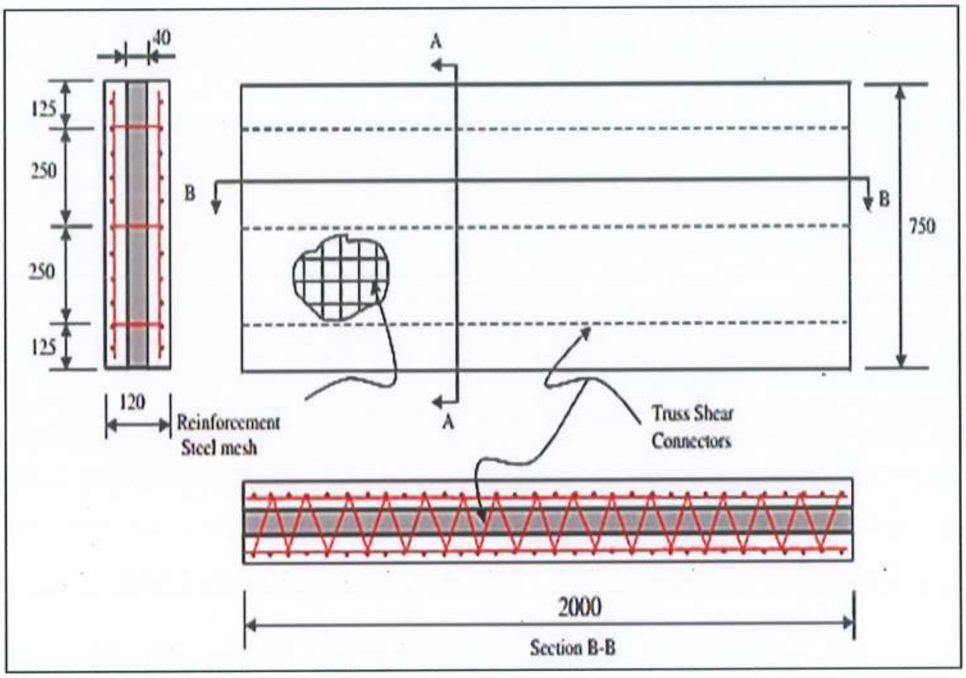

(a) One-way panels with an aspect ratio of 2.67

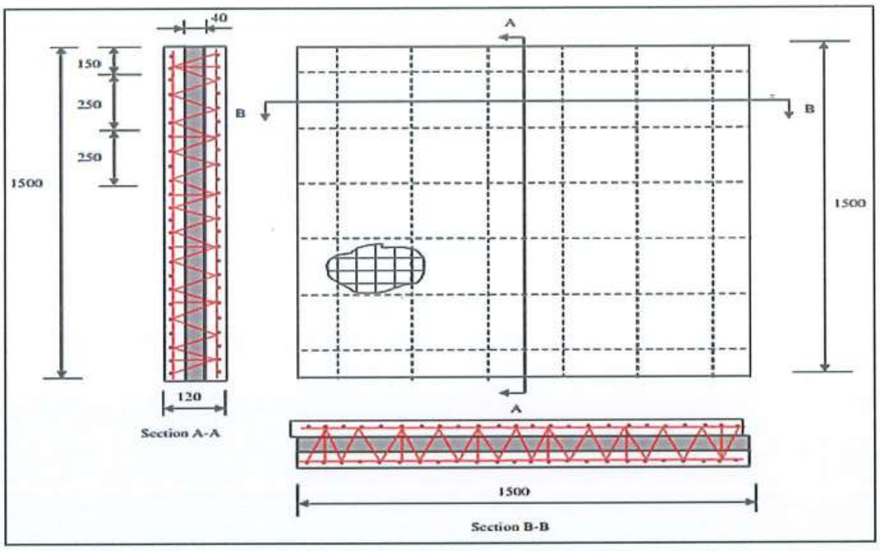

(b) Two-way panels with an aspect ratio of 1.0

Figure 2.1 Test Panels Chosen for Test as Slabs (All dimensions in mm) [12].

In 2015, Choi K.B.[7], provided the results of push-out tests on concrete sandwich panels that were conducted both with and without corrugated GFRP shear connectors to look at the in-plane shear performance. GFRP connectors are Glass Fiber Reinforced Plastic shear connectors incorporate a 45-degree angle to the shear plane and are 5 mm thick (Figure 2.2). The width, pitch, and embedded length were design parameters for corrugated GFRP shear connectors. Ten samples were examined in vertical quasi-static loading circumstances with two thermal extruded polystyrene XPS and expanded polystyrene EPS (Figure 2.3). The compressive strength of the concrete panels was 30 MPa.

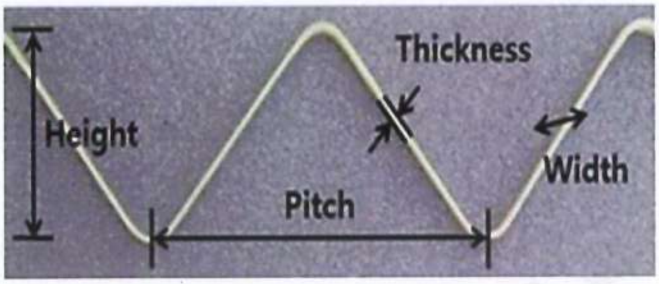

Figure 2.2 Design Parameters for Corrugated GFRP Shear Connectors [7].

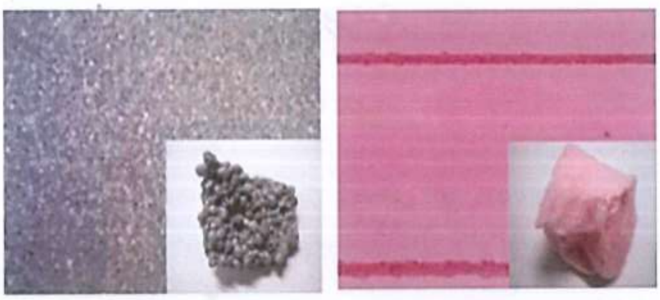

(a) EPS insulation (b) XPS insulation

Figure 2.3 Types of Insulation Material [7].

The test findings show that the bending strength between the insulation layer and the concrete walls is significantly influenced by the type of insulation material employed in the system. In this investigation, the average shear flow values for EPS insulation and XPS insulation with a 10-mm wide shear connector and a 30mm embedded length were 111 kN/m and 103 kN/m, respectively, but were 137 kN/m and 130 kN/m, respectively, with a shear connector that was 20 mm wide and had a 50 mm embedding length. The stiffness and strength of the specimen tended to rise as the corrugated GFRP shear connector's width increased. When specimens with a 15 mm-wide shear connection were embedded for 30 mm, pull-out behavior and radical splitting of the upper area occurred after reaching the maximum load. The corrugated GFRP shear connector's width tended to increase the specimen's stiffness and strength as well. The in-plane shear strength increased with pitch, giving the shear connector a high tensile strength.

In 2017, Joseph J. D. and Prabakar J.[14], conducted ten one-way concrete sandwich panels that are subjected to four-point bending as part of the experimental program. Shear-resistant ribs, panel thickness (100, 150mm), mesh size 50x50 mm or 100x100 mm, and traditional rebars attached to the wire mesh in the bottom wythe were all evaluated by the parameters. Figure 2.4 shows that expanded polystyrene (EPS) makes up the core. The panels measured 3000 x 1220 x 100/150 mm in size. Self-compacting concrete with an age cube compressive strength of 45.9 N/mm² was employed, along with truss shear connectors. Shear-resistant ribs are made of longitudinal rebars with a diameter of 2 Ø8 mm. As reinforcement, place stirrups with an 8 mm diameter at 150 mm c/c.

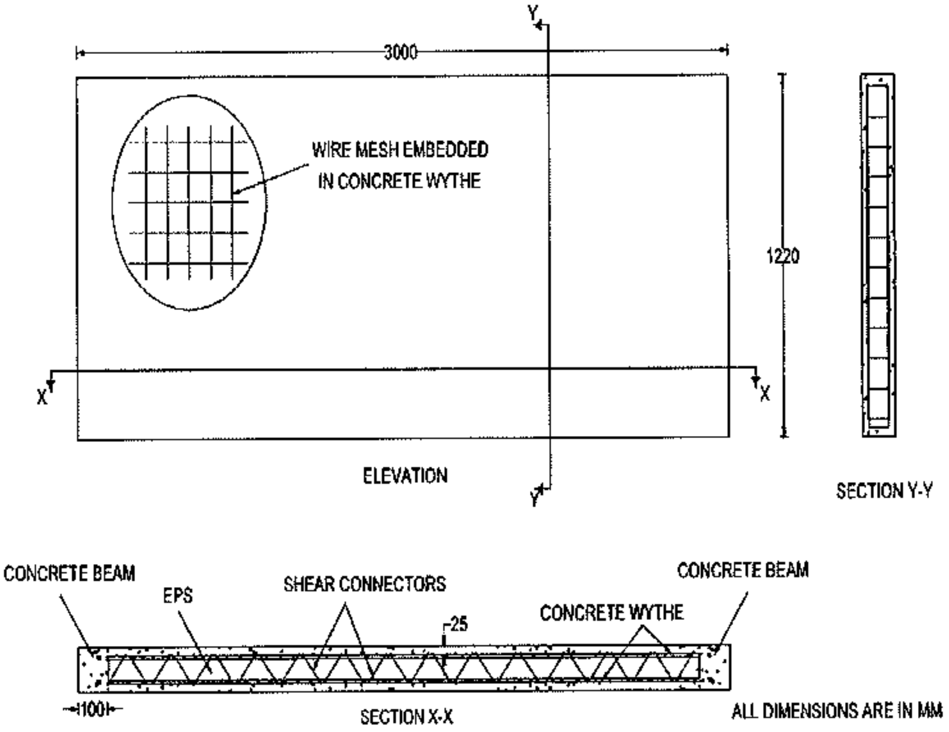

Figure 2.4 Details of Concrete Sandwich Panel [14].

The test findings reveal that all of the panels act as composite elements up until they collapse with truss connectors, where the connectors and probable frictional forces between the EPS-concrete interface resist shear force. Precast concrete sandwich panels' failure mode, failure load, load-deflection behavior, and load-strain behavior are all impacted by the addition of rebars in the bottom wythe and span-wise distributed shear-resistant ribs orientated in the spanning direction. Similar to conventional RC one-way slabs, the bond force between the concrete and reinforcements has a significant impact on influencing their cracking behavior. In ductile flexural mode, all of the panels with shear-resistant ribs fail by developing many vertical flexural cracks on their sides. Through the formation of shear cracks, the panels with traditional rebars in the bottom wythe without shear-resistant ribs failed. Concrete's ultimate load-carrying capacity is increased with reduced crack spacing when rebars are added to the bottom wythe in addition to small-size wire mesh measuring 50x50 mm. The mesh size and the presence or absence of shear-resistant ribs determine strain in shear connectors. The shear connectors strain more to ensure the panel's composite action when the mesh dimension is smaller and there are no rebars in the panel's bottom wythe.

In 2019, O'Hegarty R.[25], examined the flexural behavior of a precast concrete sandwich panel made of foam insulation, high-performance fiber-reinforced concrete wythes, and grid connectors made of carbon fiber-reinforced polymer. Three-point bending was used to test the strength of four panels (Figure 2.5). The size of each panel was 3000x750 mm, and they had a 25mm, and 40mm outer wythe, a 90-mm insulating layer of EPS, and a 40-mm inner wythe (Figure 2.6). The compressive strength of concrete wythes was of 96 MPa with 24 mm long straight fibers of 0.7 mm diameter had a tensile strength greater than 1000 MPa and an elastic modulus of 42 GPa. Two strips longitudinally carbon fiber-reinforced polymer shear grid were used in the panel.

Figure 2.5 Panel Test Under 3-Point Loading [25].

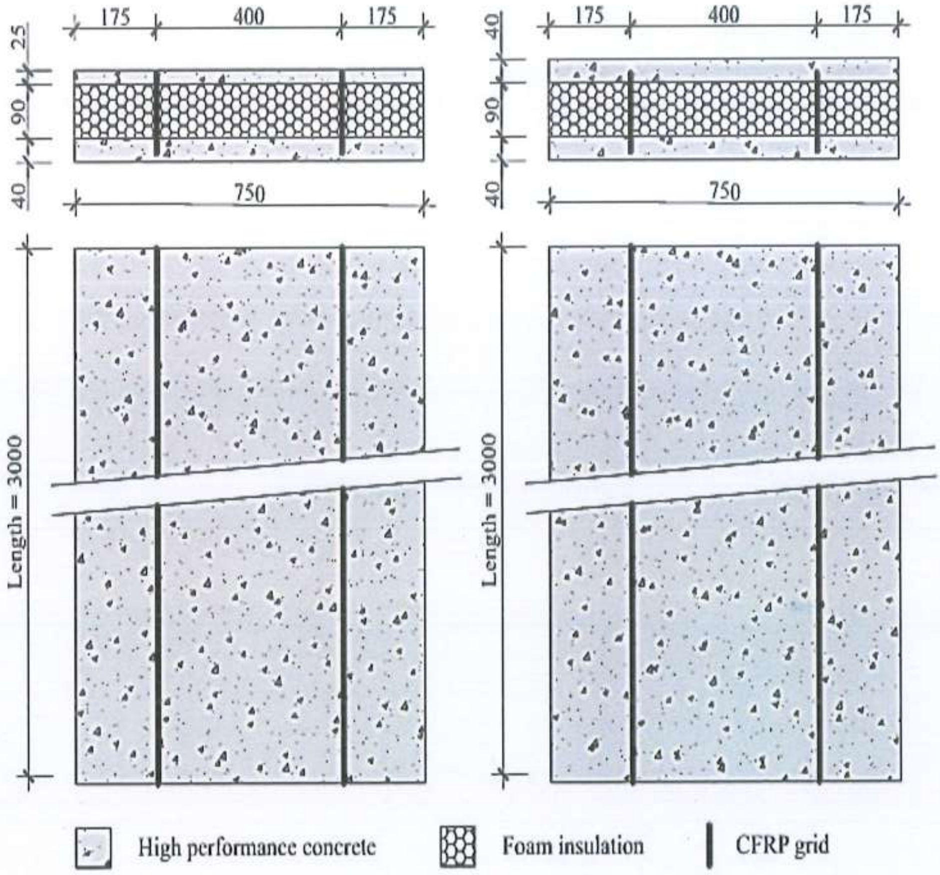

Figure 2.6 Concrete Sandwich Panels Dimensions in mm [25].

According to the experimental results, the ultimate capacity and flexural rigidity of the panel doubled when the outer layer of concrete was increased from 25 to 40 mm. All of the panels' failure mechanisms were ductile, exhibiting displacements greater than 30 mm before final collapse and high relative strain energy and bending moments of up to 6.5 kN · m for the panels of 25 mm in thickness and up to 13.1 kN · m for the panels of 40 mm. There was very little indication in the testing results that the CFRP shear grid improved the panel's composite behavior. Following failure, it was clear that the CFRP grid failed due to rupture rather than pull-out, and the 20 mm embedment depth seemed to be adequate to prevent pull-out. In addition to displacement data and visual inspections, the results from the strain gauges reinforce the fact that there is non-composite behavior, particularly before cracking. The compression and tension in both wythes mean there are two neutral axes and no full composite action. Firstly, the bottom wythe appears to crack in thinner panels, but with 40 mm thickness, the top wythe appears to crack first.

In 2020, Kandil M.A.[10], examined how modifications to the wythe and core characteristics affect structural sandwich panels. Within the experimental program, seven specimens measuring 500 x 500 mm and 120 mm in total height were created. Three grades of concrete (80.3, 70.4, and 37 MPa), three types of core materials (high-density foam, polyethylene foam, and palm bark), and three thicknesses of upper and lower concrete wythes (25, 35, and 45 mm) were used. The concrete wythes were reinforced with plain steel (5 Ø 6 mm per meter length) in both directions. In each specimen, 16 steel bar shear connectors measuring Ø 12 mm in diameter were placed at a 45° angle at their assigned positions (Figure 2.7). Every specimen underwent flexural load testing using a three-point loading system.

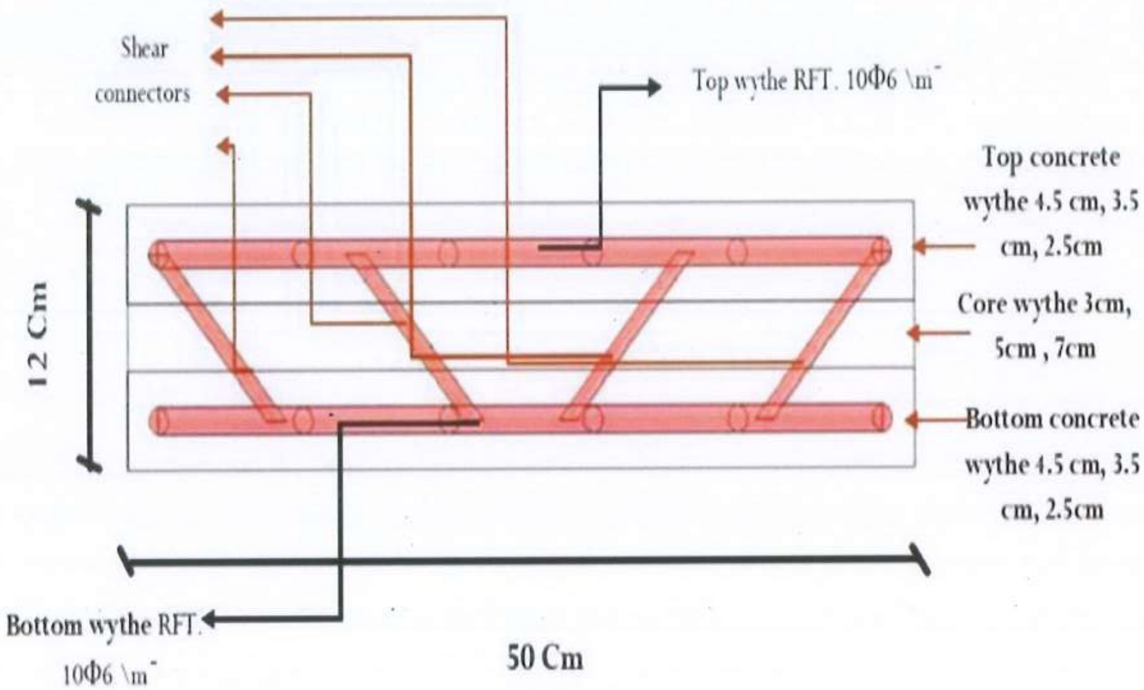

Figure 2.7 Cross Section for One Specimen [10].

The results showed that the strength-to-weight ratio, composite degree, and overall strength of slabs were all considerably enhanced by improving the concrete's grade. It was noticed that the ultimate strength and the degree of composite action and strength/weight ratio decreased with a change of concrete strength from 80.3 to 70.4 MPa by 19.3%, 19.23%, and 12.8%, respectively. The ultimate strength decreased by 32.12%, the degree of composite action reduced by 30.74%, and the strength/weight ratio lowered by 6.8% when the grade of concrete was changed from 70.4 to 37 MPa. The load capacity and the weight are influenced by the wythe thicknesses. The ultimate load and the degree of composite decreased by 18.32%, while the strength/weight ratio increased significantly by 2% when the thickness of both wythes was adjusted from 45 mm to 35 mm. The composite action decreased by 16.1%, and the ultimate load decreased by 15.8% when the wythe thickness was reduced from 45 mm to 25 mm. Conversely, the ratio of strength to weight increased by 13.3%. While the ultimate load and composite degree increased by 22.5%, the strength/weight increased by 22.7% when the core material moved from high-density foam to polyethylene foam. When the core material was changed from high-density foam to palm bark, the ultimate load and composite degree decreased by 19%, and the strength/weight decreased by 19%.

In 2022, Wang Y. and Wang J.[26], investigated insulated concrete sandwich panels with innovative dumbbell-shaped steel fiber-reinforced polymer (FRP) composite bar connectors under flexural load. The sandwich panel was 2800×1000 mm with a total thickness of 310 mm. All specimens consisted of a structural wythe of 120 mm thick at the bottom, a 60-mm-thick wythe at the top, and a 130-mm layer of foam insulation between the two wythes (Figure 2.8). The compressive strength of the two concrete layers was 35 MPa, reinforced with 8 mm diameter welded steel wire mesh. The connectors were designed based on hybrid GFRP-steel bars with an 8 mm diameter and the same 250 mm length (Figure 2.9). The thickness of GFRP jackets of hybrid bars varied from 2 to 3 mm, and the raised thickness of dumbbell ends varied also from 4 to 6 mm.

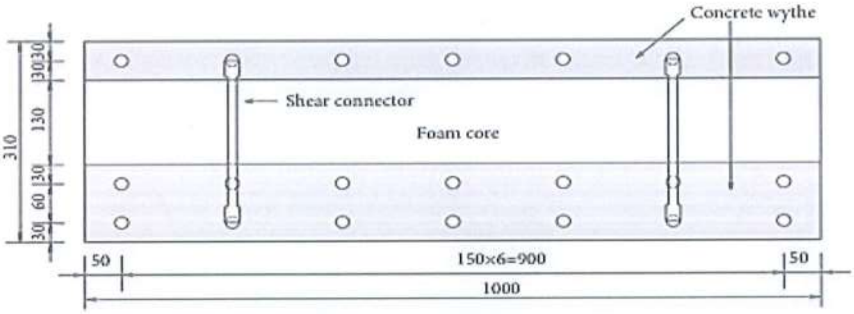

Figure 2.8 Cross Section of the Sandwich Panel with

Dumbbell-shaped Connectors [26].

Figure 2.9 Dumbbell-Shaped hybrid GFRP-Steel Bars Connectors [26].

According to the findings, the yielding of the tension rebars and the penetration of the bottom wire in the midspan controlled the failure modes of sandwich panel specimens under load. The hybrid bars' GFRP thickness and the dumbbells' increased thickness had little effects on the sandwich panel specimens' failure mechanisms. The specimens' initial cracking load, maximum load, and flexural stiffness rose by 75, 49, and 16%, respectively, when the GFRP jacket on the hybrid bar was thickened from 2 to 3 mm. The flexural stiffness of specimens was 18, 46, and 9%, respectively, and the increased thickness of dumbbell ends from 4 toppled to an increased first breaking force. Although they had little effect on ductility, the GFRP jacket's increased thickness and the dumbbell ends' increased thickness both helped to reduce the slide between the two wythes. Regarding the initial stiffness of the sandwich panels with independent hybrid connections, the estimated values of the degree of composite action ranged from 19 to 42, indicating a partially composited structure. However, the ultimate strength values of the degree of composite action were larger than the initial stiffness values, ranging from 31 to 97.

2.3 Shear Connectors in Composite Elements

In 2012, Jacquier N.[16], tested shear connections with cross-laminated timber (CLT) panels for floor systems. In order to place technical installations, the concrete was not in the form of a plate but in the form of a beam element. In Figure 2.10c, this configuration, as a floor, the CLT panel forms a platform for mounting and connecting the installations from above during the prefabrication process at the factory. In all, twelve specimens underwent shear tests as showed in Figure 2.11. For the experiments, two distinct kinds of connections were selected. The original kind of connector was called "studs" and was made of two welded-head studs attached to a steel plate that was 6 mm thick (Figure 2.10 a). The second type of mesh was created by welding an expanded metal mesh of 4 mm thickness, was fixed between two plates made of steel (Figure 2.10 b). Holes of 12 mm diameter were made inside steel plates for connecting the screws to the CLT with spacing of 80 mm. The screws were tightened rather hard with the CLT panel. Compressive concrete strength was 40.81 MPa at 28 days. Shear tests were used on CLT panels that were made of 3 layers with thicknesses of 74 and 103 mm. All CLT elements were 500 mm wide and 420 mm long. Details for the test specimens are given in Table 2.2.

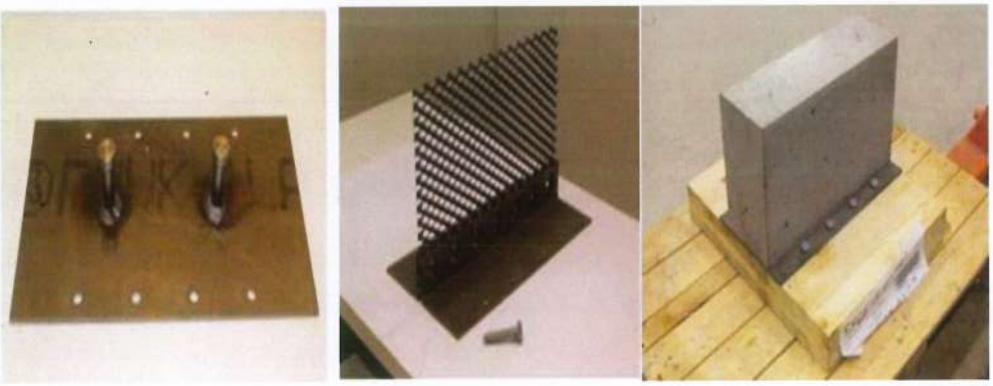

(a) (b) (c)

Figure 2.10 Shear Connectors (a) Stud (b) Mesh (c) Test specimen [16].

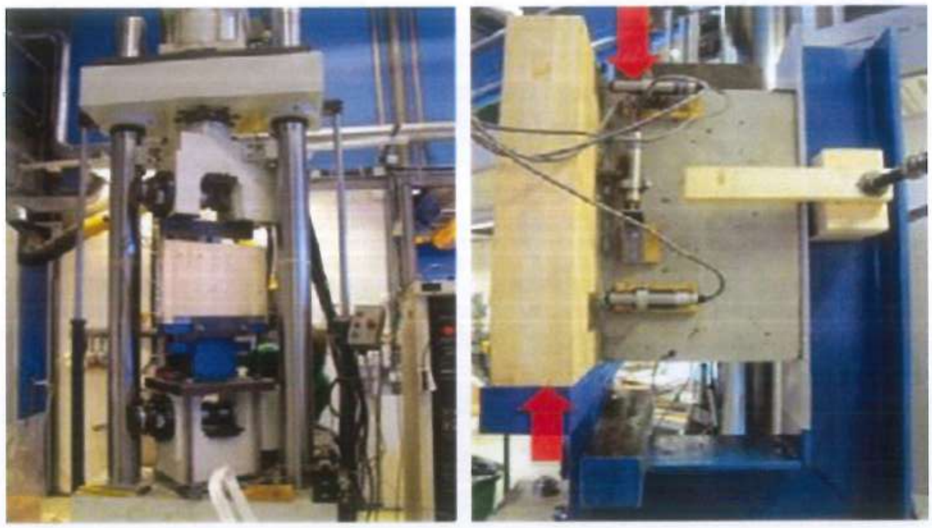

Figure 2.11 Test Setup for the Shear Test [16].

Table 2.2 Details of Series Test Specimens [16].

	Series	Test	Type of shear connector/Thickness of steel plate	Screw spacing (load direction)/ Edge distance(mm)	Thickness of CLT panel(mm)
GROUP1	S-8S-65	T1, T2, T3	Studs /6mm	80 / 90	74
GROUP2	S-4S-65	T4, T5, T6	Studs /6mm	240 / 90	74
GROUP3	M-8S-65	T7, T8, T9	Metal mesh /4mm	80 / 90	74
GROUP4	M-4S-65	T10, T11	Metal mesh /4mm	240/90	74
GROUP5	M-8S-100	T12	Metal mesh /4mm	80/90	103

According to the test results, the first group of tests with studs 6mm and 80/90 screw spacing in concrete showed semi-brittle behavior; the failures occurred in the concrete after yielding of the studs in the concrete at an applied load of about 105 kN. Test specimens for the second group exhibited a very ductile type of behavior, an almost perfect plastic behavior, with an average ultimate load of 56.3 kN, which was about half of that of the first series. The failure was caused by the CLT panel's failure as well as the screws' yielding. With an average ultimate load of 129.2 kN, the third series with a mesh in the concrete exhibited the same behavior as the second series. Additionally, with an average ultimate load of 63.7 kN, the fourth seires shared the same traits and degree of yielding as the second series. After yielding, the last series experienced a brittle failure; the concrete block broke apart in accordance with the expanded metal mesh at an applied shear stress of 157 kN. The high initial stiffness is most likely caused by friction between the CLT panel and the steel plate. Due to their ductile properties, the connection types from second, third,and fourth were appropriating for practical applications.

In 2014, Toghroli A.[27], investigated the shear strength of steel channel shear connectors with push-out specimens that consist of a steel I beam with two slabs attached to each flange of the beam. There were four different types of channels used: 30 and 50 mm in length and 100 and 75 mm in height. The flange thickness and web thickness of the 100 mm high channels were 6 mm and 8.5 mm, respectively, while the 75 mm high channels had 5 mm and 7.5 mm, respectively. One channel was welded to each beam flange, and two layers of steel bars with four 10 mm diameter steel bar hoops were placed in two perpendicular directions to all slabs (Figure 2.12). The concrete compression strength were 82 MPa and 63 MPa.

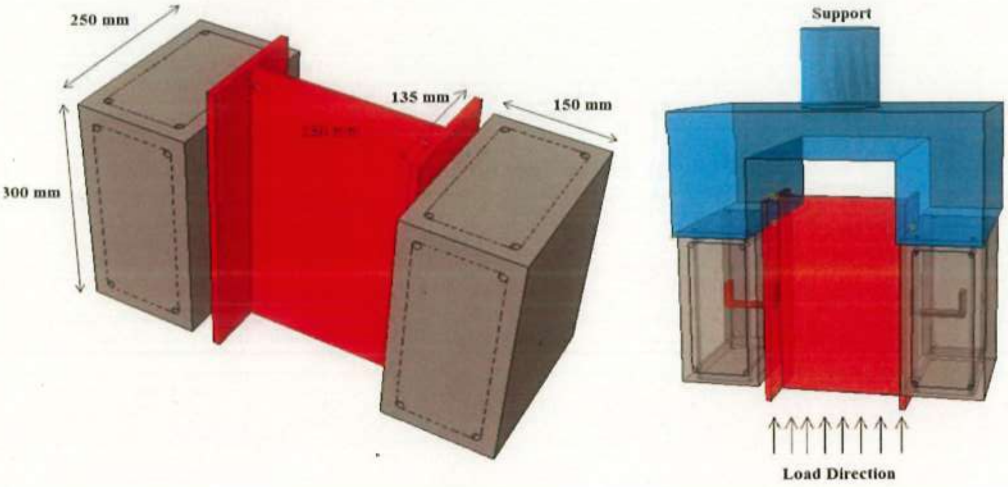

Figure 2.12 Details of Specimen Used in Experimental Push-Out Test [27].

The findings showed that when channel fractures occur, concrete cracks on the sides of slabs with prediction of shear capacity of channel shear connectors using longer channels; this is not the case with slabs with shorter channels. In comparison to the specimens with 75 mm high channel connectors, the specimen with 100 mm high channel connectors handled a somewhat more load. The shorter channel connectors' propensity to concentrate the applied load on a smaller region could be the cause of this. Compared to the specimen with 75 mm high channels, the one with 100 mm high channels is more flexible. Slip at the ultimate load level was 6.5–9 mm for the 100 mm high channels and 4–8 mm for the 75 mm high channels. The load-slip curve abruptly ends when the load capacity rapidly drops below the peak load. This demonstrates that every specimen has a yield plateau, indicating that slip increases when the load reaches its maximum.

In 2016, Titoum M. and Mazoz A.[28], presented an experimental evaluation of the push-out tests conducted on a novel I-shaped shear connector. The purpose of the test specimens was to examine how the height, length, compressive strength of the concrete, and number of transverse reinforcing bars of an I-shaped connection affected the ultimate load capacity. 24 push-out tests with three pairings in each series made up the experimental program. Level of I-shape connector (80, 100, 120 mm), width (40, 60, 80 mm), and compressive strength of concrete (21.23, 26.28, 31.47 MPa). A push-out example comprises two little substantial pieces that stood firm in an upward situation and joined to the ribs of a 160 x 360 mm steel bar through a welded I-shaped shear connector (Figure 2.13).

There were two main categories into which the failure modes found in the push-out tests fall. The first mode of failure was the shearing of the connector. The characteristic feature of this failure mode was the yielding and then shearing of the web near the welded flange fillet, especially in the specimens with higher-strength concrete and/or with connectors of smaller length. The second mode of failure is the cracking and crushing of the concrete slab in front of the connector. In specimens made using low- and moderate-strength concrete, the failure was caused by cracking and crushing of the concrete slab. Up until the specimen reached the ultimate load, slip increased with increasing load; beyond that, the load steadily dropped until failure. When the connector height was raised from 80 mm to 100 mm, the ultimate load rose by almost 10% on average. When the connector height was raised from 100 mm to 120 mm, there was an additional 6% rise. The ultimate load capacity increased by about 56% on average when the I-shaped connector's length was increased from 40 to 60 mm, and by about 27% when the connector's length was increased from 60 to 80 mm. The average increase in the final load capacity of an I-shaped connector was about 12.25% when the concrete's compressive strength increased from 21.23 to 26.28 MPa. Even so, the ultimate load capacity of the I-shape connector only rose by 3.13% when the concrete strength was further increased from 26.28 to 31.47 MPa.

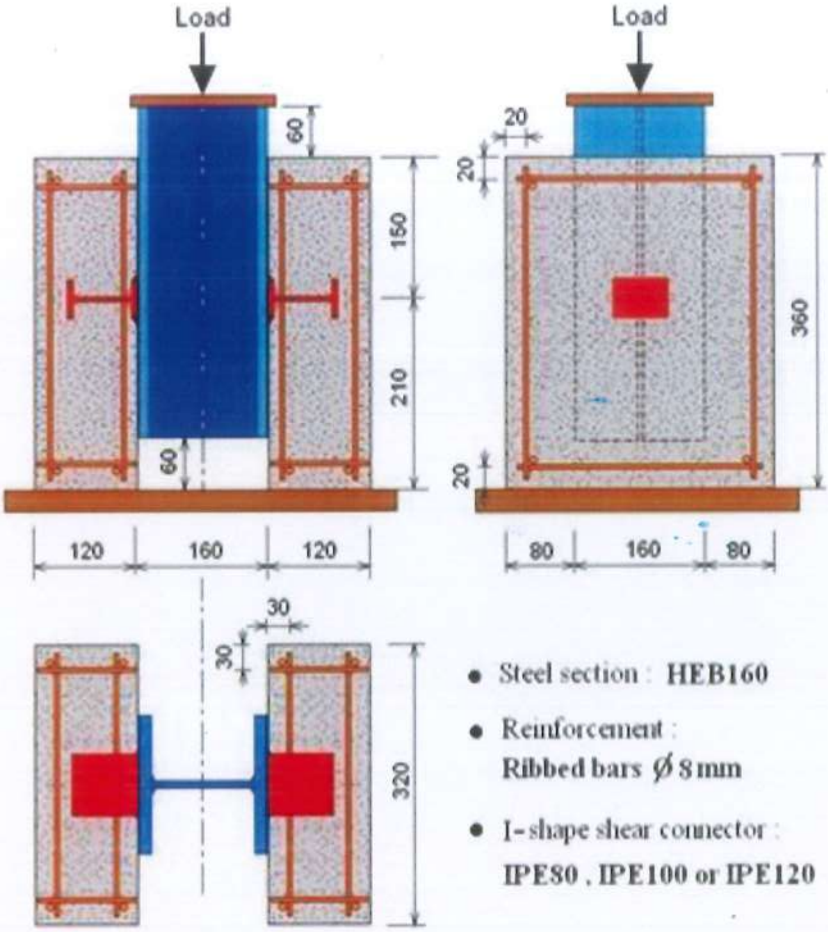

Figure 2.13 Push-Out Specimen with I-shape Connector (Dimensions in mm) [27].

In 2019, Joseph J. D.[11], tested shear behavior of precast concrete sandwich panels with truss shear connectors. The existence or absence of an EPS core, the thickness of the EPS core, the amount of open space between the two wythes, and the quantity of shear connector lines were the main test criteria taken into account in the experimental study as show in Table 2.3. All panels cast with small-scale 600×600mm used self-compacting concrete with an average compressive 45.97 MPa (Figure 2.14). The wythes were reinforced with steel wire meshes of 2.2 mm diameter with a grid size of 50×50 mm or 100×100 mm.

Table 2.3 Details of Specimens [11].

Sl. No	Dimension	Thickness of EPS Core	Total Thickness of Specimen	Number of Shear Connector Line
	(l x b)	(c)	(t)	(n)
	(mm x mm)	(mm)	(mm)	5
1	470 × 575	100	150	6
2	475 × 600			5
3	460 × 560	50	100	6
4	464 × 573			6
5	495 × 553	No EPS Core	150	5
6	475 × 546			5
7	460 × 585		100	4
8	460 × 560			4

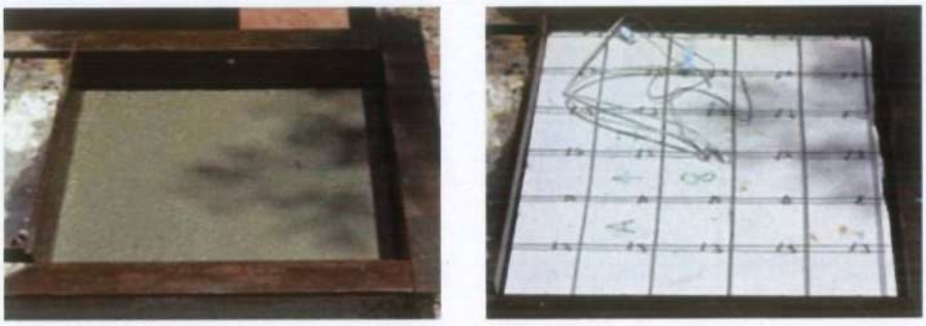

(a) Casting of Bottom Wythe

(b) EPS Core with Wire Meshes and Shear Connectors placed on Top of the Bottom Wythe Concrete

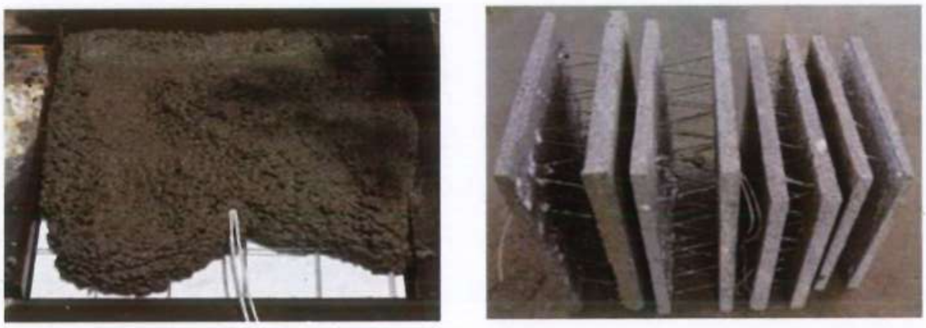

(c) Casting of Top Wythe

(d) Precast CSP Specimens without EPS Core

Figure 2.14 Casting Process Specimens without EPS- Core [11].

According to test results, shear sliding happened at the top or bottom wythe-to-EPS core interface for every specimen with an EPS core because of a loss of bonding activity. As would be clear from horizontal cracks along the loading direction at any depth of the EPS core, failure patterns of the specimens with the EPS core showed that the EPS core did not fail under shear while experiencing shear deformation. The failure patterns of the tested CSP specimens showed that buckling failure of the shear connectors under compression was the main cause of the failure of the CSP specimens with and without EPS core under push-off shear loading. The test findings showed that the shear strength rose when the EPS core's thickness decreased. Additionally, shear strength of the specimens without EPS core rose when the space between the wythes was reduced. When the EPS core was 50 mm thick, the average shear strength was 49% greater than when it was 100 mm thick. The shear strength rose by 30% with a 100 mm thick EPS core when the number of shear connector lines was increased by one. The specimen's shear strength increased by 16% when the number of shear connectors was raised by one with a 50mm thick EPS core.

2.4 High-Strength Self-Compacting Concrete (HSSCC)

Increased productivity, a more uniform and cohesive material with few or no honeycombs, better strength and durability characteristics, a good finish, adaptability in crowded reinforced sections, a reduction in the size of structural members, and more are some of the benefits of SCC over regular concrete. Self-compacting concrete SCC in one-way panels had better structural performance in terms of higher ultimate loads and lower deflections as compared to conventional concrete panels [29].

In 2015, Mohammed H.M.[29], presented an experimental investigation on the flexural behavior of reinforced concrete panels under bending load. Sixteen simply supported panels of dimensions 1000mm×450mm×50 or70mm were tested. Twelve spiecimens were constructed using self compacting concrete and four using conventional concrete. Four variables were adopted to investigate panels behavior: type of concrete, longitudinal steel ratio (ρ) (0.5, 0.33, 0.66, 1%), panel thickness and steel fiber ratio (Vf). All the components for self-compacting and conventional concrete mixes, as well as their properties, are shown in Table 2.4.

Table 2.4 Mix Proportions of Concrete [29].

Concrete Type	Conventional concrete	Self -compacting concrete		
Cement (kg/m^3)	400	400		
Sand (kg/m^3)	600	800		
Gravel (kg/m^3)	1200	770		
Limestone powder (kg/m^3)	-	170		
Water (kg/m^3)	200	190		
Superplasticizer (L/m^3)	-	8.1	9.2	10.8
Steel Fibers (kg/m^3)	-	0	31.4	62.8
Vf (%)	-	0	0.4	0.8
Slump flow (mm)		750	720	680
f'c (MPa)	27	29.7	31.1	32.9
fr (MPa)	3.91	4.41	6.32	7.02

The results showed, filling and passing abilities were decreased when steel fiber was added to self-compacting concrete up to 0.8%. Steel fiber, on the other hand, increased SCC's modulus of rupture and compressive strength by up to 60% and 10%, respectively. Compared to the longitudinal steel ratio (ρ) and steel fiber ratio (Vf), which increased the ultimate load of SCC panels by up to 64% and 75%, respectively, panel thickness was the most effective factor (up to 111%). The ultimate loads of nonfibrous SCC panels increased by roughly 63–111% when the thickness was increased from 50 to 70 mm. This is greater than the comparable ratios of 43–85% for fibrous SCC panels. Nonfibrous SCC panels performed better than fibrous ones when the longitudinal steel ratio (ρ) was increased from 0.5% to 1% and from 0.33% to 0.66% for slabs with thicknesses of 50 and 70 mm, respectively.The load-deflection curves for conventional concrete and SCC panels are stiffened by increasing panels thickness, longitudinal steel ratio (ρ), and steel fiber ratio (Vf), which results in fewer deflections at a given load. As thickness, ρ, or Vf increased, load-deflection curves showed increased toughness and ductile failure.While increasing panel thickness or steel fiber ratio (Vf) had little effect on the fracture patterns of the tested panels, increasing longitudinal steel ratio (ρ) increased the number of cracks and decreased their widths and spacing.

High-strength self-compacted concrete (HSSCC) is known to be a commonly used building material that has been developed to satisfy the engineer's demand for more workable concrete.

In 2020, Fares A.[30], examined the flexural behavior of rigid geogrid as a potential reinforcement in high strength self-compacted concrete panels. A34 concrete panels measuring 1100 × 450 × 50 mm and reinforced with two diameters (6 and 8 mm) were evaluated under three-piont loads.High strength self-compacted concrete had a compressive strength of MPa 64.5 with slump flow and t500 (660mm, 4sec), respectively. All proportions of the concrete mixture were shown in Table 2.5. In one, two, and three layers, three different rigid geogrid types-uniaxial, biaxial, and triaxial-were employed. High-density polyethylene was used to make the uniaxial kind. Polypropylene was used to make the biaxial and triaxial varieties (Figure 2.15).

Table 2.5 Concrete Mixture Proportions [30].

Cement (Kg/m^3)	Silica fume (Kg/m^3)	Fine aggregate (Kg/m^3)	Course aggregate (Kg/m^3)	Water (L)	Superplasticizer (L)
500	25	810	810	168	6.825

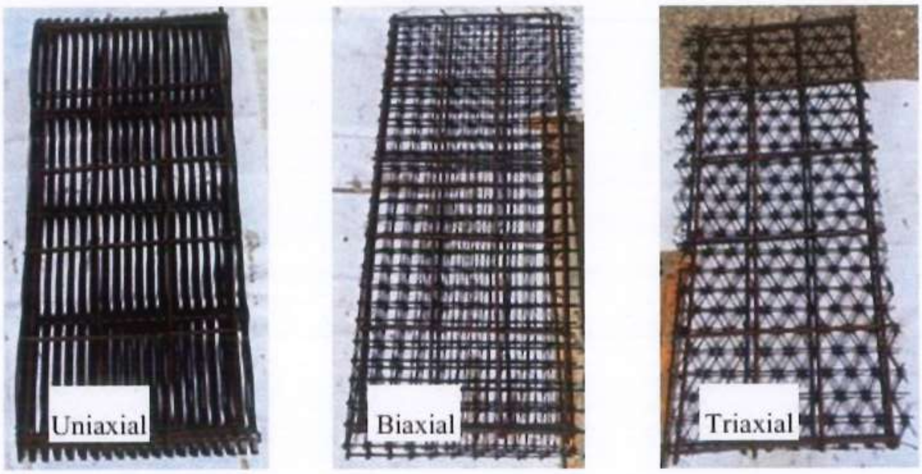

Figure 2.15 Types of Geogrid with Steel Reinforcement of Panels [30].

The findings demonstrated that adding geogrids to HSSCC concrete panels enhanced their ductility and had a positive impact on the panel' load-deflection behavior. For every HSSCC panel, flexural failure was the mode of failure. Two failure fractures were found at the ends of the aperture beneath the loading point in certain panels reinforced with uniaxial geogrids. Results were better when two geogrid layers were utilized as reinforcement for a simple concrete panels than when one or three geogrid layers were employed. Compared to uniaxial and triaxial geogrids, biaxial geogrids provide better results when utilized as reinforcement for concrete panels, especially when two layers of each kind were employed. The ultimate load of the HSSCC panels was increased by roughly 20% when three layers of two geogrid types (one uniaxial layer between two triaxial layers) were used instead of three triaxial geogrid only.

A thorough understanding of the mechanical properties of HSSCC is crucial since its manufacture calls for different ingredients and mix proportions than standard vibrating concrete (NVC).Numerous studies are trying to enhance HSSCC's overall performance due to its many benefits.

In 2023, Zende A.A.[17], investigated the characteristics of three mixes of high-strength self-compacting concrete (HSSCC) (M1, M2, and M3) in the split tensile strength and compressive strength of ranges of 70–79, 80–89, and 90–99 MPa. These mixes consist of cement, water, aggregate, and chemicals to regulate the slump of the concrete and mineral admixtures to enhance its strength. Ordinary Portland cement is used with fly ash (FA), silica fume (SF), and coarse aggregates (CA) of 10 mm. Ten mix trials with a water/cement ratio varying from 0.26 to 0.34 were used, as shown in Table 2.6. For the intended flowability and stability, a high powder content is needed. Slump flow between 650 and 800mm. Additionally, a high dosage of superplasticizers should be used, and the water-to-cement ratio should be minimized.All mixes were evaluated against the guidelines set by the specifications and guidelines for self-compacting concrete of the European Federation of Specialist Construction Chemicals and Concrete Systems(EFNARC).

Table 2.6 Proportions of Trial Mix [17].

Mix trial no.	W/C ratio	Cement (kg/m^3)	FA (%)	SF (%)	Sand (kg/m^3)	CA (kg/m^3)
MF1	0.34	430	10		950	800
MF2	0.32	430	20		850	800
MF3	0.32	430	30		870	770
MA1	0.32	480		10	900	800
MA2	0.30	480		20	890	860
MA3	0.28	480		30	755	995
MC1	0.30	480	5	5	890	860
MC2	0.28	480	10	10	755	960
MC3	0.28	480	15	15	755	995
MC4	0.26	480	20	20	780	945

After the tests, three mixes were selected that have a compressive strength within the limits required for the study. Their respective compressive strengths are 79.57 MPa for MC2, 86.93 MPa for MC4, and 94.36 MPa for MC3. All mixes achieved the slump flow from 650 to 800 mm. MF1 achieved 702 mm, which a 0.34 has a water ratio, and 650 mm for MA3.

The strength of HSSCC is influenced by the water-to-binder ratio as well as the type of binders. Compared to specimens without silica, the use of microsilica as a mineral admixture increased strength more quickly. The compressive strength of HSSCC with 30% silica fume (MA3) was 40% greater than that of SCC with fly ash (MF3). Split tensile strength was related to the compressive strength and depended on the type and particle size of aggregate, age of the concrete, and curing processes. The split tensile strength of SCC with silica fume mixtures was around 15% higher than that of SCC with FA. In comparison to SCC with FA alone, Mix MC3 achieves a 19.5% higher split tensile strength (Table 2.7).

Table 2.7 Results of HSSCC Mixes.

Mix trial no.	Compressive strength[a] (MPa)	Split tensile strength (MPa)	slump flow(mm)
MF1	45.87(1.63)	3.67	702
MF2	46(1.15)	3.80	699
MF3	50.31(1.78)	3.96	685
MA1	65.67(2.33)	4.11	684
MA2	71.25(2.4)	4.39	665
MA3	85.65(2.36)	4.67	650
MC1	84.43(2.7)	4.55	692
MC2	79.57(2.8)	4.32	680
MC3	94.36(1.1)	4.95	675
MC4	86.93(1.8)	4.39	670

Compressive strength[a] = Average of three tests with standard deviation

In 2024, Azare A.A.[19], examined the mechanical characteristics of high-strength self-compacting concrete (HSSCC) in order to determine the ideal proportions of cement substitutes, such as silica fume and fly ash. This study used ordinary Portland cement with a 2% superplasticizer of types G and F. The sand had a specific gravity of 2.62 and a particle size of 4.75 mm. A 20 mm sieve was used to filter the coarse material, which was natural gravel with a specific gravity of 2.6. Table 2.8 contains a list of all the materials utilized. With different replacement materials, including SF (0-15%) and FA (0-30%), with w/c 0.30 at the lower limit and 0.36 at the upper limit of SF and FA. All mixes were evaluated by EFNARC. In each mix, three 100 mm cubic specimens were used for the compressive strength test. Three cylinders measuring 100 × 200 mm were used to test the splitting tensile strength, and three prisms measuring 100 × 100 × 400 mm were utilized to test the modulus of rupture.

Table 2.8 Proportions of HSSCC [19].

Cement Kg/m^3	Sand kg/ m^3	Coarse Aggregate kg/m^3	W/C ratio	Superplasticizer %
530	900	1200	0.33	2

In general, the mechanical properties of the HSSCC mix improved when FA and SF were added at the ideal content. According to the average test results at 28 days, the highest strengths were achieved with cement replacement materials, where with 15% SF and 30% FA, a compressive strength of 78.5 MPa was achieved, and with 5%–10% SF and 20% FA, a maximum compressive strength of 86.5 MPa was achieved. Because of the silica fume's fine particle size and large surface area, the maximum splitting tensile strength of 3.4 MPa was achieved for 15% and 30% replacement of both SF and FA. The maximum flexural strength attained was 5.8 MPa at 15% and 30% SF and FA. By reducing excess calcium hydroxide and forming more calcium silicate hydrate at the right amount of pozzolans, interactions that increase the amount of binder are responsible for the strength of concrete.

2.5 The Performance of Concrete Structures with Expanded Metal Mesh

There was an increasing use of expanded metal in numerous concrete applications.

In 2017, Shaheen. I. [31], investigated the feasibility and effectiveness of reinforcing U-shaped slabs with expanded mesh, welded metal, and other non-metallic meshes. Ten panels measuring 500 x 100 x 2500 mm in total, with 40 mm thickness (Figure 2.16). Concrete mortar was used at 35 MPa. Expanded metal mesh size (16×31 mm), welded metal mesh size (12.5x12.5 mm), fiberglass mesh size (12.5x11.5mm), and polypropylene fibers 300-e3 with a dosage of 0.9 were used in concrete mixes to improve the concrete characteristics (Figure 2.18). All details of specimens are listed in Table 2.9. Figure 2.17 shows the U-shape reinforcement with meshes. All slabs tested under a two-point loads.

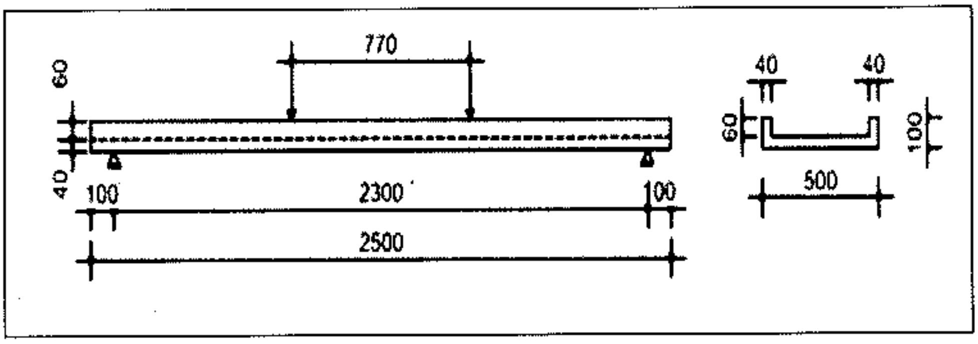

Figure 2.16 Dimension of U-Slab [31].

Table 2.9 Details of Experimental U-Shaped Slab [31].

Series	No. of Slab	Reinforcement			
		Tension steel bar, Ø10mm	Compression steel bar,Ø6 mm	No. of stirrups,Ø6mm	No. and Type of Mesh Layers Compression steel bar,,6 mm
A	1	4	2	15	–
	2	4	2	15	–
B	3	4	2	2	One layer of expanded mesh
	4	4	2	–	2 Layer
C	5	4	2	4	Two layer of welded mesh
	6	4	2	2	4 Layers
D	7	4	2	4	One layer of fiber glass mesh
	8	4	2	4	2 Layer
E	9	–	2	–	Two layer of expanded mesh
	10	6	2	–	1 Layer

Figure 2.17 Reinforcement in U-Slabs [31].

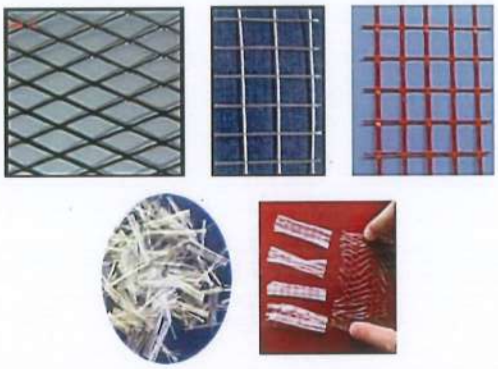

Figure 2.18 Types Fibers and Meshes [31].

All the tested slabs failed by flexure and crushing of the concrete. Using two layers of expanded mesh with compressive steel yielded the lowest ultimate load (16 kN), while the highest ultimate load was 25 kN with one layer of expanded mesh and reinforcement in both compressive and tensile regimes. High results in first crack load were achieved when using 4 layers of welded mesh and using one layer of expanded mesh with both compressive and tensile reinforcement. Reinforcing U-shaped slabs with two to four layers of welded mesh will increase the energy absorption. Reinforcing slabs with steel bars and welded steel mesh resulted in higher energy absorption than using steel bars alone. The addition of polypropylene fibers to the mortar results in an increase in energy absorption, increased stiffness, first crack load, and ultimate load. But it led to reduced deflection at the maximum load level and a decline in the ductility ratio. The ductility ratio and energy absorption are enhanced by using four steel bars with a single layer of expanded metal mesh.

In 2021, Erfan A.M. [32] investigated the flexural behaviour of reinforced beams strengthened by using layers of expanded, welded, and woven meshes. The experimental program included testing seven simply supported beams to the point of failure under a two-point load. Each specimen measures 150 mm by 250 mm by 2000 mm. Layers of steel meshes were used to reinforce six beams, as shown in Table 2.10. Self-compacted concrete with a compression strength of 30 MPa. Welded wire mesh with an opening of 10 x 10 mm and a diameter of 0.7. The expanded wire mesh was 31 x 16.5 mm in size and 1.25 mm in thickness. Woven wire mesh size of 4x4 mm with a thickness of 2 mm. As reinforcement in all beams, 2Ø12 steel on the bottom, 2Ø10 on the top, and 10 Ø 10/m for stirrups.

Table 2.10 Specimens Descriptions and Notations [32].

Group	**Specimen ID.**	**Description of specimens**	**Reinforcement**	
			tension	**Comp.**
Control	B01	Control specimen	2 ϕ12	2 ϕ10
A	B02	One layer welded wire mesh	2 ϕ12	2 ϕ10
	B03	Two layer welded wire mesh	2 ϕ12	2 ϕ10
B	B04	One layer expanded wire mesh	2 ϕ12	2 ϕ10
	B05	Two layer expanded wire mesh	2 ϕ12	2 ϕ10
C	B06	One layer woven wire mesh	2 ϕ12	2 ϕ10
	B07	Two layer woven wire mesh	2 ϕ12	2 ϕ10

For the control specimen, the ultimate failure load was 64.0 kN with a deflection of 47.0 mm. The failure loads were 68.5 kN and 85.6 kN for the beam with one and two layers of welded wire mesh, respectively, with deflections of 32.0 mm and 20.4 mm, which decreased, and the failure load increased due to the high tensile strength of the steel layers. When using one and two layers of expanded wire mesh, the recorded failure loads were 64.31 kN and 71.0 kN, respectively, with deflections of 30.0 mm and 22.3 mm, respectively. With woven wire mesh, there were 78.5 kN and 89.0 kN in experimental failure loads versus 24.4 mm and 20.3 mm in deflection for one and two layers, respectively. Woven wire mesh shows the most ratios in failure load capacity and deflection, at 22.6% and 39.1% in carrying load capacity and 48.1% and 57.1% in deflections with respect to the control specimen. The failure mode was flexural failure for all beams. A slightly greater ultimate load and lower deflection caused by an increase in the volume of steel reinforcement. There is an enhancement in ductility in beams using one and two layers of mesh; with welded mesh, the ductility varied between 44.5% and 48.4% , respectively, while with expanded mesh, the ductility varied between 47.3% and 48.30%, and woven mesh, the values were 36.4% and 52.0% respectively.

In 2025, El-Dehemy H.[33], investigated expanded metal meshes as a unique type of internal shear reinforcement in order to improve the structural performance of reinforced concrete (RC) beams with numerous web apertures. Eleven full-scale beams were subjected to three-point loading tests (Figure 2.20). Each beam was 1500 mm long, 200 mm deep, and 80 mm wide. Each beam was 1500 mm long, 200 mm deep, and 80 mm wide. To prevent premature failure, welded wire mesh (750 x 180 mm) was employed as shear reinforcement on the left (solid) side of each beam. Instead of employing traditional stirrups, expanded mesh (730 x 180 mm) were used to support the right side, which has web openings (Figure 2.19).

Three square apertures (60 x 60 mm) and three circular web openings (60 mm in diameter and 160 mm apart). One layer of welded mesh and one, two, and three layers of expanded metal mesh were applied to each beam. Two post-cages with four Ø2.5mm vertical bars and Ø2.5mm stirrups spaced 41mm apart. The 40 MPa tested beams were cast using self-compacting concrete (SCC).

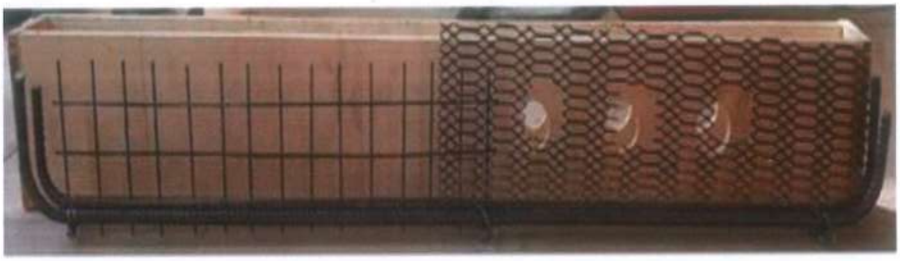

Figure 2.19 Reinforced Concrete Beam with Expanded Mesh [33].

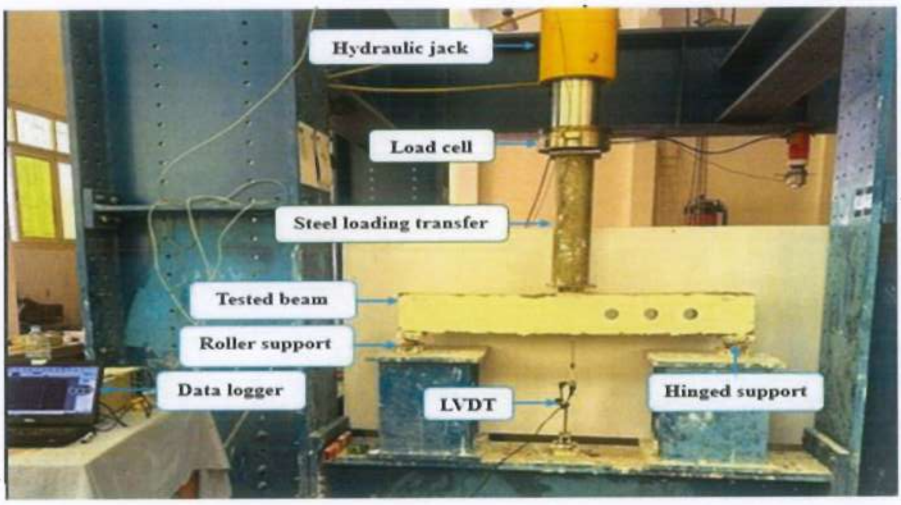

Figure 2.20 Test Set-Up of Reinforced Concrete Beam with Openings [33].

The results showed, all of the specimens failed under shear, exhibiting diagonal cracks that stretched from the support to the load application point. The results indicate that increasing the number of expanded meshes around circular openings enhances shear crack load by delaying the onset of cracking. Using an expanded mesh as a shear reinforcement inside the beams did not affect the shear crack angle where all beams with openings showed angles between 30° and 35°.When compared to solid beams, adding many web openings decreased shear strength and energy absorption by roughly 50% and 80%, respectively. Shear resistance, ductility, and energy absorption were all enhanced by adding more expanded mesh layers. At an opening ratio of 0.18, beams with three expanded mesh layers exceeded unreinforced beams by up to 71% (circular) and 100% (square). Due to lower stress concentrations, round apertures regularly performed better than square ones, attaining up to 32% higher ultimate loads and greater energy absorption.

When openings are closely spaced or there is a strong shear demand, post-cage strengthening is recommended to boost load capacity by about 45%.

2.6 Summery

Several studies were conducted in terms of experimental application to examine the behavior of precast composite concrete panels, shear connectors, self-compacting concrete, properties of high-strength self-compacting concrete, and characteristics of expanded metal mesh in concrete structural, it was conceivable to set the subsequent points from previous investigations:

1. The type of shear connections, the volume of steel reinforcement, the thickness of concrete face wythes, the grade of concrete in concrete face wythes, the distribution of shear connectors, and the rigidity of core material are some of the parameters that affect the composite structural behavior.
2. The overall behavior of the precast concrete sandwich panel is dependent on the behavior of the connections, so the bond is always a concern. Several techniques have been proposed to determine the type of shear connector that is effective to achieve composite activity of the panels.
3. Any created shear connector is required to understand how it behaves; therefore, experimental tests are needed to provide data by using fully or partially scaled slabs with varying supports or only simply supported beams.
4. The concrete wythes have a thin thickness; with self-compacting concrete, there are no problems in casting, like flowing to reach the narrow sides and achieving full compaction.
5. The panel's load resistance depended partially on the structure's concrete layers. In order to obtain high-strength concrete greater than 60 MPa, the highest doses of superplasticizer and silica fume are required within the recommended limits for the type used.
6. Expanded mesh has been the subject of numerous studies aimed at reinforcing structures and has been utilized as a shear connector in certain investigations.
7. The bond strength between concrete layers plays a significant role in achieving the composite behavior.

Therefore, the following are the identified research gaps that this study will attempt to fill:

1-The effectiveness of self-compacting concrete characteristics as high compressive strength structural layers with expanded mesh shear connectors.

2-The performance, stiffness, ductility, and load capacity of high strength self-compacting composite beams with expanded shear connectors and the influence of old and new concrete layers on the behavior.

3-The overall structural performance of EPS-insulated high-strength self-compacting concrete panels equipped with expanded mesh connectors as a composite system, as well as the impact of both new and old concrete layers.

CHAPTER THREE: EXPERIMENTAL WORK

3.1 Introduction

The experimental methodology employed for this study is outlined in this chapter. It displays the properties and specifications of the materials used, phases of the three experimental programs, details of specimens for each stage, casting steps, method of curing, and instruments and devices for examination methods.

3.2 Materials Properties

The materials utilized in the testing program are described in general terms and according to their specifications.

3.2.1 Cement

Ordinary Portland cement (type II) was utilized for casting all specimens in this study. The Technical Institute of Amara's laboratory is where the tests are conducted. As stated by the Iraqi standard No. 5/2019 [34] with ASTM C150-07 [35], the physical and chemical characteristics of the cement are shown in Tables 3.1 and 3.2, respectively.

Table 3.1 Physical Properties for Cement.

Property	Result from test	Limit of IQS NO.5/2019	ASTM C150-07
Fineness using Blaine air permeability apparatus (m^2/kg)	311	≥230	260min 430max
Vicat's instruments for setting time:			
Initial time (hrs:min)	111	≥45 min	> 45
Final time (hrs:min)	5:10	≤10 hrs	> 375
Compressive strength at:			
3 days (MPa)	20	>15	> 10
7 days (MPa)	26.24	>23	> 16

Table 3.2 Chemical Composition for Cement.

Chemical components	Chemical symbol	Percentage by weight %	Limit of IQS NO.5/2019	ASTM C150-07
Lime	CaO	62.8	-	Not applicable
Silica	SiO2	19.8	-	Not applicable
Alumina	Al2O3	4.34	-	6 max
Iron Oxide	Fe2O3	4.8	-	6 max
Magnesia	MgO	2.93	≤ 5	6 max
Sulfate	SO3	1.9	≤ 2.8	
Loss on Ignition	L.O.I	1.5	≤ 4	3 max
Non soluble substances	I.R	0.76	≤ 1.5	0.75 max
Lime Saturation Factor	L.S.F	0.963	0.66 to 1.020	

Aluminum oxide to ferric oxide ratio more than 0.64 (main compounds (Bogue's equation) percentage by weight of cement)

Tricalcium silicat (C3S)	63.73
Dicalcium silicate (C2S)	8.69
Tricalcium aluminate (C3A)	3.37
Tetracalcium aluminoferrite (C4AF)	14.6

3.2.2 Fine Aggregate (Sand)

Natural sand has been a part of every concrete mixture. 4.75 mm is the maximum grain size, and the modulus of fineness is 2.71. The laboratory tests on sand were conducted in compliance with Iraqi regulations No.45/1984 [36] and ASTM C33a-08 [37]. The outcomes for the test are presented in Table 3.3.

Table 3.3 Fine Aggregate Grading.

N0.	Sieve size (mm)	Passing by weigh(%)			
		Test results	Retained Weight %	Zone 2 IQS No. - 45/1984 Limits	ASTM C33-08
1	10	100	-	100	100
2	4.75	98	2	90-100	95-100
3	2.36	88	12	75-100	80-100
4	1.18	72	28	55-90	50-85
5	0.60	46	54	35-59	25-60
6	0.30	17	83	8-30	5-30
7	0.15	8	92	0-10	0-10
Fineness Modulus of Sand MF			2.71		

3.2.3 Coarse Aggregate (Gravel)

In compliance with ASTM C33-08 [37] and Iraqi standard No. 45/1984[36], dry and cleaned aggregate with a maximum size of 10 mm is utilized. Tables 3.4 provide the aggregate grading in Figure 3.1.

Figure 3.1 Coarse Aggregate.

Table 3.4 Grading for Coarse Aggregate.

N0.	Sieve size (mm)	Passing (%)		
		Test results	Limits of IQS No. -45/1984	ASTM C33-08
1	20	100	100	100
2	10	95.4	90-100	85-100
3	4.75	16	10-30	10-30
4	2.36	1.8	0-10	0-5
5	PAN	0	0	0

3.2.4 Water of Mixing

Every specimen was cast using water as reverse osmosis (R.O.) treatment.

3.2.5 Silica Fume

In Portland cement systems, silica fume is employed to improve mechanical and lasting qualities (Figure 3.2). 10% silica fume has been used in place of some cement in concrete. According to ASTM C 1240-04 [38, 39], this kind of silica was used in the current study. Tables 3.5 and 3.6, with Table 3.7, display the typical properties of silica fume.

Figure 3.2 Silica Fume.

Table 3.5 Silica Fume Technical Description.

NO.	Property	Value
1	Colour of powder	Grey to medium grey
2	Specific of gravity	2.10-2.40
3	Bulk density	500 to 700 kg/m^3

Table 3.6 Chemical Requirements of Silica Fume.

NO.	Property	Value
1	SiO2, min, %	85%
2	Moisture content (Max)	3%
3	Loss on ignition (Max)	6%

Table 3.7 Physical Requirements of Silica Fume.

NO.	Property	Value
1	Specific Surface Area	Minimum (15m^2/g)
2	Pozzolanic Activity Index at 7 days	Maximum (105% of control)
3	Retained on a 45 micron sieve are particles of excess size.	Maximum (10%)

3.2.6 Superplasticizer

To better concrete's performance and high compressive strength, 2% super-plasticizer of type ViscoCrete®-171 Precast (3rd Generation) was used to reduce the percentage of water content for concrete mixtures. This particular kind of plasticizer complies with ASTM C494 class C [40, 41]. Table3.8 shows all technical descriptions of the superplasticizer used.

Table 3.8 Superplasticizer Technical Descriptions.

NO	Property	Value
1	Appearance and colour	Brownish liquid
2	Specific gravity	1.080 ± (0.02) g/cm^3
3	Recommended dosage	(0.5 % - 2 %) by weight of total cementitious materials.

3.2.7 Reinforcement with Steel Bars

For this study, steel bars of grade 60 were utilized. The steel bar used in beams and panels had a diameter of Ø10 mm. The bottom layers of the slabs were reinforced with the same dimension in both directions. The yield stress (fy) and ultimate stress (fu) of three 45 cm long samples were determined by routine tension testing. Table 3.9 displays the test results, which complied with ASTM (A615/A615-12) [42] (Figure 3.3).

Table 3.9 Steel Bar Reinforcement Properties.

NO.bar	Nominal (mm)	Measured (mm)	Yielding stress f_y(MPa)	Ultimate strength f_u(MPa)	Elongation %
1	10	9.7	467.5	583.7	21.6
2	10	9.7	463.17	578.5	20.8
3	10	9.7	462.3	577.6	21.2
Avg.	10	9.7	464.3	579.9	21.2

Figure 3.3 Reinforcement Test Bars' Tensile Strength.

3.2.8 Wire Mesh

Welded-wire mesh with square openings made of stainless steel was used in reinforcing both concrete layers. Compared to other mesh types, square welded-wire meshes are more structurally rigid because of their greater modulus, which causes smaller crack widths in the load-deformation curve's initial region [43]. According to ASTM (A1064/A1064M) [44], the test piece was machined into a suitable shape for the grips of the test machine to ensure that the test piece is held in such a way that the force is applied as axially as possible-the welded joint is located at the center of the wire being tested. Total length 280mm, cross wire extended 25mm inside grips Figure 3.4. The properties of the wire mesh and test results are given in Table 3.10.

Figure 3.4 Wire Mesh Testing.

Table 3.10 Properties for Wire Mesh.

Wire mesh type	Properties					
Square mesh	Diameter (mm)	Opening size of mesh (mm)	Sheet dimension (LXB)(mm)	Yield strength (MPa)	Ultimate tensile strength (MPa)	Elongation %
	5	100x100	2000x2000	343	491	12.6

3.2.9 Expanded Metal Mesh

Sheet perforation expanded metal (standard type) with an overlapped diamond-shaped mesh pattern was used in this study, as shown in Figure 3.5. By utilizing the volume fraction, effective modulus for steel meshes in the loading direction (transverse direction), and minimum values of the yield strength with stress-strain curves, direct tensile testing on expanded mesh samples that are 360 mm in length and 150 mm in breadth can yield the ultimate tensile strength. The test specimens had extra reinforcement for grip at their ends, according to ACI 549.1R [43]. The properties of the selected expanded metal are given in Table 3.11.

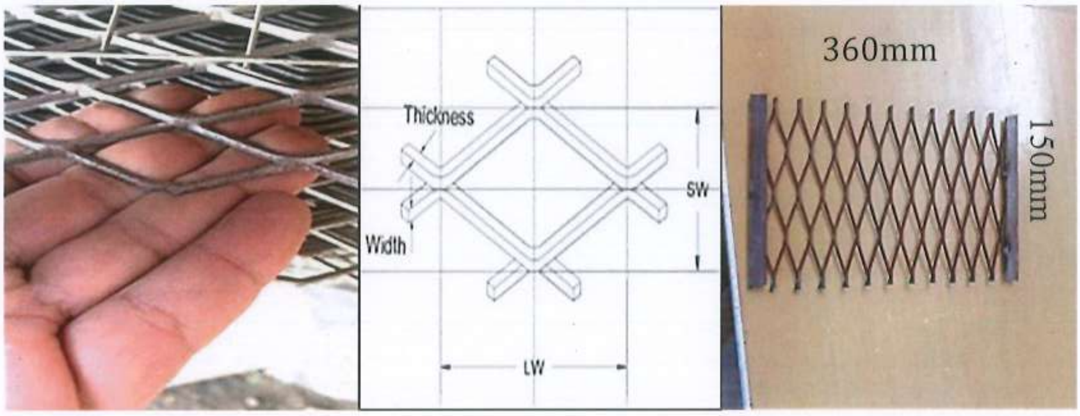

Figure 3.5 Expanded Metal Mesh.

Table 3.11 Properties of Expanded Metal.

Type	SW (mm)	LW (mm)	Width (mm)	Thickness (mm)	Weight (Kg\m^2)	Size (mm)
Standard	22	50.8	3	3	5.75	1000x2000
Yield strength (MPa)		Ultimate tensile strength (MPa)			Elongation %	
310		420			34.9	

3.2.10 Steel Angle

Metal angles, also known as angle iron, are a type of steel product that is used in a variety of applications. The dimensions are (20x20x2mm) and it is up to 6 meters long. According to ASTM A36, yield strength is 248MPa and ultimate tensile strength is 400MPa.

3.2.11 Expanded Polystyrene (EPS)

The insulation material is commonly either extruded polystyrene or expanded polystyrene. The insulation of the panel specimens in this study consisted of an expanded polystyrene panel with a density of 20 kg/m³ (Figure 3.6) [45]. Insulation sheets were laid between concrete layers as one of the components of the composite system. Technical specifications are given in Table 3.12.

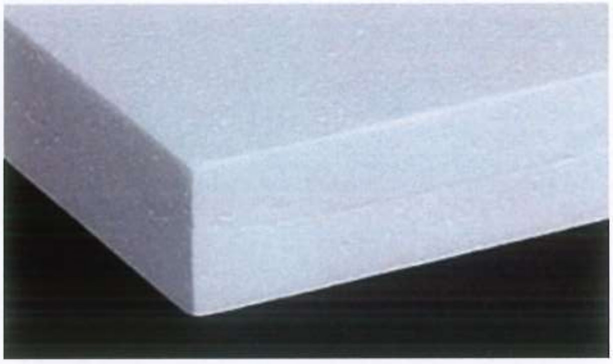

Figure 3.6 Expanded Polystyrene EPS.

Table 3.12 Properties for Insulation Material.

Type	Size (mm)	Thickness (mm)	Bulk Density (Kg/m^3)	Compressive strength at 10% deformation, in kg/cm^2, Min.	Water vapour Permeance in g/m^2, 24 h, Max.
Expanded Polystyrene EPS	1000x2000	50	20	13-18	3.0

3.2.12 Flat Bar

A flat steel bar was used in the shear connector with an I-shape to hold the lengths to the required shape, and the model was checked according to the ASTM A 370 specification [46], as shown in Figures 3.7 and 3.8. Product specifications and dimensions with the results from the test are presented in Table 3.13.

Table 3.13 Properties of Flat Bar.

Type	Thickness T(mm)	Gauge length G (mm)	Colour	Length (mm)	Yield strength (MPa)		Ultimate tensile strength (MPa)
Mild steel	2	200	Grey	6000	322		519
L (mm)		A (mm)	B (mm)	C (mm)	R (mm)	W (mm)	Elongation%
395		225	75	40	10	20	24.9

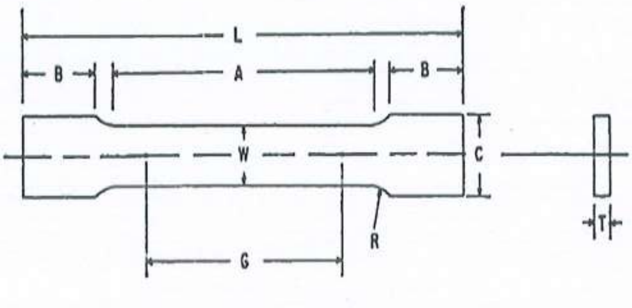

Figure 3.7 Dimensions of Test Specimens [46].

Figure 3.8 Flat Bar Tension Test Specimens.

3.3 Experimental Program

The experimental investigation consists of three levels for each step's specifics and work procedures. The outcomes of the first stage are reported in this chapter, while the final results of the other two phases are presented in the following chapter.

3.4 Phase

The first phase aims to study the fresh and hardened characteristics of a high-strength self-compacting concrete mix that provides advantages in strength, workability, and effective bonding with reinforcing bars.

3.4.1 Concrete Mix

The first step is choosing the required target of concrete. The maximum sizes of aggregate are subsequently taken into consideration while determining the water-to-cement ratio. All specimens for the study were casted by using self-compacting concrete with high-strength cube compressive strength f_{cu}=70 MPa following IS 10262-2019 [47]. Several tries have been made to identify the ideal dosage of superplasticizer and silica fume. The aggregate's size was 10 mm. Based on the results from experimental attempts, the water ratio has been reduced to 24.5% (Appendix A). Table 3.14 shows the weight mixing ratios of the materials used. The mixtures were combined using a 40 L mixer. After adding silica to the cement, it was mixed for two minutes. Dry sand was gradually placed over cementitious material for mixing for about 3 minutes. An equal amount of water and superplasticizer-171 were combined and added to the admixture, followed by adding the remaining water and superplasticizer with the maximum speed of the mixer. The gravel was added to the mixture and left to homogenize for 3 minutes, then the cubes, cylinders, and prisms were poured. The compressive strength of concrete is tested at 56 days because superplasticizers and silica accelerate and enhance the chemical reactions and improve the filling, resulting in a significant increase in strength after 28 days. Therefore, long-term tests demonstrate the true strength of HSSCC and are essential to ensure the achievement of final specifications and target strength in projects, especially with silica, which reduces its permeability and whose reactions last longer compared to ordinary concrete.

Table 3.14 Material quantities of Concrete Mix.

Cement (kg/m^3)	Sand (kg/m^3)	Gravel (kg/m^3)	Water (L)	Silica fume (kg/m^3)	Superplasticizer (L)
802.14	726.9	851.3	219.48	89.12	17.8

3.4.2 Characteristics of Fresh High- Strength SCC

One of the best points of interest in utilizing silica fume in SCC is its small size, which makes self-compaction possible. Because the majority of the aggregate utilized is similar to or less than 10 mm, the fine spherical granules of silica fume fill the gaps between the cement blocks of Portland cement, filling the sand spaces between the granules of aggregate, leading to a smaller volume of gaps. Increasing the volume of the excess paste provides a coating of paste for each aggregate particle and renders workability to the concrete mix [17]. The fresh form features of high-strength SCC were examined in order to confirm filling, passage, and segregation resistance standards. When there are no obstacles present, the horizontal free flow of SCC is assessed using the slump flow. The method of testing is very similar to the test method of determining concrete slump. The distinction is that the diameter of the spread concrete is measured in two perpendicular directions and recorded as slump flow rather than the height loss. The time it takes for the concrete to reach a 500 mm diameter is likewise measured and recorded as t500 during the slump flow test BS EN 12350-8:2010 [48]. The concrete's capacity to pass the J-ring test is ascertained when the height differential between the concrete inside and immediately outside the ring is measured using ring equipment by BS EN 12350-12:2010 [49]. When assessing the viscosity or flowability of concrete, the V-funnel test is utilized. About 0.012 m^3 of concrete are poured into the funnel, and the amount of time it takes for the concrete to pass through the device is timed. It would take little time for good, stable, and flowable concrete to flow out (BS EN 12350-9:2010) [50]. The measured fresh properties are presented in Table 3.15. All tests for fresh high strength self-compacting concrete are as shown in Figure 3.9.

Table 3.15 Fresh High-Strength SCC Properties.

Character	Slump flow (mm)		V-funnel	J-ring step height (mm)
	D	t500		
Limits	(760-850)mm	(2-5)sec	(10-22)sec	≥10
Result	770	4	18	8

(a) J-ring test (b) Slump flow test

(c) V-funnel test

Figure 3.9 Test of Fresh High-Strength SCC

3.4.3 Characteristics of Hardened SCC

Mechanical properties are essential for preliminary design purposes. Silica fume with superplasticizer has a great impact on the strength of the concrete produced, especially water-reducing admixtures and high compressive strength at an early age. Concrete with SF could improve other mechanical properties, such as flexural strength and modulus of elasticity. Tests for compressive, flexural, and splitting tensile strength were used to examine HSSCC in the hardened state. Compressive strength was determined according to BS EN 12390-3:2019 [51], flexural strength according to ASTM C78 [52], splitting tensile strength, and elastic modulus according to ASTM C496 [53].

3.4.3.1 Cube Compressive Strength (fcu)

Cubical specimens of 150×150×150 mm were used to test the compressive strength of concrete, as shown in Figure 3.10. The goal values for the required strength were the 3rd, 7th, 28th, and 56th days. The results are shown in Table 3.16.

Table 3.16 Results of Compressive Strength Test.

No.	fcu (3day) MPa	fcu (7day) MPa	fcu (28 day) MPa	fcu (56day) MPa
1	53.6	60.3	74.7	76.7
2	54.7	59.4	68.3	74.13
3	46.5	49.7	73.6	81.6
Avg.	51.6	56.46	72.2	77.47

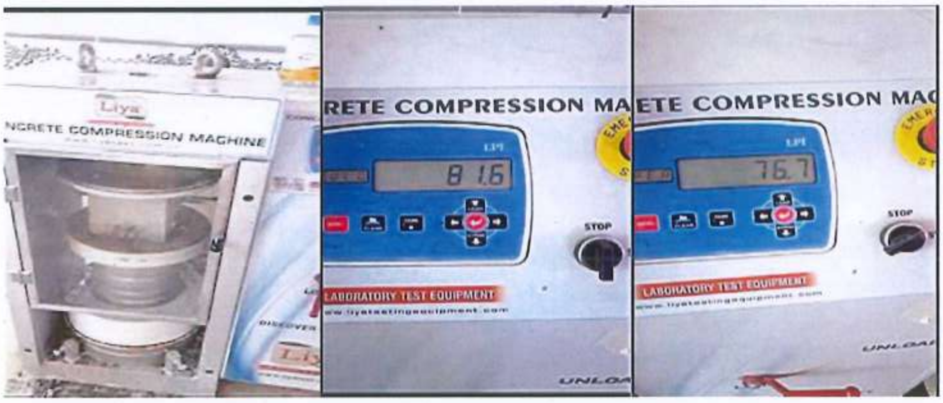

Figure 3.10 Compressive Test of Concrete Cube.

3.4.3.2 Splitting Tensile Strength (f_t)

A total of six cylinders (150×300 mm) were tested as shown in Figure 3.11. The test result is shown in Table 3.17 and used to calculate ft by the following formula:

$$f_t = \frac{2P}{\pi DL} \tag{3.1}$$

Where:

f_t: Splitting tensile strength (MPa)

P: Maximum applied load (N)

D: Diameter of specimen (mm)

L: Length of the specimen (mm)

Table 3.17 Results for Splitting Tensile Strength Test.

NO.	Maximum applied load (N)		f_t (MPa)	
	7day	28day	7day	28day
1	404.9	513.3	5.73	7.26
2	379.3	514.75	5.36	7.28
3	388.5	511.3	5.49	7.23
Avg.	390.9	513.1	5.52	7.25

Figure 3.11 Split Tensile Strength Test of Concrete.

3.4.3.3 Flexural strength (f_r)

The calculation of the modulus of rupture was performed using six prisms with dimensions of 100 x 100 x 500 mm, as shown in Figure 3.12. The modulus of rupture and the data are displayed in Table 3.18 are computed using the expression provided below:

$$f_r = \frac{3PL}{bd^2} \qquad 3.2$$

Where :

f_r: Modulus of rupture (MPa)

b: Average width of specimen (mm)

P: Maximum applied load (N)

L: Span length (mm)

d : Average depth of specimen (mm)

Table 3.18 Results for Flexural Strength Test.

NO.	Maximum applied load (N)		f_r (MPa)	
	7day	28day	7day	28day
1	7.78	9.02	11.67	13.53
2	7.50	9.99	11.25	14.98
3	8.37	9.60	12.55	14.4
Avg.	7.88	9.53	11.82	14.3

Figure 3.12 Flexural Strength Test of Prisms.

3.5 Phase II

The ultimate strength capacity in a reinforced concrete beam under a two-point load with four types of shear connectors of expanded mesh was the primary goal of the current phase.

3.5.1 Beam Details

All beams were designed as one-layer-reinforcement solid sections according to ACI 318-14 [54] (Appendix B), with specimen details as follows:

1. The total length for all beams was 1200 mm, the width was 200 mm, and the total depth was 200 mm. Also, each beam has the same compressive strength of 70 MPa and the same bottom reinforcement of 2Ø10 mm without stirrups (Figure 3.13, 3.14, 3.15, 3.16, and 3.17). Overall details of the beams are shown in Table 3.19.
2. Four types of continuous connectors run the full length of the beam. The most commonly used sections in steel structures are rectangular sections (Figure 3.19), I-sections (Figure 3.21), and Z-sections (Figure3.23).The dimensions were designed according to ANSI /AISC, 2005 [55]. Also, expanded mesh was experimented with as two-line trusses in one direction (Figure3.25).
3. Because of the impossibility of nailing, screwing, or welding, each section of shear connectors was made by cutting expanded sheet with an electric cutter to the dimensions shown in the details of Figure 3.18, 3.20, 3.22, and Figure 3.24. To form the required structural element, each meeting edge was connected with another by stick welding, and then a steel angle from the top and inside was welded along the connector.
4. All shear connectors are oriented in such a way that the strong axis of the cross-section is perpendicular to the loading plane; therefore, the diagonal side of the Z-section is placed vertically.
5. Because there are no stirrups in beams, shear connectors were related by welding over the reinforcement steel using a cross-section steel Ø10 mm with a length of 100 mm to fix the shear connector over the rebar and also prevent movement.
6. The truss connector was welded directly on the rebar, and an angle steel was added in the middle as vertical stiffeners.

7. In the symbolization of the specimens in the table, the first letter indicates the group, the next letter represents the type of shear connector, and the last digits define the numbers of the beam specimens (Figure 3.26).

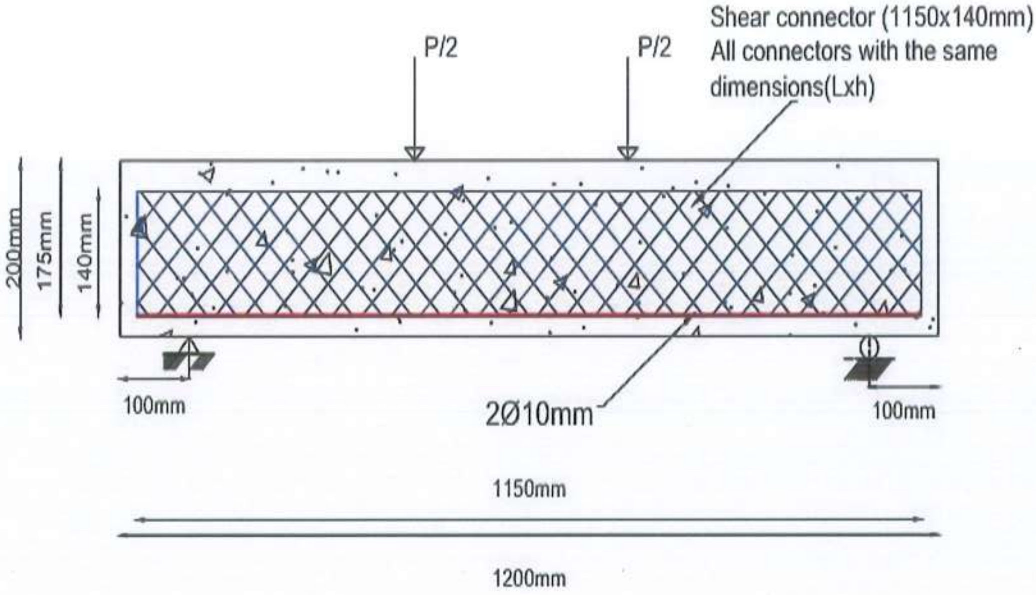

Figure 3.13 Beam Details.

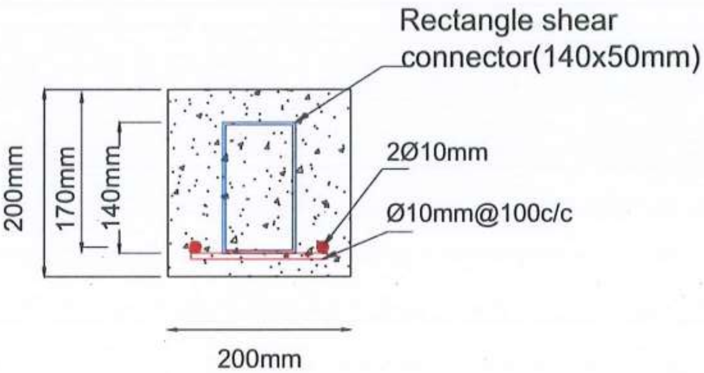

Figure 3.14 Cross-Section for Beam with Rectangle Shear Connector.

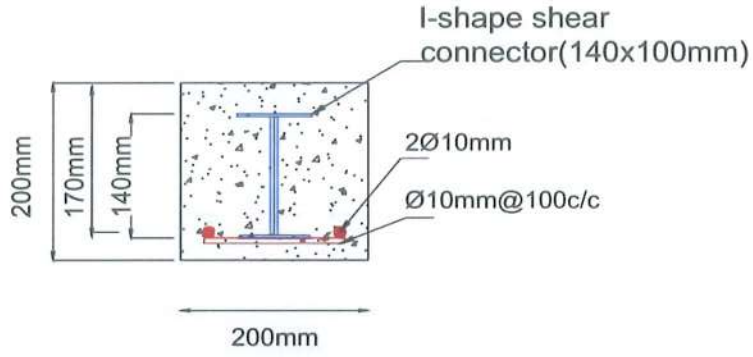

Figure 3.15 Cross-Section for Beam with I-Shape Shear Connector.

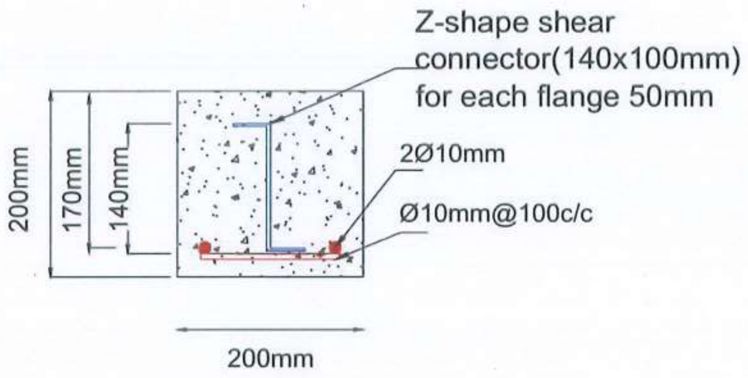

Figure 3.16 Cross-Section for Beam with Z-Shape Shear Connector.

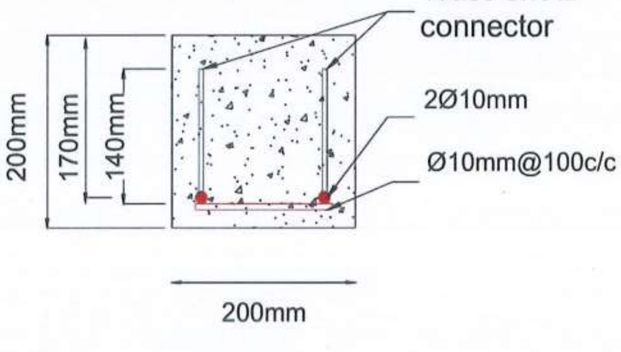

Figure 3.17 Cross-Section for Beams with Truss Shear Connectors.

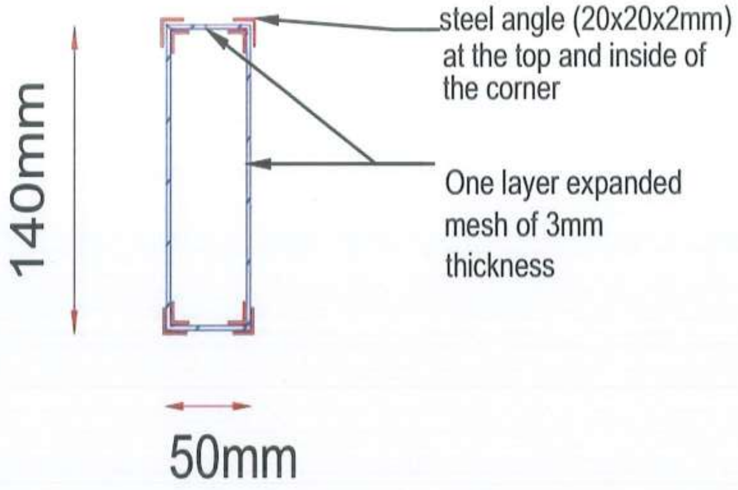

Figure 3.18 Rectangle Shear Connector Details.

Figure 3.19 Rectangle Shape Shear Connector.

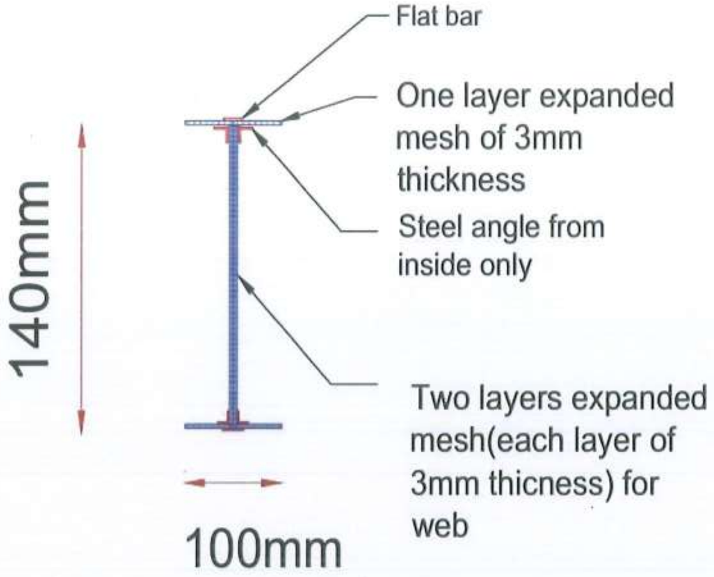

Figure 3.20 I-Shape Shear Connector Details.

Figure 3.21 I- Shape Shear Connector.

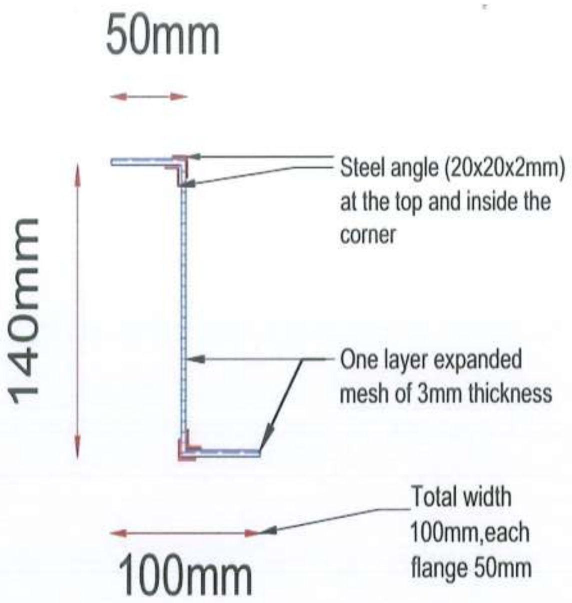

Figure 3.22 Z- Shape Shear Connector Details.

Figure 3.23 Z-Shape Shear Connector

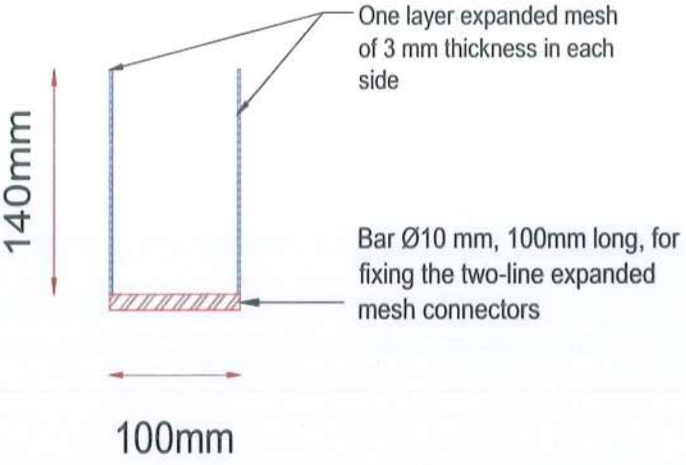

Figure 3.24 Truss-Shape Shear Connector Details.

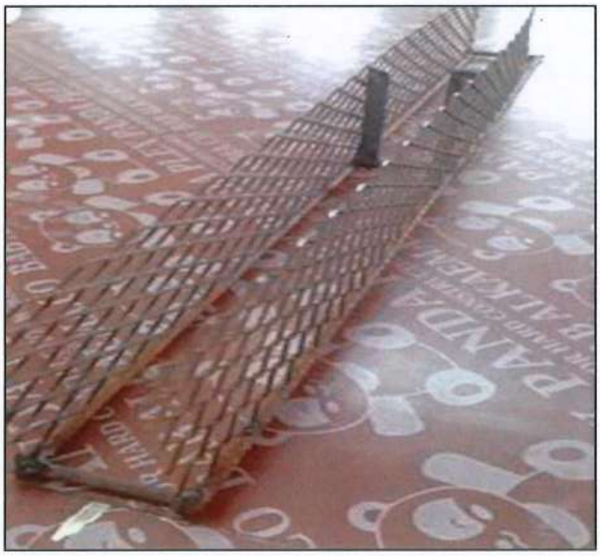

Figure 3.25 Truss-Shape Shear Connector.

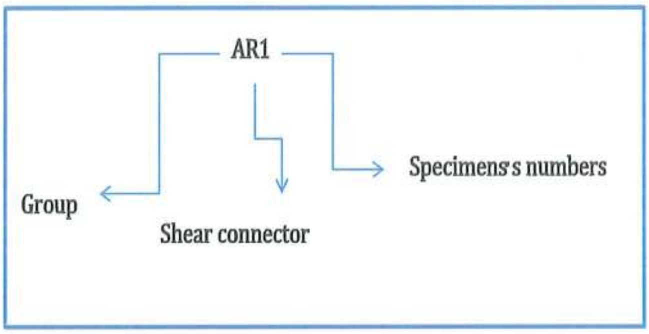

Figure 3.26 Symbols of Beam Specimens.

Table 3.19 Details of Beams With Shear Connectors.

Specimens	Casting	Type of shear connectors	Tension steel bars	Dimension (mm)	Additional steel area (mm^2)		Finding
					Flat bar (bxt)	Steel angle tx(2b-t)	
AR1,AR2 , AR3	One stage	Rectangular	2Ø10	1200x200x200	-	608	All groups A: 1. Average ultimate load 2. Stiffness, ductility 3. Failure mode
BR1, BR2, BR3	Two stages						
AI1, AI2, AI3	One stage	I-shape	2Ø10	1200x200x200	160	304	
BI1, BI2, BI3	Two stages						
AZ1, AZ2, AZ3	One stage	Z-shape	2Ø10	1200x200x200	-	304	All groups B: 1. Average ultimate load 2. Stiffness, ductility 3. Failure mode 4. Influence of concrete interface
BZ1, BZ2, BZ3	Two stages						
AT1, AT2 , AT3	One stage	Truss- shape	2Ø10	1200x200x200	-	-	
BT1, BT2, BT3	Two stages						

3.5.2 Casting Procedure of Beam Specimens

All of the concrete beams were casted using wooden formwork. Before beginning the mixing process, all of the ingredients were weighed and prepared. Shear connectors with bars were placed inside the molds, and plastic spacers were used to maintain the cover of concrete and to keep the right position of reinforcement during the casting of concrete. Mixing quantities was done by a truck concrete mixer. 12 beams were designated as an A team, which were completely cast and served as reference models. In contrast, 12 further specimens were cast to a thickness of 50 mm, and a day later, they were completely casted. As a collective, they were a B team. The previous method of treating the concrete layer was simply wetting the surface with water without adhesives being used. The casting procedure was done without compaction for all specimens. After a day, the prepared and poured concrete cubes, cylinders, and prisms were taken out and put inside a curing tank. Figure 3.27 illustrates the casting of beams.

Figure 3.27 Casting of the Beam Specimens.

3.5.3 Curing for Second Phase

The curing of the cast specimens was done by the normal methods of curing by sprinkling water and keeping the elements moist for 28 days using wet burlap. The models were also covered using thick nylon, as in Figure 3.28.

Figure 3.28 Beams Curing.

3.5.4 Test Setup for Second Phase

Figure 3.29 shows the setup for testing the specimens and a schematic diagram. All specimens were cleaned and colored white. The test method covers the determination of the flexural strength of reinforced concrete beams with two-point loading by using an automated 600 kN compression machine in the engineering lab at Misan University, according to ASTM C78 [52]. The vertical position of the loading and support blocks was maintained. Under the loading steel plate, rubber matting was positioned to guarantee that the load was distributed evenly throughout the beam. The beams had a 1000 mm clear span. An LDVT with a 100 mm sensor was used to record the deflection at the beam mid-span. The deflection readings were captured using a portable electronic data logger. The load was applied at a rate of 1 MPa/min, which constantly increases the maximum stress on the tension face. As the loading increased, the crack patterns were observed and noted.

(a) Flexural Testing Machine

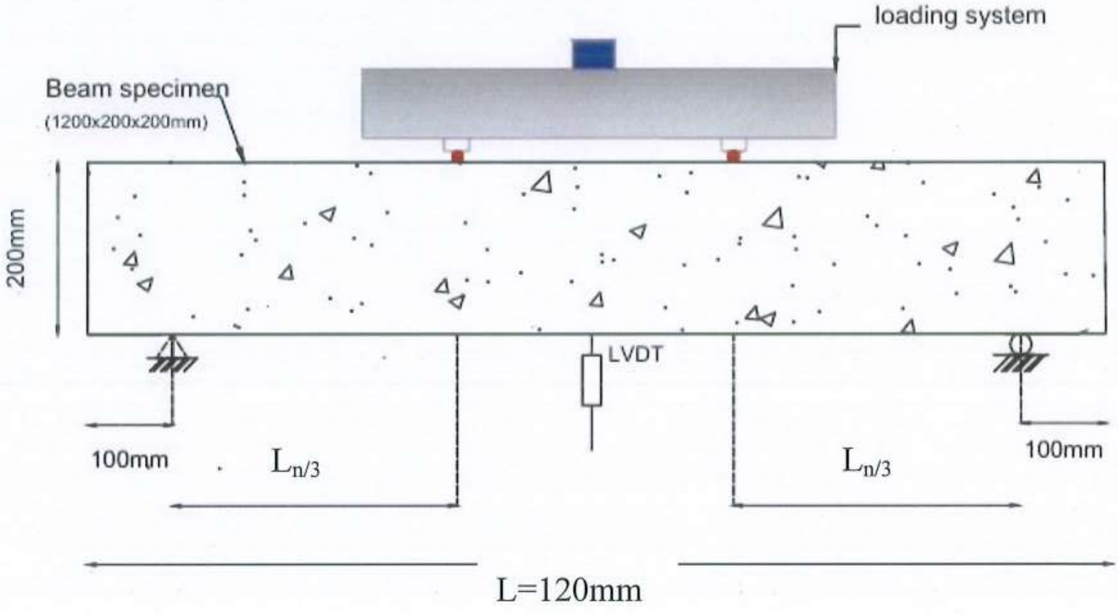

(b) Schematic Diagram of Test

Figure 3.29 Test Set-up and Instrumentation for Beam Specimens.

3.6 Phase III

Examining the behavior of insulated concrete with the rectangle shear connector from the second phase was the focus of the third phase.

3.6.1 One-Way EPS Insulated Concrete Panel Details

The slab panels studied in this research consisted of a core from an expanded polystyrene (EPS) insulator sandwiched by two concrete wythes with the same value of compressive strength of concrete (fcu) of 70 MPa. Six panels were prepared, 180 mm in thick, 610 mm in wide and 1220 mm in long, designed as solid slabs according to ACI 318-14 [54] (Appendix D). For the structural performance of the layer and also because of the concrete cover and for the fixing of the conductors, each wythe had a 65mm height; the same reinforcement Ø10@150 mm c/c was welded with overlapped splices in both directions of the bottom wythe of concrete, tied together with shear connectors and mesh using stick welding instead of tie wires. With this arrangement, the structure as a single unit became easy to move. The top wythe was reinforced only by wire fabric mesh. Because of the mesh's adequate thickness, just one layer was needed in concrete wythes. Between the concrete layers, 50 mm of EPS was fixed. 100 mm concrete from both sides, so the length of the EPS board was 1020 for each model. Each panel was prepared with two rectangular shear connectors with the same dimensions as those used in the beam specimen for the second phase (140 mm in height, 50 mm in width). The bond force between the reinforcements and concrete plays an important role in influencing their cracking behavior and supports the internal demands (compression, tension, and shear stresses) as a composite section, so for increasing the bond, an additional 200 mm length steel bar of Ø10 @ 200 mm was extended at the top face of the rectangle connector as tie reinforcement [56]. All details of panels are shown in Figure 3.31, 3.32,and 3.33. Table 3.20 presents the details of panels that were identified by codes.

The specimens' symbolization: the slab modal is represented by the first letter, the group is represented by the next letter, and the specimen number is defined by the final digits (Figure 3.30).

Table 3.20 Details of Panels with Shear Connectors.

Model	Casting	Dimensions (Lxbxt)mm	Top reinforcing	Bottom reinforcing	Type shear connector	N0.of shear connector
SA1	One stage	1220x610x180	wire mesh Ø5 mm (opining 100x100mm)	Ø10@150mm, wire mesh Ø5 mm	rectangle	2
SA2						
SA3						
SB1	Two stages					
SB2						
SB3						
Thickness of each concrete layer						65 mm
Total area of all the Panel						0.744 m2
Length of shear connector						1020 mm
Width of shear connector						50mm
Height of shear connector						140 mm
Length of EPS						1020mm
Width of EPS						470mm
Thickness of EPS						50mm
Length of tie						200mm

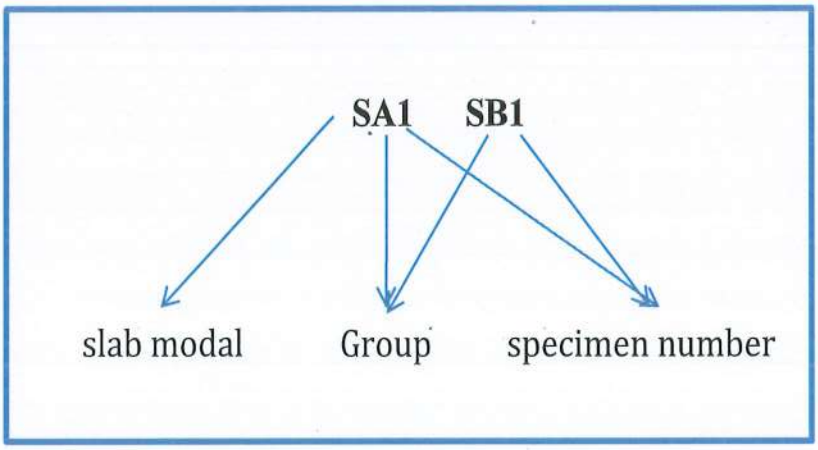

Figure 3.30 Symbols of Panel Specimens.

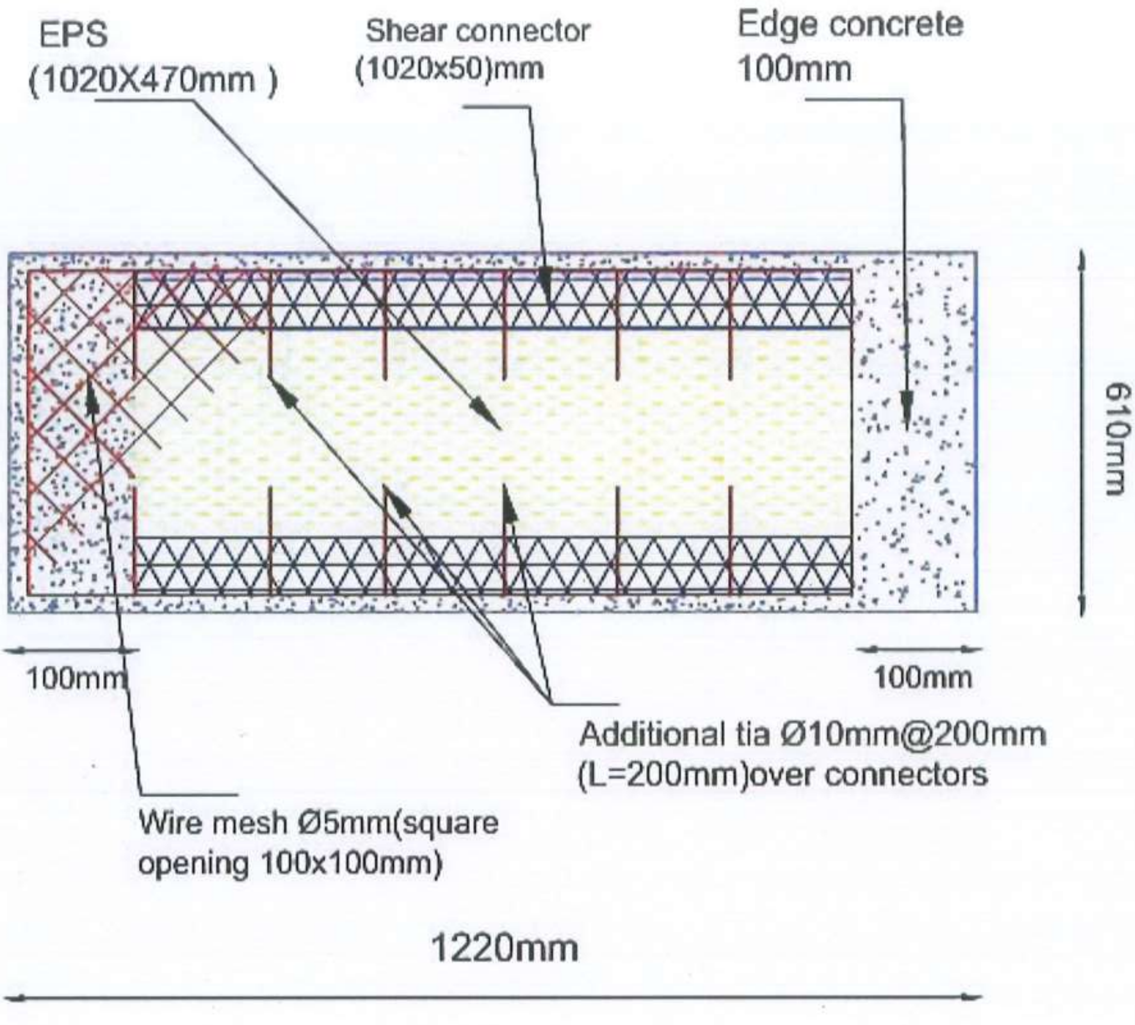

Figure 3.31 Panel Details-Top View.

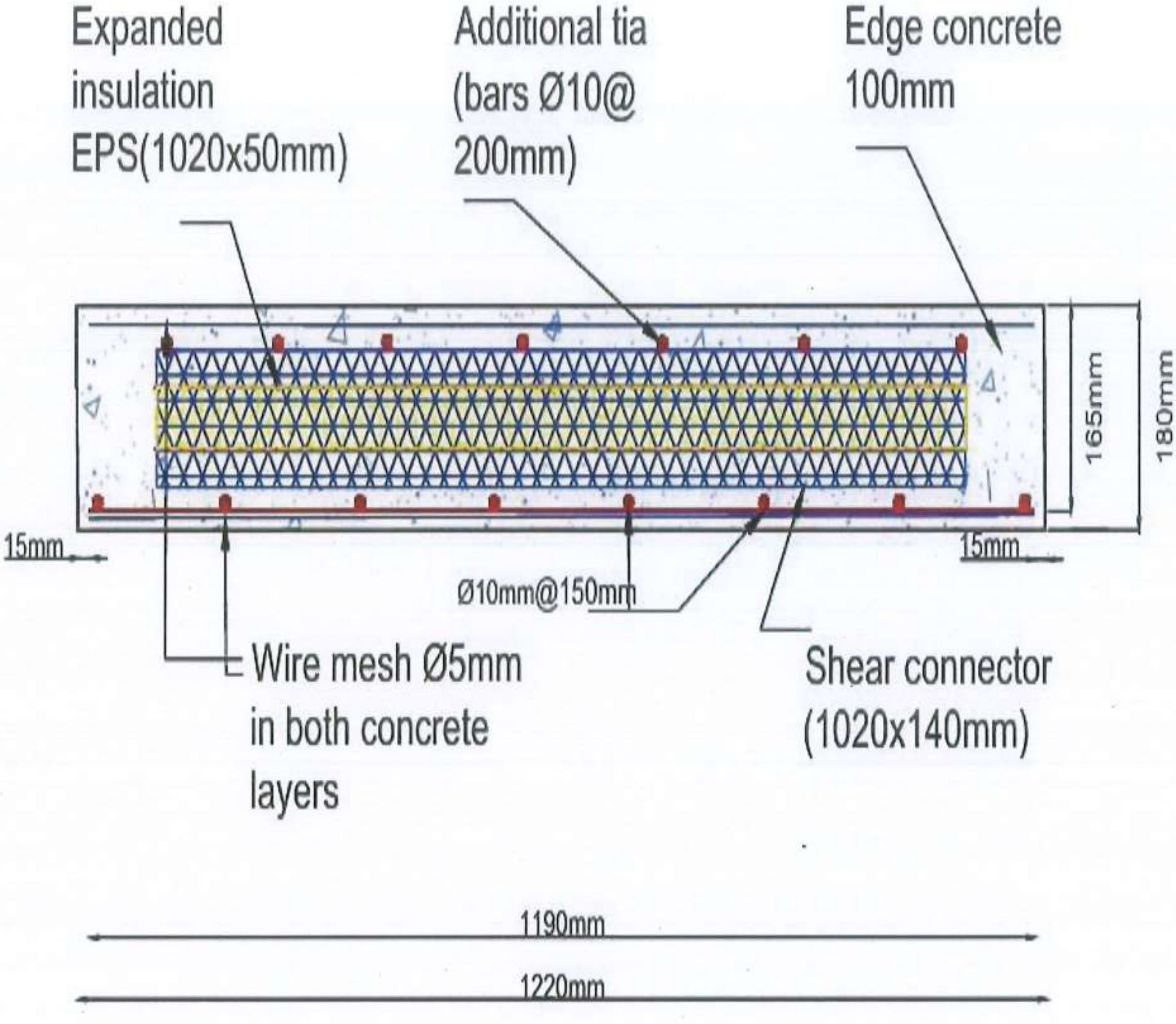

Figure 3.32 Panel Details-In Front View.

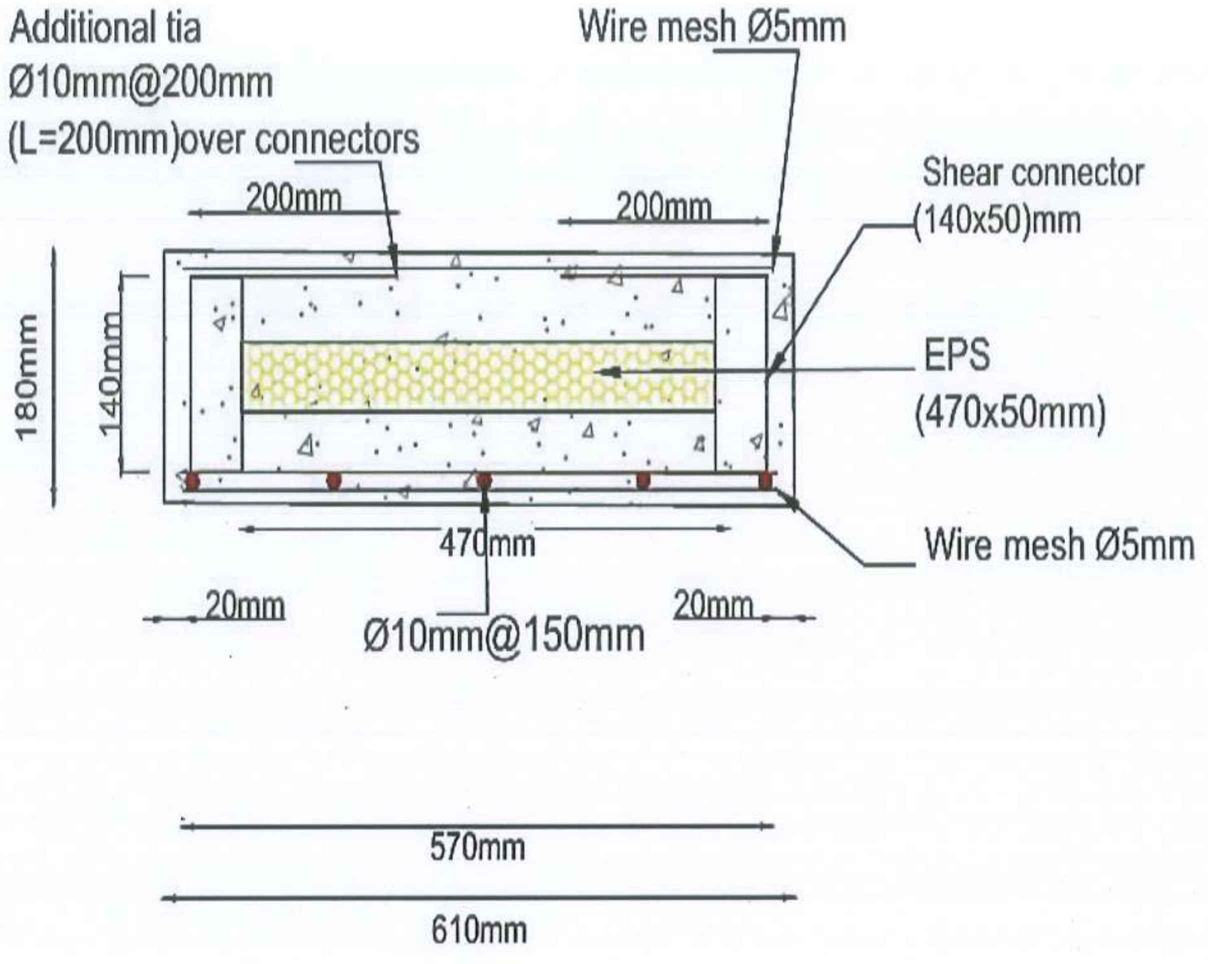

Figure 3.33 Panel Details-Side View.

3.6.2 Attachment of Strain Gauges

All EPS concrete panels have uniaxial strain gauges (FLAB-5-11-3LJC-F) measuring 5 mm in length that were affixed for measuring strains during the full loading in mid-span at the top wire mesh and bottom steel reinforcements (Figure 3.34). Following the smoothing of a portion of the reinforcement (steel or wire mesh), the strain gauges were placed tightly with CN adhesive. The strain gauge wires were carefully positioned to avoid damage during the concrete pouring process, and plastic bags surrounded them to ensure the strain gauges functioned properly.

(a) (b) (c)

Figure 3.34 Strain Gauges (a) Strain gauge of steel (b) Adhesive strain gauge of steel on reinforcement (c) Strain gauge on wire mesh.

3.6.3 Casting Procedure of EPS Panel Specimens

According to the pouring method, two groups of composite EPS concrete panels were considered: (SA1, SA2, SA3) and (SB1, SB2, SB3). The quantities needed for the models were calculated, weighed, and kept in a dry place. Also, the quantities were mixed by a truck concrete mixer. For the first group, high-strength SCC was poured into a plywood mold of 1220 x 610 mm on a horizontal surface to create the specimens' bottom wythe. The mold was filled to a depth of 65 mm. The cover for the reinforcement was 15 mm. The EPS core with 50 mm thickness was set atop the concrete laid, and the top wire mesh was connected with the additional bars pre-pouring with self-locking plastic cable ties (2.5x200 mm). To create the top wythe, the concrete was poured 65 mm above the EPS core. To effectively transfer the stresses between the two layers with shear connectors, parts of the connectors' webs were embedded inside the concrete layers. In the casting process for the models of the second group, the same steps were followed, except that the upper layer was poured the next day. Before starting pouring, the old concrete layer treatment consisted of moistening the surface with water only and no adhesives. The stages of casting panel samples are shown as in Figure 3.35.

(a) Installing reinforcement and connectors.

(b) Pouring down concrete wythe.

(c) Installing steel mesh and EPS.

(d) Pouring top concrete wythe.

Figure 3.35 Casting of the Panel Specimens.

3.6.4 Curing for the Third Phase

Curing is necessary to develop the required properties of concrete strength. After casting, all exposed surfaces were sprayed with water and also covered with burlap and thick nylon throughout the treatment period, which lasted for 28 days. Figure 3.36 shows the curing for the third phase.

Figure 3.36 Curing for Panels.

3.6.5 Test Setup for the Third Phase

The flexural performance of the concrete panels was assessed by using two-point loading for transverse load tests at a distance of one-third of the span from the supports, toward the middle of the span, according to ASTM C78 [52], as shown in Figure 3.38. The third stage was conducted using the same screening apparatus as in the previous phase. The loading system consists of three steel I-beam portions. The supporting system comprises two steel I-beams. The support base in the examination device was smaller in width than the dimensions of the models, so a rectangular steel base was added for the purpose of installing the models (Figure 3.37). In the vertical direction, one LVDT was placed in the center of the slabs, and all deflection data were taken until the ultimate load was applied. Moreover, load versus horizontal slide is investigated at the end of the panel. Two LVDT devices are installed at the end of the panel for the two layers of concrete at mid-width of the specimens. All test specimens had the load applied to them in steps that were carefully calibrated to ensure that enough readings would be collected to definitively identify the load-deformation curve. An electronic data logger was used to record the applied load, deflection, and stresses.

Figure 3.37 Loading and Support System for Panels Test.

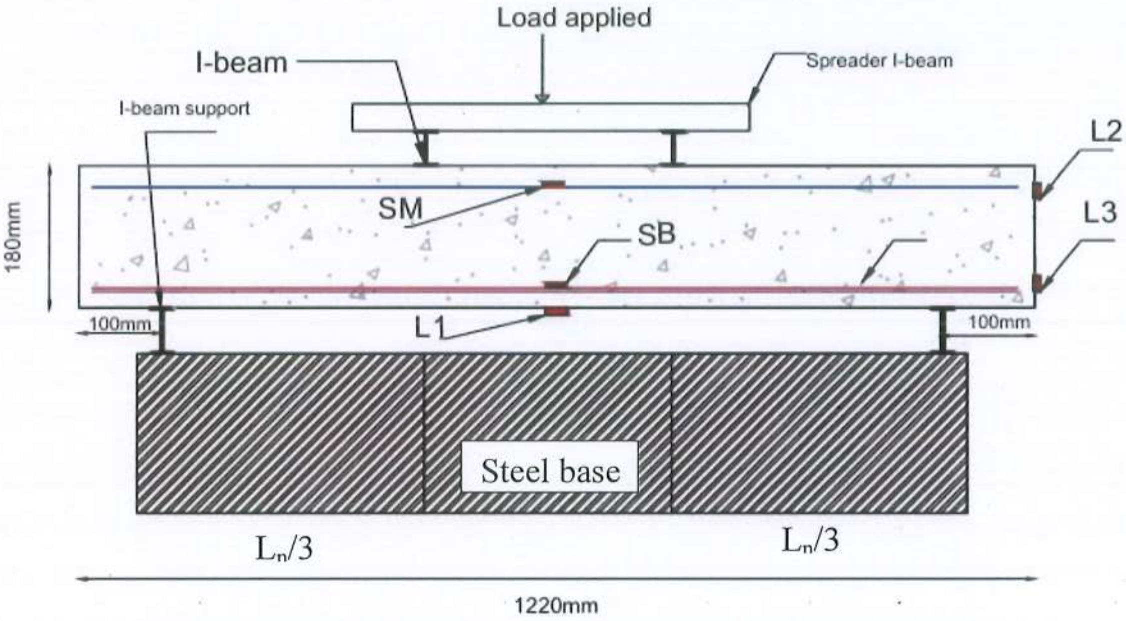

SM (strain gauge in wire mesh), SB (strain gauge in steel bar),
L1, L2, L3 (LVDT)

Figure 3.38 Two-Point Bending Test Instrumentation and Setup Details.

CHAPTER FOUR: RESULTS AND DISCUSSIONS

4.1 Introduction

The experimental work's findings, which were detailed in the preceding chapter, are presented in this chapter for phases II and III. To generate data for the models of the developed shear connectors, experimental testing is required. The second phase is investigating the performance of using different types of expanded shear connectors with beams. Twenty-four models were examined in the same way and according to the required specifications. Through their results and observations, the final models were made in the third phase of this study. The results of the final stage of testing six models of a slab, the details of which were mentioned in the previous chapter, may contribute to the development of the composite concrete system.

In this chapter, statistical methods are used to construct results and make statements to provide a basic comparison of the relative effects of variables across cases and to compare cases directly to each other.

4.2 Results for Phase II

In this chapter, the beams efficiency studied through the first crack load (P_{cr}), ultimate load ($P_{u)}$, the deflections at the first crack load (Δ_{cr}), the deflections at ultimate load (Δ_u) ductility, the difference of ultimate load between specimens, failure mode, load-deflection relationships, and strain in tension and compression zones.

All test data were displayed in Tables 4.1, 4.2, and 4.3, with the calculated averages for each group and variance values from the mean.

Table 4.1 Second Phase Experimental Results for Ultimate Load and Deflection.

Specimens	Ultimate load, P_u (kN)	Avg.	Difference in P_u (%)	Deflection at ultimate load Δ_{max} (mm)	Avg.	Difference in Δ_{max} (%)
AR1	264	246.66	0	15.28	15.41	0
AR2	230		12.87	14.62		4.32
AR3	246		6.81	16.34		-6.94
C.0.V %	5.63			4.59		
BR1	219	212	17.04	9.50	8.78	1.45
BR2	205		22.34	8.12		15.77
BR3	212		19.69	8.72		9.54
C.0.V%	2.69			4.43		
AI1	216	215.33	8.09	7.22	8.09	25.10
AI2	195		17.02	7.42		23.03
AI3	235		0	9.64		0
C.0.V %	4.56			3.55		
BI1	190	195.67	19.15	7.31	7.68	24.17
BI2	207		11.91	8.21		14.83
BI3	190		19.15	7.53		21.89
C.0.V %	4.09			4.99		
AZ1	175	169	6.42	8.94	8.67	-3.35
AZ2	151		19.25	7.95		8.09
AZ3	181		3.21	9.12		-5.43
C.0.V %	4.58			5.93		
BZ1	164	175	12.30	8.01	8.83	7.40
BZ2	174		6.95	9.83		-13.64
BZ3	187		0	8.65		0
C.0.V %	5.38			6.53		
AT1	131	134	3.68	7.86	7.93	1.13
AT2	135		0.74	7.989		-0.49
AT3	136		0	7.95		0
C.0.V %	1.61			0.68		
BT1	130	127	4.41	6.73	5.97	15.35
BT2	123		9.56	5.21		34.47
BT3	128		5.88	5.98		24.78
C.0.V %	2.31			4.39		

Table 4.2 Second Phase Experimental Results for First Crack Load and Deflection.

Specimens	First crack load, P_{cr} (kN)	Avg.	Coefficient of Variation for First crack load C.0.V (%)	Deflection at first crack load, Δ_{cr} (mm)	Avg.	Coefficient of Variation for, Δ_{cr} C.0.V (%)	Failure mode
AR1	60	70	5.83	1.688	1.92	4.30	Shear
AR2	75			2			Shear
AR3	75			2.108			Shear
BR1	70	70	0	1.027	1.14	4.13	Shear
BR2	70			0.98			Shear
BR3	70			1.416			Shear
AI1	50	60	4.78	1.415	1.19	4.12	Shear
AI2	65			1.045			Shear
AI3	65			1.132			Shear
BI1	55	53.3	4.42	1.09	1.04	5.27	Shear
BI2	55			1.08			Shear
BI3	50			0.97			Shear
AZ1	60	61.7	3.82	1.311	1.63	4.31	Shear
AZ2	60			1.861			Shear
AZ3	65			1.72			Shear
BZ1	45	48.3	3.76	1.22	1.20	3.54	Shear
BZ2	45			1.25			Shear
BZ3	55			1.15			Shear
AT1	45	48.3	4.76	1.55	1.40	3.88	Flexural
AT2	45			1.07			Flexural
AT3	55			1.59			Flexural
BT1	40	38.3	4.15	1.08	1.06	2.04	Flexural
BT2	35			1.03			Flexural
BT3	40			1.07			Flexural

Table 4.3 Tensile and Compressive Strain for Beam Specimens.

Specimens	Ultimate load, P_u (kN)	Tensile Strain	Avg.	Compressive Strain	Avg.
AR1	264	2.83 x10^{-3}	2.62 x10^{-3}	1.03 x10^{-3}	9.5 x10^{-4}
AR2	230	2.36 x10^{-3}		9 x10^{-4}	
AR3	246	2.69 x10^{-3}		9.6 x10^{-4}	
BR1	219	2.33 x10^{-3}	2.25 x10^{-3}	8.5 x10^{-4}	8.26 x10^{-4}
BR2	205	2.14 x10^{-3}		8 x10^{-4}	
BR3	212	2.29 x10^{-3}		8.3 x10^{-4}	
AI1	216	2.30 x10^{-3}	2.26 x10^{-3}	8.4 x10^{-4}	8.4 x10^{-4}
AI2	195	2.09 x10^{-3}		7.6 x10^{-4}	
AI3	235	2.38 x10^{-3}		9.2 x10^{-4}	
BI1	190	2.04 x10^{-3}	2.08 x10^{-3}	7.4 x10^{-4}	7.63 x10^{-4}
BI2	207	2.17 x10^{-3}		8.1 x10^{-4}	
BI3	190	2.04 x10^{-3}		7.4 x10^{-4}	
AZ1	175	1.60 x10^{-3}	1.61 x10^{-3}	6.8 x10^{-4}	6.6 x10^{-4}
AZ2	151	1.42 x10^{-3}		5.9 x10^{-4}	
AZ3	181	1.82 x10^{-3}		7.1 x10^{-4}	
BZ1	164	1.50 x10^{-3}	1.66 x10^{-3}	6.4 x10^{-4}	6.83 x10^{-4}
BZ2	174	1.60 x10^{-3}		6.8 x10^{-4}	
BZ3	187	1.89 x10^{-3}		7.3 x10^{-4}	
AT1	131	1.25 x10^{-3}	1.29 x10^{-3}	5.1 x10^{-4}	5.23 x10^{-4}
AT2	135	1.29 x10^{-3}		5.3 x10^{-4}	
AT3	136	1.33 x10^{-3}		5.3 x10^{-4}	
BT1	130	1.20 x10^{-3}	1.19 x10^{-3}	5.1 x10^{-4}	4.97 x10^{-4}
BT2	123	1.18 x10^{-3}		4.8 x10^{-4}	
BT3	128	1.2 x10^{-3}		5 x10^{-4}	

4.3 Ductility

The performance objectives (life safety and limiting degradation) are critical in the design of structures and cannot be understated. The concept of "ductile design" refers to a structural system's capacity to guarantee that specified zones, referred to as "plastic hinges", are capable of developing deformations in response to strong seismic action and preventing the collapse of the structure. Also, controlling the ductility avoids the possibility of non-economic design of structures [57]. As a result of loads, concrete members rotate, shift, or curve; when a member yields, its stiffness drastically reduces, and a significant deformation occurs. A range of methods to assess ductility are generally simple and effective:

4.3.1 Ductility Index

Tables 4.1 and 4.2 display the maximum deflection and the recorded ultimate load. Thus, as shown in equation 4.1 below, the global ductility μ can be represented as a ratio between the system's ultimate displacement (Δmax) and the displacement that corresponds to the structure's global yielding (Δy) [58]. Table 4.4 presents the ductility of all beams in terms of the ductility index (Figure 4.1).

$$\mu = \frac{\Delta u\ max}{\Delta y} \qquad 4.1$$

Where:

μ : Ductility index

$\Delta_{u\ max}$: Maximum deflection (mm)

Δ_y: Yielding displacement (mm)

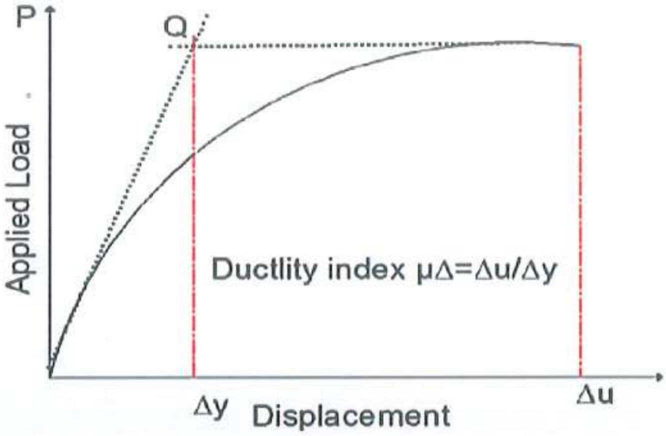

Figure 4.1 Index of Ductility [58].

Table 4.4 Index of Ductility for Beam Specimens.

Specimens	Deflection at ultimate load Δ_{max} (mm)	Yield Deflection Δ_{y} (mm)	Ductility Index	Avg.	C.O.V (%)	Increasing (%)
AR1	15.28	7.42	2.05	2.26	4.69	0
AR2	14.62	6.13	2.38			-16.10
AR3	16.34	6.91	2.36			-15.12
BR1	9.50	3.21	2.95	2.6	5.71	-43.90
BR2	8.12	2.87	2.83			-38.05
BR3	8.72	4.28	2.03			0.98
AI1	7.22	2.89	2.49	2.4	2.66	-5.96
AI2	7.42	3.13	2.36			-0.43
AI3	9.64	4.09	2.35			0
BI1	7.31	3.76	1.94	1.97	2.67	17.45
BI2	8.21	4.06	2.02			14.04
BI3	7.53	3.68	2.04			13.19
AZ1	8.94	3.82	2.33	1.97	3.52	-5.43
AZ2	7.95	4.68	1.69			23.53
AZ3	9.12	4.78	1.90			14.03
BZ1	8.01	4.44	1.80	2.01	4.35	18.55
BZ2	9.83	4.83	2.03			8.14
BZ3	8.65	3.91	2.21			0
AT1	7.86	4.51	1.74	2.08	4.67	13.86
AT2	7.989	3.21	2.48			-22.77
AT3	7.95	3.93	2.02			0
BT1	6.73	3.51	1.91	1.7	3.70	5.45
BT2	5.21	3.61	1.43			29.21
BT3	5.98	3.42	1.74			13.86

4.3.2 Initial Stiffness

The load-deflection relationship can be used to define the yield point by the yield strength and yield displacement. Initial stiffness can be calculated by equation 4.2 [59]. The initial stiffness of second-phase specimens is shown in Table 4.5.

$$\text{Initial Stiffness} = \frac{Py}{\Delta y} \tag{4.2}$$

where;

P_y: Yield Load (kN)

Δ_y: Yielding displacement (mm)

Table 4.5 Beam Specimens' Initial Stiffness.

Specimens	Yield Deflection Δ_y(mm)	Yield Load P_y(kN)	Initial stiffness (kN/mm)	Avg.	C.O.V (%)	Increasing (%)
AR1	7.42	128.28	17.27	16.01	5.80	0
AR2	6.13	96.48	15.73			8.92
AR3	6.91	104.06	15.05			12.85
BR1	3.21	74	23.03	24.18	3.70	-33.35
BR2	2.87	72.37	25.21			-45.98
BR3	4.28	104.22	24.303			-40.72
AI1	2.89	86.55	29.904	26.83	4.57	-22.71
AI2	3.13	82.28	26.24			-7.67
AI3	4.09	99.73	24.37			0
BI1	3.76	97.75	25.95	25.46	1.36	-6.48
BI2	4.06	102.47	25.21			-3.45
BI3	3.68	92.98	25.22			-3.49
AZ1	3.82	74.8	19.56	19.45	1.86	9.49
AZ2	4.68	88.87	18.97			12.22
AZ3	4.78	95.04	19.84			8.19
BZ1	4.44	91.01	20.46	19.91	4.29	5.32
BZ2	4.83	85.49	17.68			18.19
BZ3	3.91	84.52	21.61			0
AT1	4.51	75.2	16.66	16.88	1.06	2.57
AT2	3.21	54.24	16.89			1.23
AT3	3.93	67.24	17.10			0.00
BT1	3.51	67.77	19.30	21.43	4.21	-12.87
BT2	3.61	85.47	23.61			-38.07
BT3	3.42	73.3	21.40			-25.15

4.3.3 Energy Absorption

Energy absorption is an increasingly important function of structure and materials, and it's also an important requirement in the design. Energy absorption can be calculated by the total area under the load deflection curve as shown in Table 4.6.

Table 4.6 Energy Absorption for Beam Specimens.

Specimens	Energy Absorption (kN.mm)	Avg.	C.O.V (%)	Increasing (%)
AR1	2233.98	2124.48	5.66	0
AR2	1956.94			12.40
AR3	2182.52			2.30
BR1	1213.24	1112.25	4.97	45.69
BR2	997.36			55.36
BR3	1126.17			49.59
AI1	772.87	870.62	5.74	29.01
AI2	750.29			31.08
AI3	1088.71			0
BI1	783.43	847.18	5.46	28.04
BI2	933.32			14.27
BI3	824.8			24.24
AZ1	797.47	753.45	2.21	3.10
AZ2	625.47			24.00
AZ3	837.43			-1.76
BZ1	702.53	821.21	2.72	14.63
BZ2	938.17			-14.00
BZ3	822.94			0
AT1	188.23	199.08	3.86	8.10
AT2	204.19			0.31
AT3	204.83			0
BT1	169.31	142.07	5.70	17.34
BT2	114.69			44.01
BT3	142.23			30.56

4.4 Composite Beam with Expanded Mesh Shear Connectors

4.4.1 Beams in Groups A and B with Rectangular Shear Connector

A total of six beams are investigated under two-point bending from groups AR and BR. Both series, AR and BR, had a linear relationship between load and deflection, where the initial flexural cracking of AR manifested at an average displacement of 1.92 mm; after that, deflection increased as the load increased to the ultimate load with an average maximum displacement of 15.41 mm (Figure 4.2). There is a clear difference in the diagram in the displacements of group B, where the maximum displacement rate reached 8.78 mm. All beams developed enough cracks before failure. The transverse force is initiating, causing the diagonal cracks. Thus, it can be stated that all the beams were destroyed due to the shear in the support zones (Figure 4.4). In BR3, after the crack pattern reaches the interface, after a short propagation along the interface, it appears in the upper layer, and the failure is caused by exceeding the shear resistance of the beam; also, the partial separation with a vertical crack of the edge of the model is observed in the lower layer (Figure 4.3). This behavior was observed in composite beams with a low ratio of transverse reinforcement, in which the height of the upper layer was greater than the height of the lower layer (Halicka, 2011).

All concrete beams reach high resistance, which may be attributed to the resistance of the concrete or because of the shear connecter and its properties (cross-section, orientation and volume fraction of expanded mesh, and steel angle). The average first crack load is 70 kN for all beams. For the specimens (AR1, AR2, AR3), which represent the control specimens poured at the same time completely, the obtained experimental failure load on average, Pu, is 246.66 kN. For specimens BR1, BR2, and BR3, the average failure load was 212 kN. The superiority of the first group in terms of maximum displacement and load may be attributed to the lack of cohesion in composite concrete layers in group BR (Halicka, 2011) [21]. It is noted in two-stage casting without using adhesion or stirrups between concrete layers that the models BR are decreasing in average ultimate load, maximum deflection, and energy absorption by 16.35%, 75.5%, and 91%, respectively. The initial stiffness and ductility index values for group A were lower than group B by 51% and 15%, because the deflection and load at the yield point for A are greater than B.

Strains were found by applying a load to yield strain. Strains of models AR1, AR2, and AR3 were higher than the strains of BR1, BR2, and BR3. The strain values were $2.83\text{x}10^{-3}$, $2.36\text{x}10^{-3}$, and $2.69\ \text{x}10^{-3}$in the tension area and $1.03\ \text{x}10^{-3}$,$9\ \text{x}10^{-4}$, and $9.6\ \text{x}10^{-4}$ in the compressive area for the AR series, respectively, while the BR series has tensile strain of $2.33\ \text{x}10^{-3}$,$2.14\ \text{x}10^{-3}$, and $2.29\ \text{x}10^{-3}$, in the compressive area $8.5\ \text{x}10^{-4}$, $8\ \text{x}10^{-4}$, and $8.3\ \text{x}10^{-4}$as shown in Table 4.3. These strains of the beams in groups AR and BR were found to be more fairly commensurate with their load-carrying capacity.

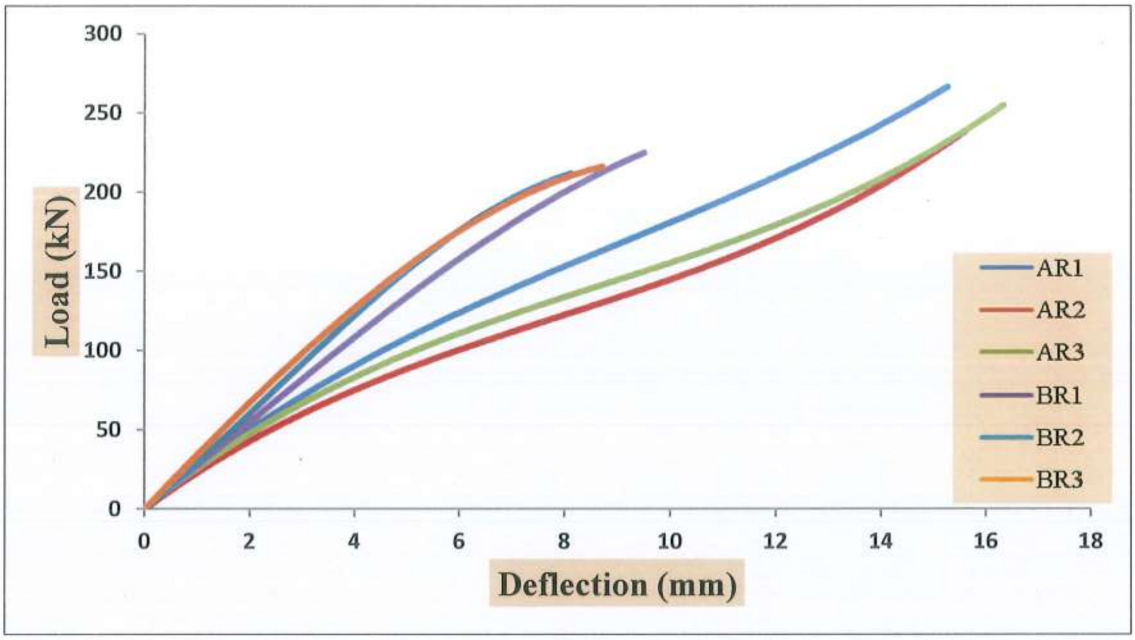

Figure 4.2 Relationship Between Load and Deflection for Series AR and BR Beams.

Figure 4.3 Slip Concrete Lower Layer in BR3 Beam.

Figure 4.4 Crack Pattern of Beams with Rectangle Shear Connector.

4.4.2 Beams in Groups A and B with I-Shape Shear Connector

For the second series of beams, Figure 4.5 shows all the readings recorded during the test, where the first crack was at an average reading of 1.19 mm and 1.04 mm, and the average higher readings were 8.09 mm and 7.68 mm for groups AI and BI, respectively. All beams failed due to imbalance because of shear forces (Figure 4.6). The same behavior was observed in BI1: the crack moves through the interface and into the point load of the beam before moving on to the upper layer, causing a slip at the end of the beam (Figure 4.7).Due to bonding new concrete to old concrete in the second series BI, this influences the mechanical characteristics of the members (Halicka, 2011) [21]. In average ,first crack and ultimate load, first crack and maximum displacement, energy absorption, ductility index, and initial stiffness averages for AI are higher by 11.16%, 9.13%, 12.6%, 5%, 2.7%, 17.9%, and 5.1%, respectively, indicating that group AI is more controlled than BI. Although it has less load resistance, an I-section connector with a beam has more stiffness.

Section I differs from a rectangle in that the total area of additional material (steel angle and flat bar) used in the I-section connector was less than that of the rectangular section. While the AI series is 14.5% less resistant to stresses than the AR series, they are 40% more resistant to elastic deformations and 5.8% more resistant to inelastic deformations. As for the BR group, BI is 5% stiffer and less resistant to load and plastic deformations by 8.34% and 32%, respectively. The rates of strain for BI1, BI2, and BI3 were lower than group AI by 16.6% for tension strain and 15% for compressive strain, as shown in Table 4.3, proportional to their capacity to support loads.

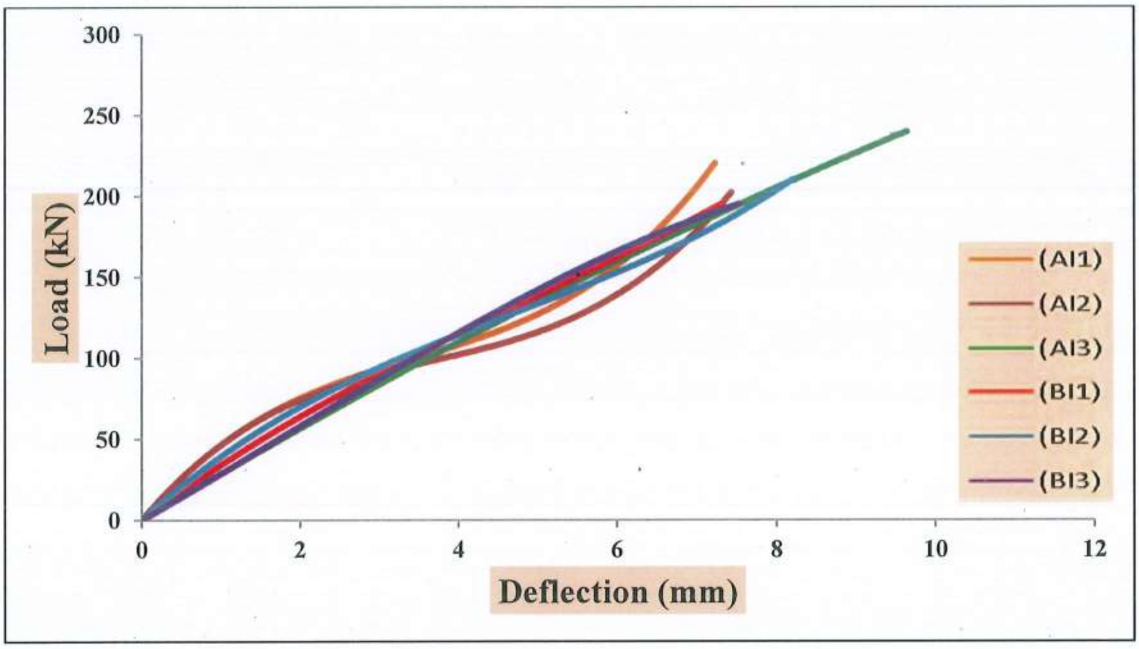

Figure 4.5 Relationship Between Load and Deflection for Series AI and BI Beams.

Figure 4.6 Crack Pattern of Beams with I-Shear Connector.

Figure 4.7 Slip Concrete Layer in BI1 Beam.

4.4.3 Beams in Groups A and B with Z-Shape Shear Connector

For the third type of shear connector (Figure 4.8), the deflections of the beams were approximately the same from before the first crack load to the yielding point until the ultimate loads, with the same crack pattern and failure mode as prior beams with rectangular and I-shaped connectors (Figure 4.9). It also shows in beam BZ1and BZ3 that the bottom layer was subjected to separation because of the lack of cohesiveness in the composite concrete layers in group BZ (Figure 4.9). In this group, the average of first crack deflection and first crack load for AZ is more than BZ by 21.6% and 26.4%, respectively. It noted a difference in the average ultimate load in beams AZ, which is lower than that in beams BZ by 3.55%; despite the convergence of the values of the two beams, AZ3 and BZ3 were 181 kN and 187 kN, respectively; perhaps the cause is due to the large amount of cementitious materials in high-performance concrete mixtures, which causes an increase in the temperature of the concrete during hydration, which leads to an increase in resistance for group BZ (Carrasquillo, 2000) [60].

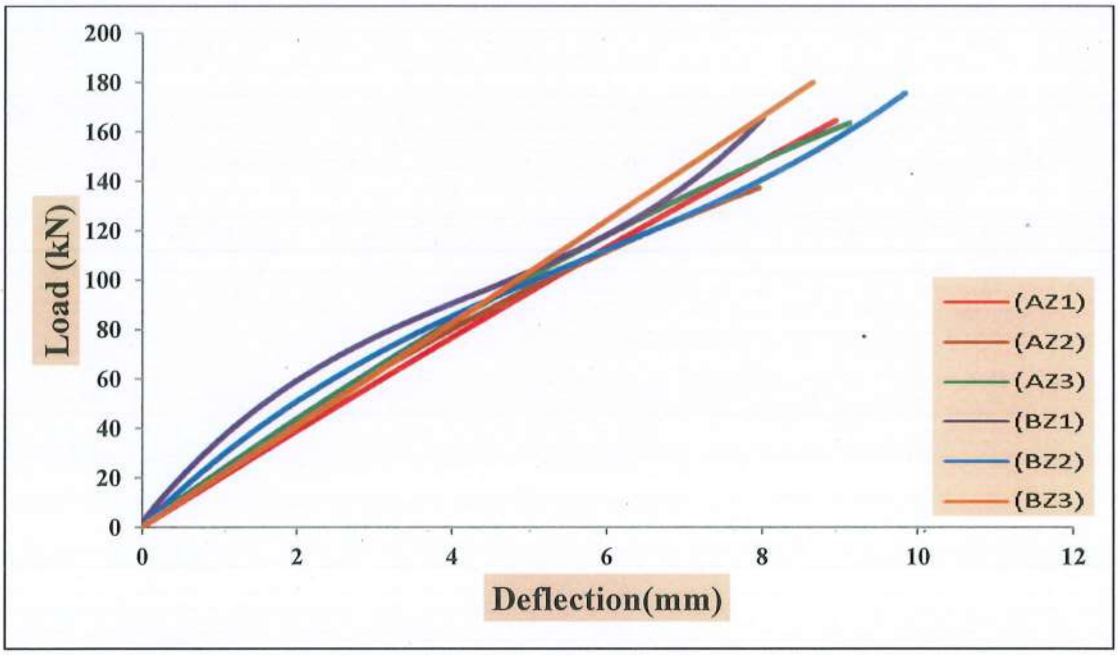

Figure 4.8 Relationship Between Load and Deflection for Series AZ and BZ Beams.

Because the yield load of BZ is less than AZ by 0.68%, it appears in ductility and initial stiffness, by 2%, 2.3%, respectively. Compared to the rectangular section, the volume fraction of the expanded mesh and the area of the steel angle used were lower. Beams with Z-shaped shear connectors have a lower load capacity and reduced ductility. The AZ group reduced the concrete beams' load resistance by 45% and reduced their ductility by 14.7% but increased their stiffness by 17.6% concerning AR. BZ reduced beams' stiffness, load resistance, and ductility by 21.4%, 21%, and 29.4%, respectively, with respect to BR.

Figure 4.9 Crack Pattern of Beams with Z-Shear Connector.

4.4.4 Beams in Groups A and B with Truss-Shape Shear Connector

In the last series where truss-shaped shear connectors were used, the load-deflection relationship is shown in Figure 4.10. The series AT, with an average maximum displacement of 7.93 mm, failed in flexure at the average ultimate load of 134 kN. Also, series BT of beams failed in flexure, as shown by vertical cracks in the middle of the specimens (Figure 4.11) at average maximum load and maximum deflection 5.5% and 32.8% lower than series AT; this difference between the two groups also comes from the influence of casting concrete layers at different times. The series BT had less AT in the averages of first crack load and its deflection, ductility, and energy absorption by 31%, 32%, 22%, and 40%, respectively. Figure 4.11 shows separation of the bottom concrete layer due to loading in beam BT3, as well as in model BT1, with hairline cracking.

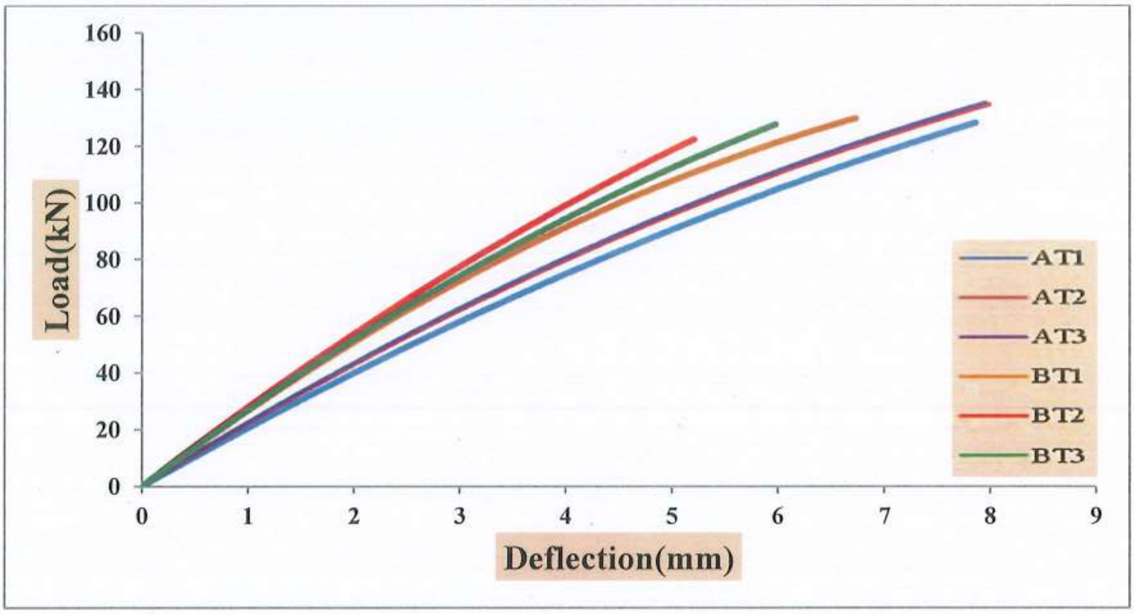

Figure 4.10 Relationship Between Load and Deflection for Series AT and BT Beams.

The maximum load rates were lower than those with other shear connectors, possibly due to the lower volume fraction of the expanded mesh used in the truss connector, without increasing their number to equalize the volume with the other connectors or strengthening the ends with angle iron, as was used in bending and fixing the corners of the rectangle, I, and Z connectors. These beams from the AT and BT series are less ductile and have a lower load capacity than the beams of rectangular connectors. In terms of AR, the AT group increased the concrete beams' stiffness by 5.15 percent while decreasing their ductility by 8.7 percent and their load resistance by 84%. In comparison to BR, BT decreased the ductility, load resistance, and stiffness of beams by 52%, 67%, and 12.8%, respectively.

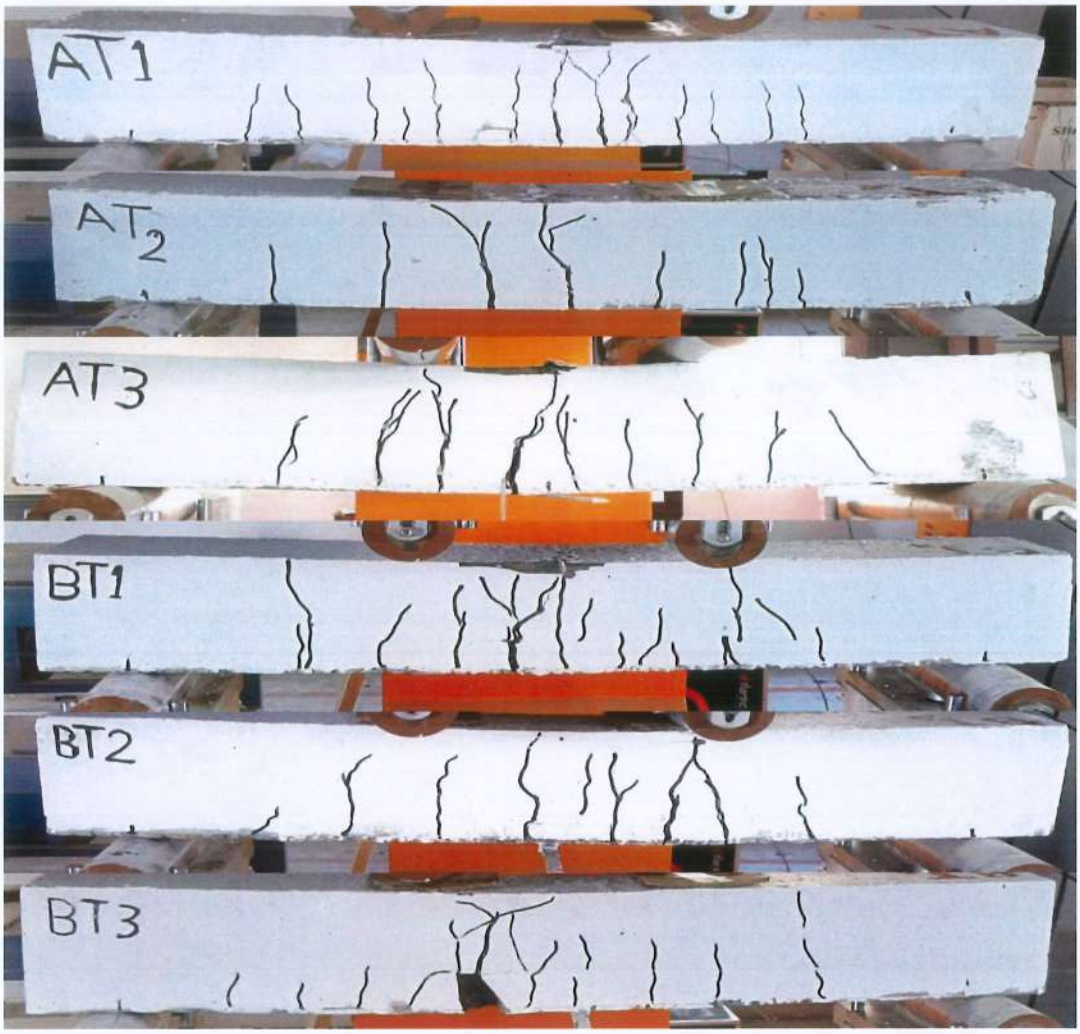

Figure 4.11 Crack Pattern of Beams with Truss-Shear Connector

4.5 Data Normalization for Beams

Data normalization is a process of transforming data into a consistent and comparable format, which can improve data quality and analysis. Experimental data is used to verify objectives through engineering tests that demonstrate the mechanical properties of materials or structural members. Bending stresses are the most typical cause of failure; therefore, the preference for a higher load value was the criterion used. Min-max normalization is a simple technique that is useful when the data has a fixed range [61]. The models were divided into groups A and B using values from Tables 4.7 and 4.8; the results obtained are shown in Figures 4.12 and 4.13. If the ideal solution signifies the highest grade, 100%, then a percent of the relative closeness may be used as a measure of the closeness of preferred alternatives. For example, AI3 can be used as an alternative, as it has a percentage of 89%, which allows for its use. Without repeating the data, Figure 4.13 shows the same normalization data for group B.

According to Figure 4.14, in the case of using the alternative in the casting method for rectangle connectors, the percentage of convergence is 13%, which is an average value (less than 20) that can be developed by adhering to specific curing techniques to the bond strength.

Based on the previous results and depending on the maximum stresses and stiffness, the types of connectors can be arranged in descending order from rectangle, I, Z, and truss shape. This arrangement makes the rectangular shape the most effective shear connector to be adopted in the following phase.

Table 4.8 Normalization Data for Beams Casting in One Stage.

Model	Pu (kN)	Normalization data
AR1	264	1.00
AR3	246	0.93
AI3	235	0.89
AR2	230	0.87
AI1	216	0.82
AI2	195	0.74
AZ3	181	0.69
AZ1	175	0.66
AZ2	151	0.57
AT3	136	0.52
AT2	135	0.51
AT1	131	0.50

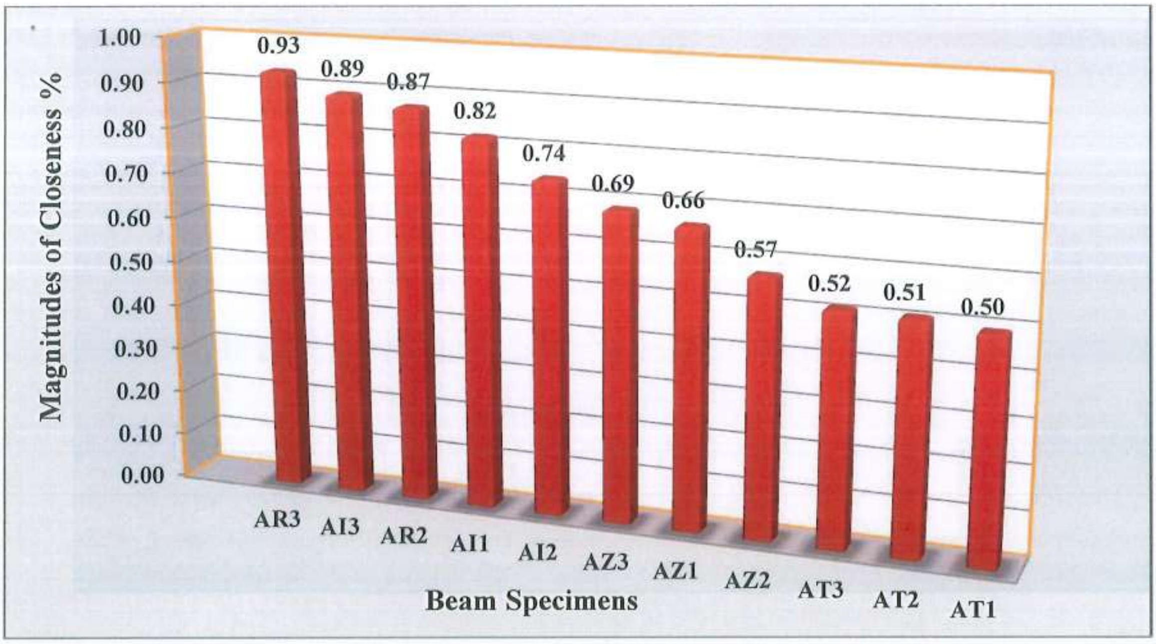

Figure 4.12 Results of Normalization Norm Relative to the Closeness for AR1 Casting in One Stage.

Table 4.9 Normalization Data for Beams Casting in Two Stage.

Model	Pu (kN)	Normalization data
BR1	219	1.00
BR3	212	0.97
BI2	207	0.95
BR2	205	0.94
BI1	190	0.87
BZ3	187	0.85
BZ2	174	0.79
BZ1	164	0.75
BT1	130	0.59
BT3	128	0.58
BT2	123	0.56

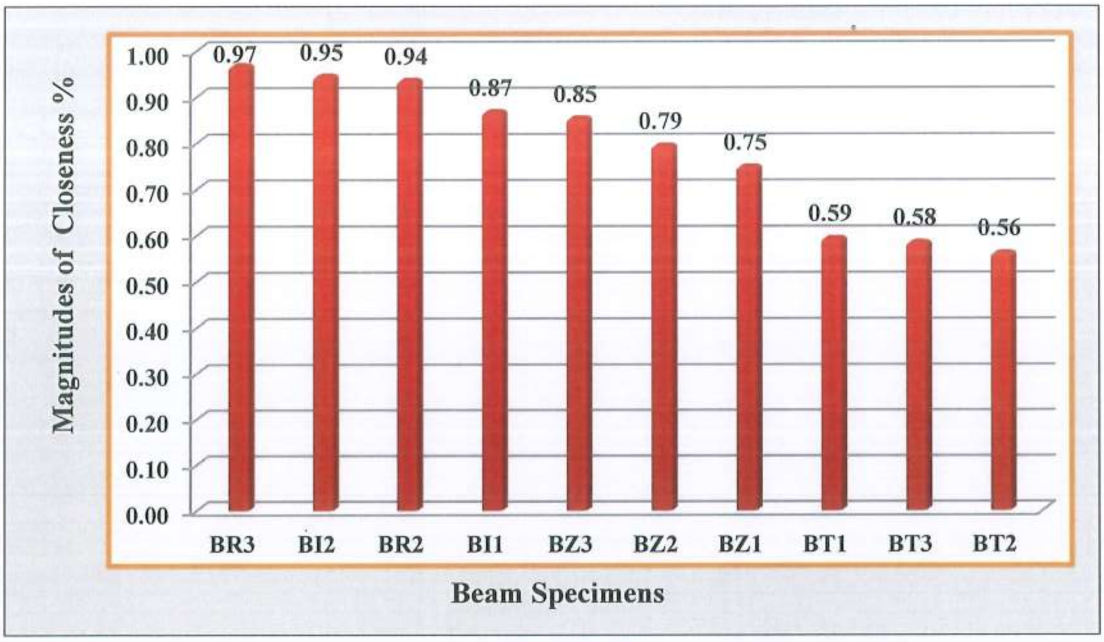

Figure 4.13 Results of Normalization Norm Relative to the Closeness for BR1 Casting in Two Stage.

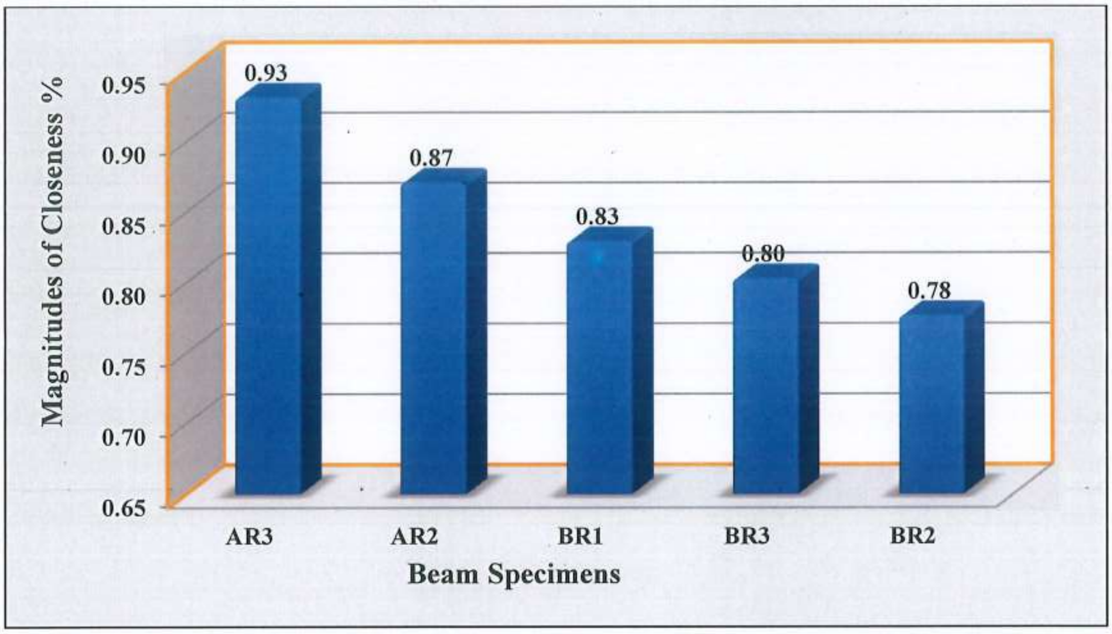

Figure 4.14 Results of Normalization Norm with Rectangle Connector Relative to the Closeness for Group A.

4.6 Results for Phase III

The structural behavior of insulated concrete sandwich panels with rectangular shear connectors subjected to two-point loading has been evaluated by

4.6.1 General Behavior and Mode of Failure

Figures 4.16,4.17, and 4.18 displays typical failure modes. The initial fracture was observed on the borders of the panel, as it was challenging to detect from the model's underside. The control samples (SA1, SA2, and SA3) initially behaved in a straight-line elastic way, and as the load grew to 32%, 29%, and 32%, respectively of the maximum load, cracks started at the bottom layer and spread to the top in the middle. The same pattern was seen in SB, with the cracking load being 30% for SB3 and 31% for both SB1 and SB2 respectively. All panels developed enough cracks before failure. The transverse force is initiating, causing the diagonal cracks. Thus, it can be stated that all the specimens were destroyed due to the shear in the support zones. The concrete did not collapse, and the presence of cracks indicates the flexibility of the panels and that the steel in the tension zone had reached the yielding stage before the concrete. The wythes were completely bonded with the foam core without slip between the structural wythes and foam core, despite the occurrence of hair cracks in series SB, indicating that the connectors achieved the composite action and transferred the load.

4.6.2 Responses of Load-Displacement

Figure 4.15 illustrates the load-deflection behavior at the midspan of control panels; it began with a linear load-deflection relationship, with initial flexural cracking occurring at an average load of 129 kN and an average deflection of 2.84 mm (Table 4.9).. Subsequently, deflection increased as the load escalated to the ultimate load of 415 kN at an average deflection of 15.61 mm. Comparing the sandwich panels (SA1, SA2, and SA3) to the second series B, the bond between the concrete wythes when the model was fully cast in one stage resulted in increased initial cracking load, ultimate load, ductility index, and energy absorption by 3.6%, 4.09%, approximately 14%, and 34%, respectively (Table 4.10).. The panels in group B were able to develop an initial stiffness 27% higher than group A, meaning that their cross-sectional stiffness can resist early loads resulting from their weight, or that the higher grade of concrete reaches a large part of its strength at an early age.

All panels showed high resistance that could be attributed to the resistance of high strength of concrete, the presence of rectangular shear connectors and the EPS-concrete bond, also the additional ties with mesh reinforcement in the upper layer, and the reinforcement of the layers. The metal mesh in composite panels distributes the applied loads in two directions and over a large area instead of concentrating them at a single point due to its uniform shape. Additionally, it provides bonding to the concrete, which increases its tensile strength and resists cracking. Consequently, it increases the initial cracking load, the ultimate strength, and energy absorption.

From the side of the panel and in the middle of the cross-section in both the upper and lower concrete layers, the deflection was measured by using two LVDT. Figure 4.19 to Figure 4.24 illustrates the recorded displacement under applied loads. The relative movement between the top and bottom wythes under ultimate load was low due to the presence of concrete edges at the ends; the distribution of reinforcing steel and metal mesh extended into the supports, which contributed to transferring and distributing loads from the slabs to the supports while providing stability and balance to the sample and preventing the layers from shifting.

Table 4.9 Ultimate Load and First Crack Load with Deflection for Panels.

Specimens	P_u (kN)	Increasing Pu between A,B (%)	Δ_{max} (mm)	Increasing P_u between A,B (%)	P_{cr} (kN)	Δ_{cr} (mm)	Failure Mode
SA1	410	4.65	15	6.17	130	2.98	Shear
SA2	405	5.8	15.87	0.72	120	2.62	Shear
SA3	430	0	15.98	0	137	2.90	Shear
Ava.	415		15.61		129	2.84	
C.0.V%	2.6		2.82		5.4	5.53	
SB1	401	6.74	10.25	35.84	127	2.38	Shear
SB2	403	6.27	11.27	29.46	125	2.27	Shear
SB3	390	7.44	11.18	30.07	121	2.53	Shear
Ava.	398		10.90		124.33	2.39	
C.0.V%	1.44		4.21		2	4.42	

Table 4.10 Ductility Index ,Initial Stiffness and Energy Absorption for Panels.

Specimens	P_y (kN)	Δy (mm)	Ductility Index	Increasing (%)	Initial stiffness (kN/mm)	Increasing (%)	Energy Absorption (kN.mm)	Increasing (%)
SA1	257.58	9.42	5.02	8.73	27.33	-1.64	3322.05	15.86
SA2	225.71	8.84	6.05	-10.00	25.51	5.13	3806.82	3.58
SA3	245.01	9.12	5.5	0	26.89	0	3948.31	0
Ava.	242.77	9.54	5.53		26.57		3692.39	
C.0.V%	5.39	4.99	7.61		2.91		7.26	
SB1	294.01	7.52	4.30	21.82	39.09	-45.37	2207.56	44.09
SB2	261.5	7.31	4.96	9.82	35.73	-32.87	2639.63	33.15
SB3	284.2	8.14	4.42	19.64	34.88	-29.71	2461.97	37.64
Ava.	279.9	7.65	4.56		36.56		2436.38	
C.0.V%	4.86	4.60	6.29		4.97		7.27	

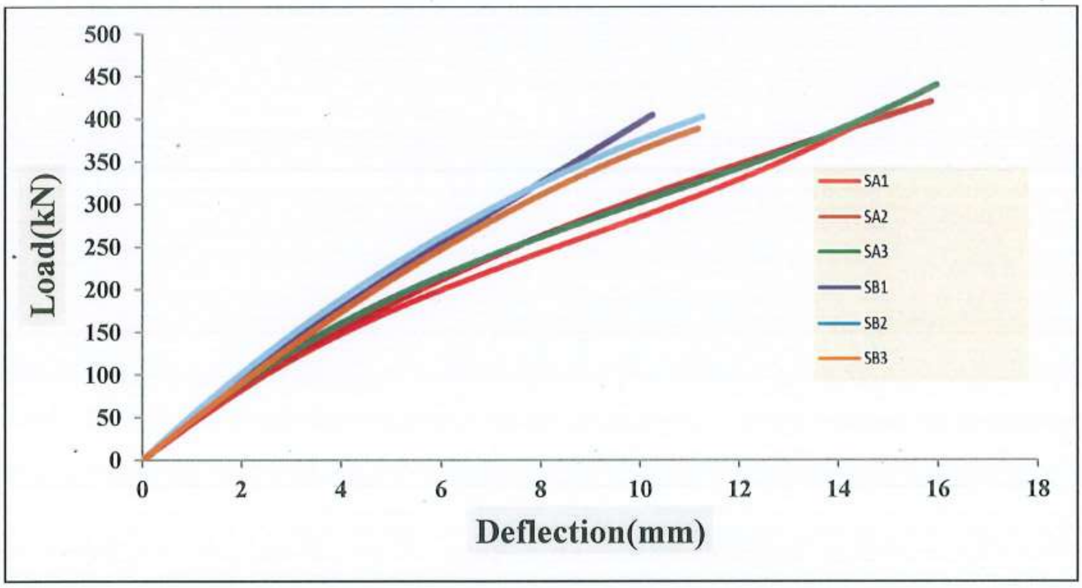

Figure 4.15 Load-Deflection Relationship for Panels.

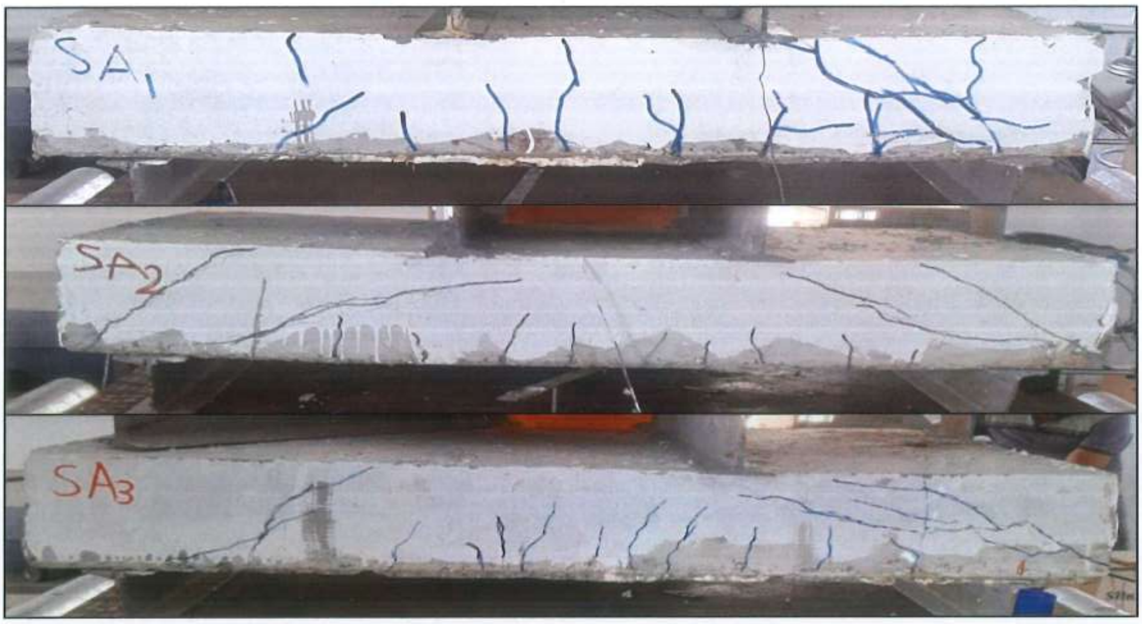

(a) Crack Pattern of SA Series.

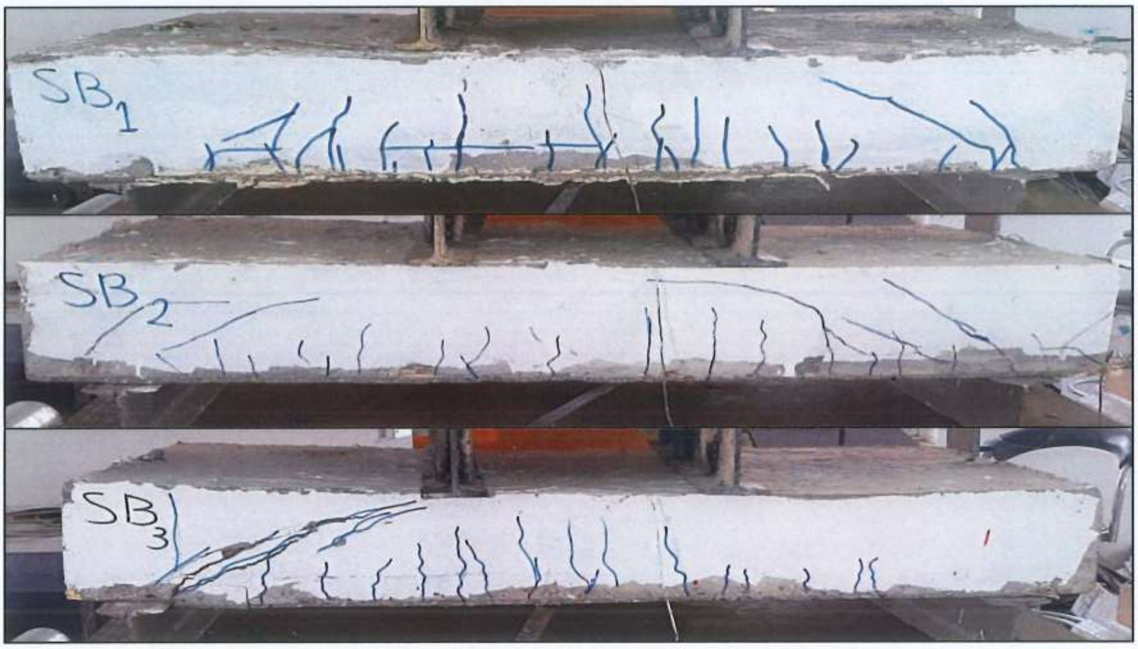

(b) Crack Pattern of SB Series

Figure 4.16 Crack Pattern of Panels with Rectangular- Shear Connector from Sides.

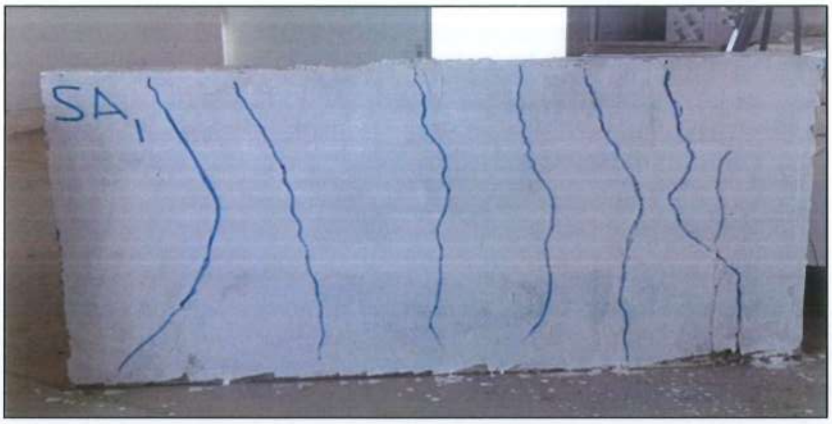

Panel SA1

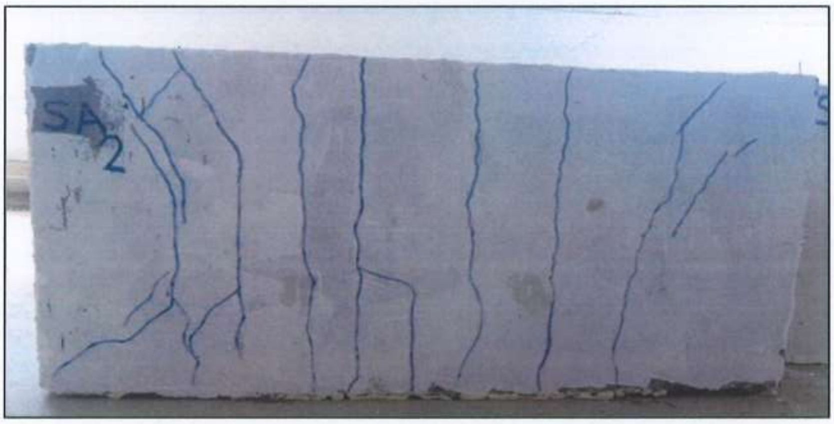

Panel SA2

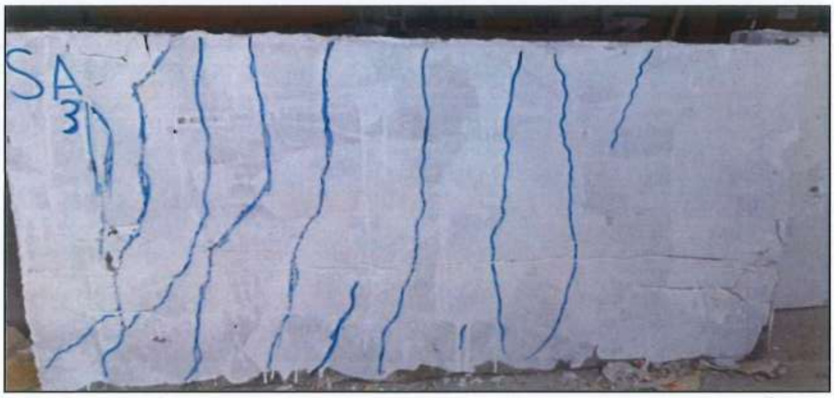

Panel SA3

Figure 4.17 Crack Pattern of SA Series from the Bottom Layer.

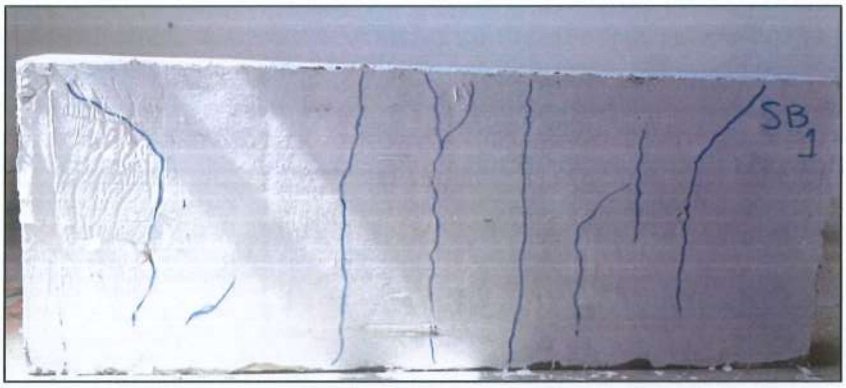

Panel SB1

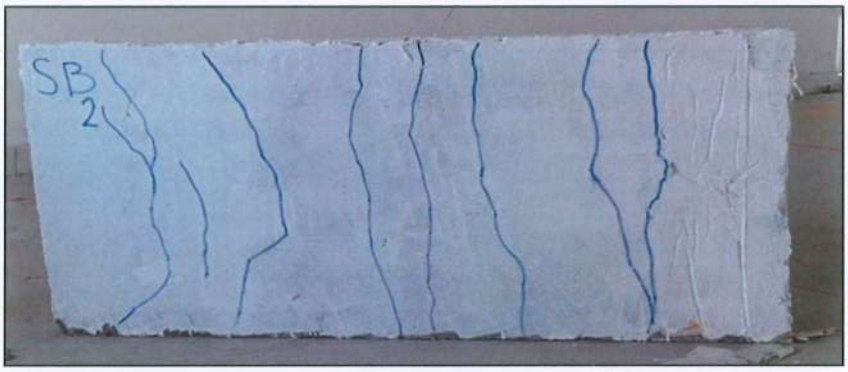

Panel SB2

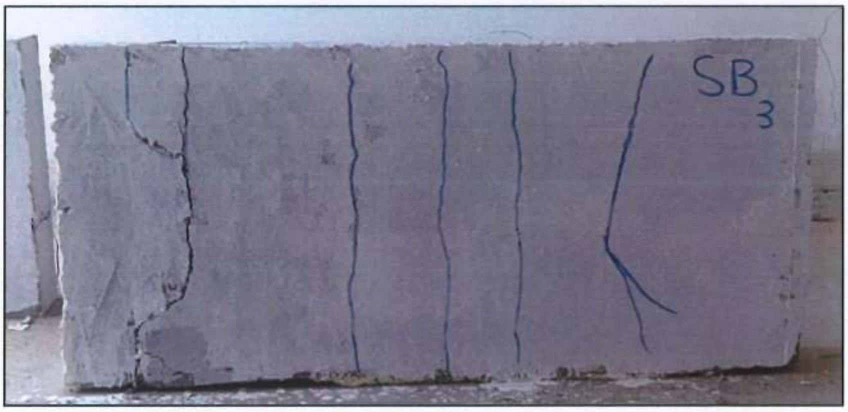

Panel SB3

Figure 4.18 Crack Pattern of SB Series from the Bottom Layer.

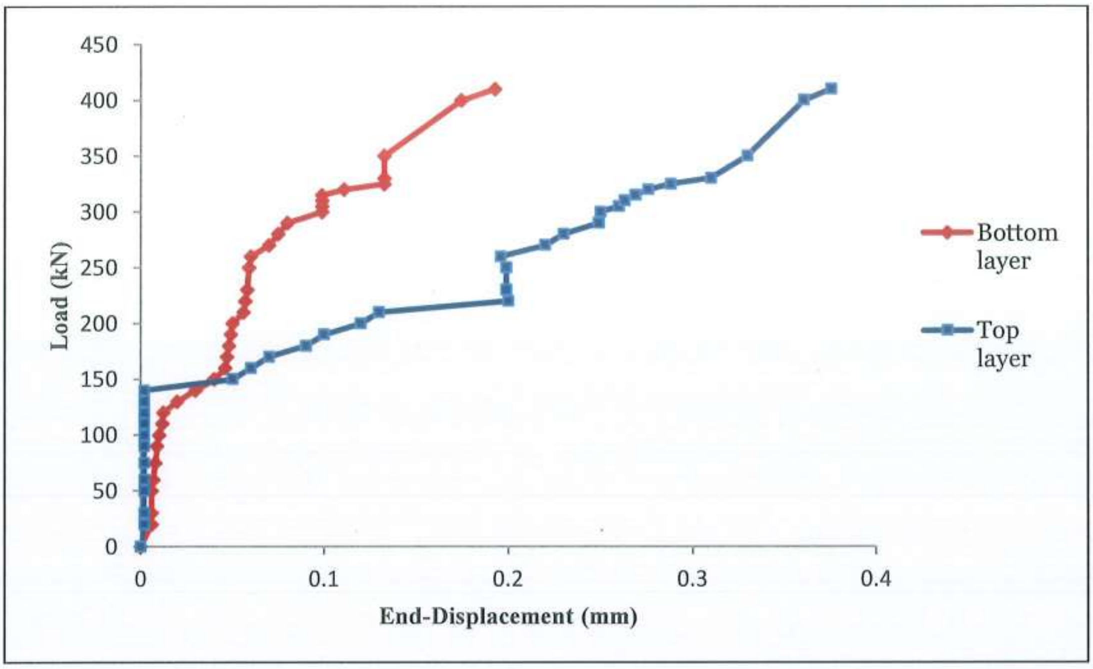

Figure 4.19 Load-End Displacement Relationship for Panel SA1.

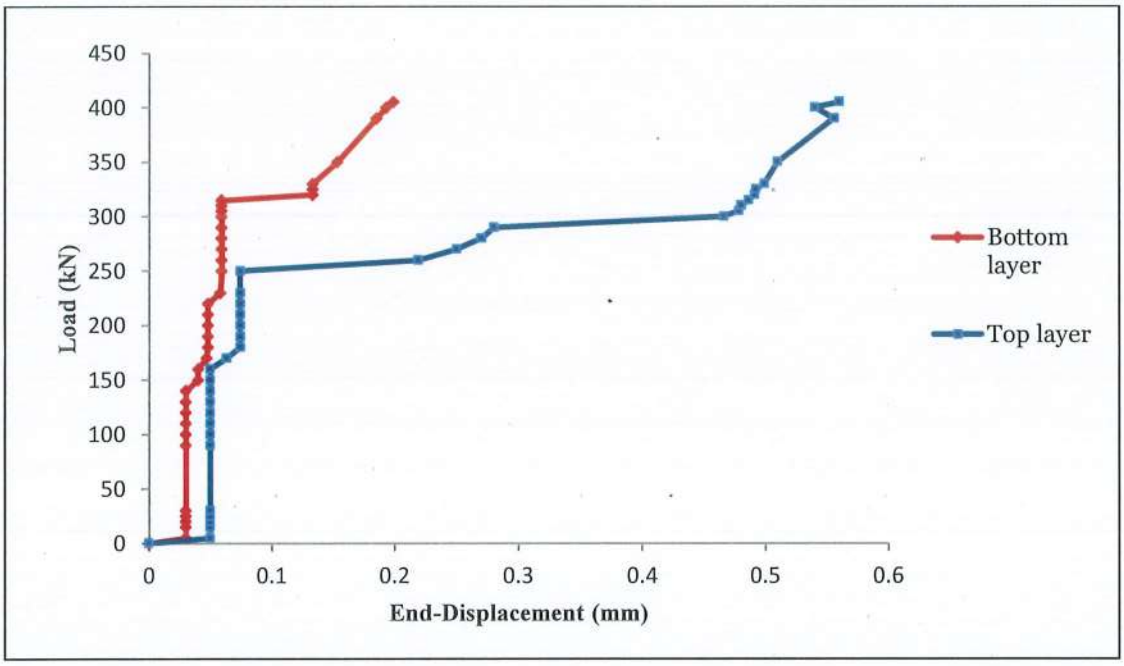

Figure 4.20 Load-End Displacement Relationship for Panel SA2.

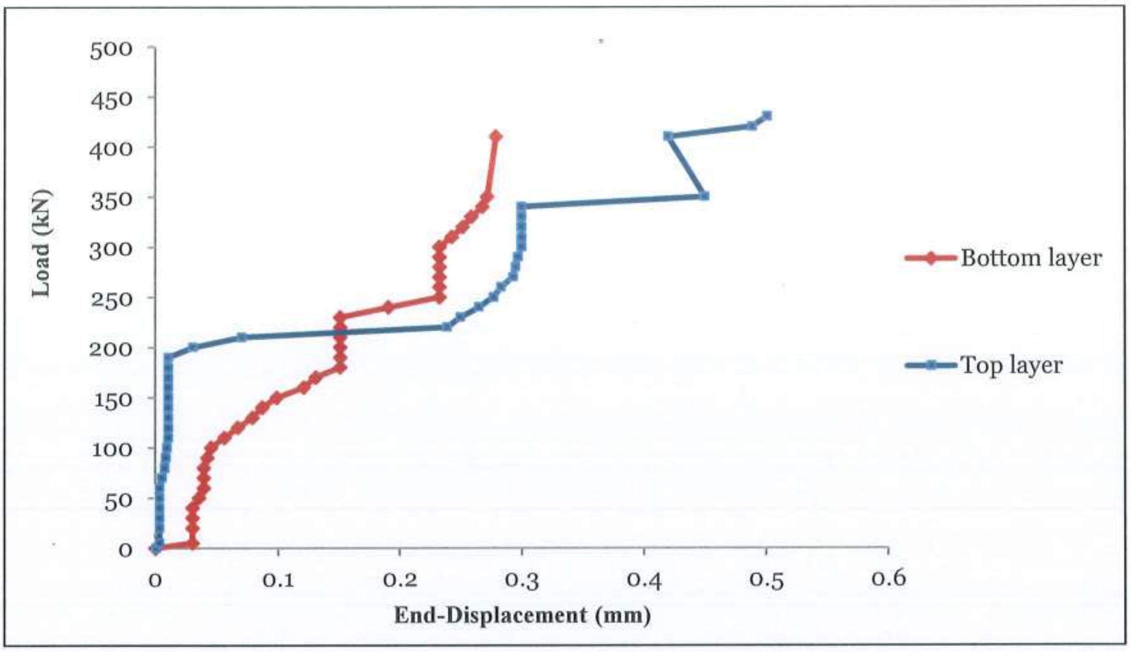

Figure 4.21 Load-End Displacement Relationship for Panel SA3.

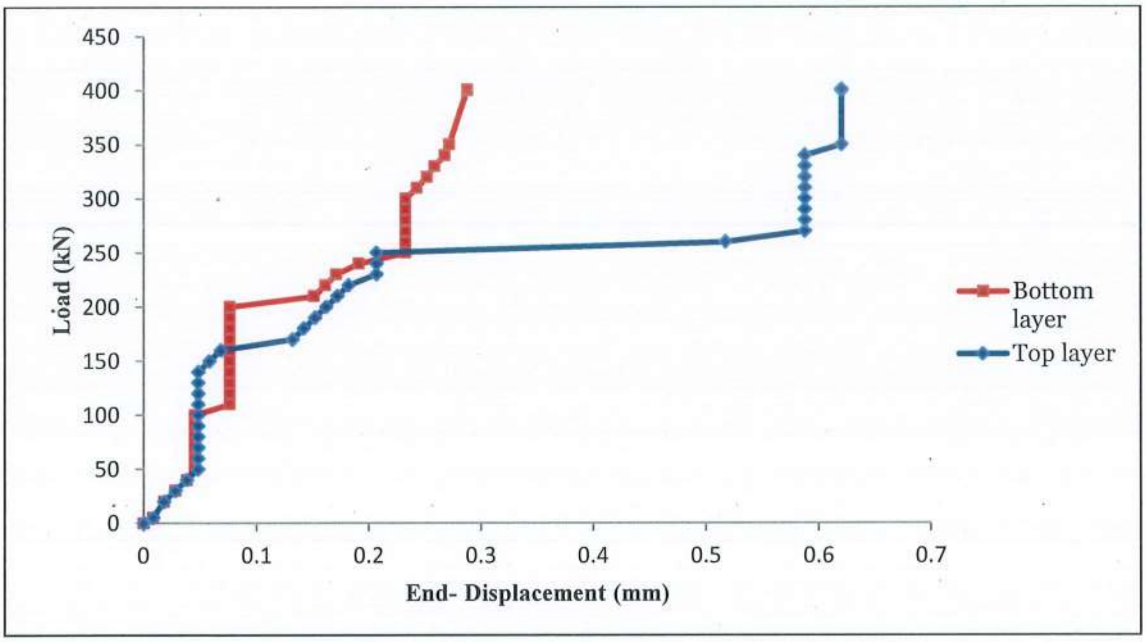

Figure 4.22 Load-End Displacement Relationship for Panel SB1.

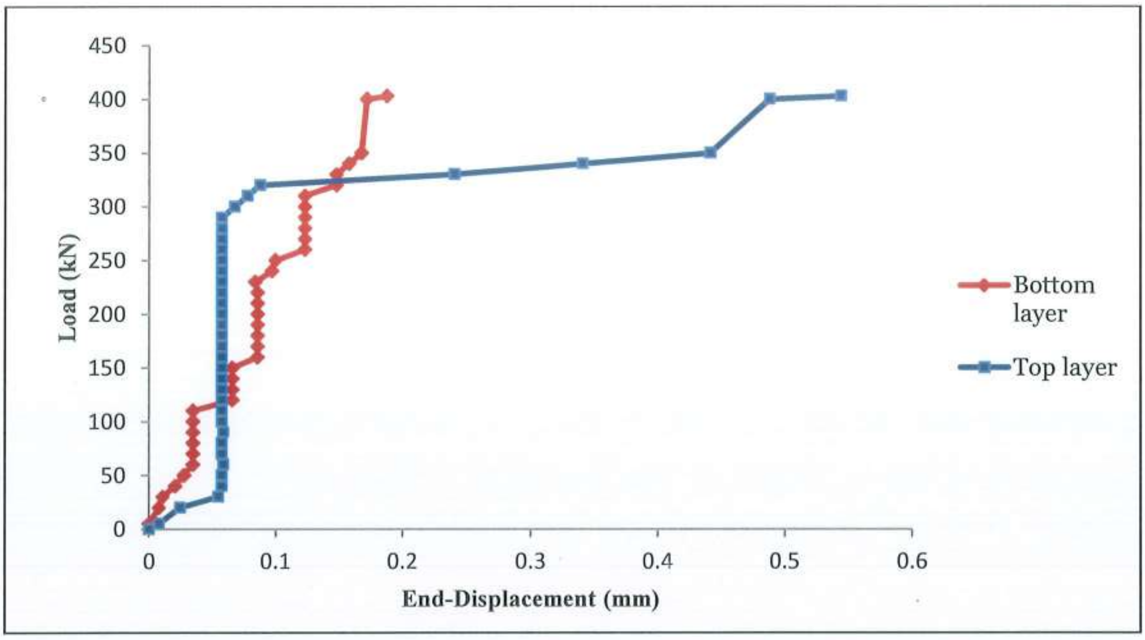

Figure 4.23 Load-End Displacement Relationship for Panel SB2.

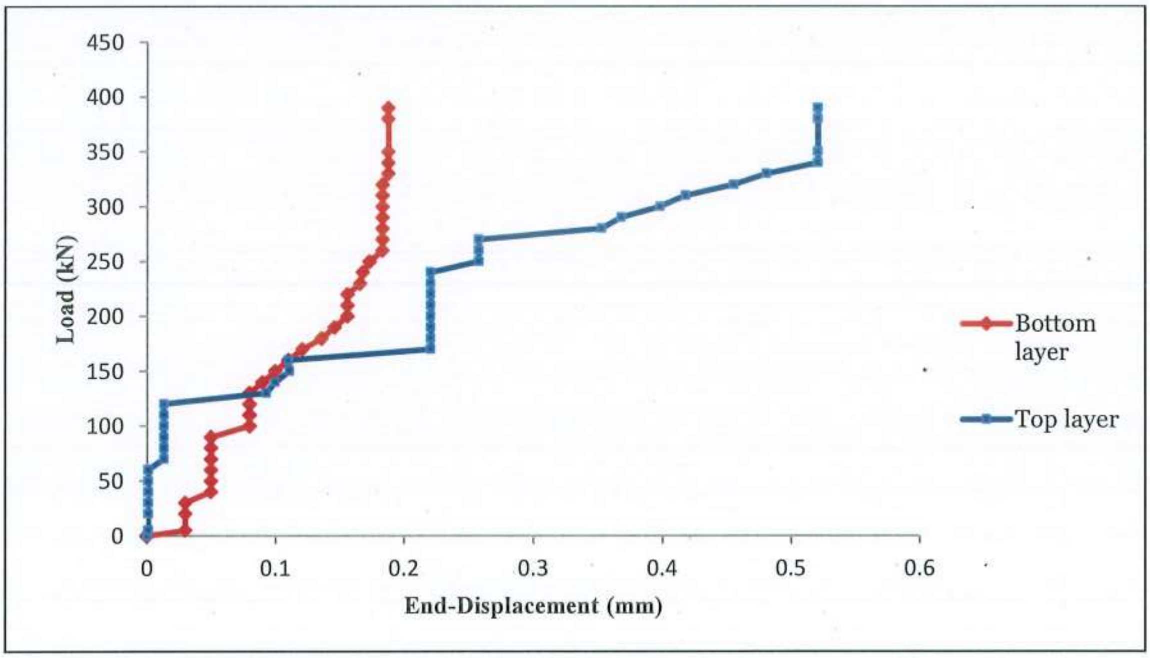

Figure 4.24 Load-End Displacement Relationship for SB3.

4.6.3 Responses to Load-Strain

Figure 4.25 displays the development of reinforcing strains at the midspan of representative specimens. In general, for all specimens, and according to the nature of the strain values, the bottom wythe experiences tensile stress while the top wythe experiences compressive stress. In composite panels, the code allows the use of one or more layers of metal mesh in both concrete layers as additional reinforcement with the steel bars or as a replacement for them. Concrete is a brittle material that can withstand compressive loads on its particles, but it separates under tension. In this study, mesh was added to the lower layer along with the reinforcement to increase tension resistance, while mesh was used only in the upper layer to provide tensile strength to the concrete in anticipation of a possible incident of partial or non-composite, which makes the concrete layers work separately.

Table 4.11 shows the magnitude of strains measured, the average maximum tensile strain is $4.20x10^{-3}$ for group SA and $2.58x10^{-3}$for group SB. This observed difference between the strains for the two groups is attributed to the effect of casting, where the high load-carrying capacity of SA1, SA2, and SA3 may allow for more tensile concrete strains before ultimate collapse.

Table 4.11 Ultimate Tensile and Compressive Strain at Failure Load for Panels.

Specimens	Ultimate Tensile Strain	Ultimate Compressive Strain
SA1	$4.15x10^{-3}$	$9.81\ x10^{-4}$
SA2	$3.95\ x10^{-3}$	$9.93\ x10^{-4}$
SA3	$4.45\ x10^{-3}$	$1.\ 12\ x10^{-3}$
Avg.	$4.20\ x10^{-3}$	$9.96\ x10^{-4}$
C.0.V%	2.23	2.14
SB1	$2.61\ x10^{-3}$	$9.30\ x10^{-4}$
SB2	$2.67\ x10^{-3}$	$8.96\ x10^{-4}$
SB3	$2.45\ x10^{-3}$	$8.75\ x10^{-4}$
Avg.	$2.58\ x10^{-3}$	$9.00\ x10^{-4}$
C.0.V%	3.16	3.55

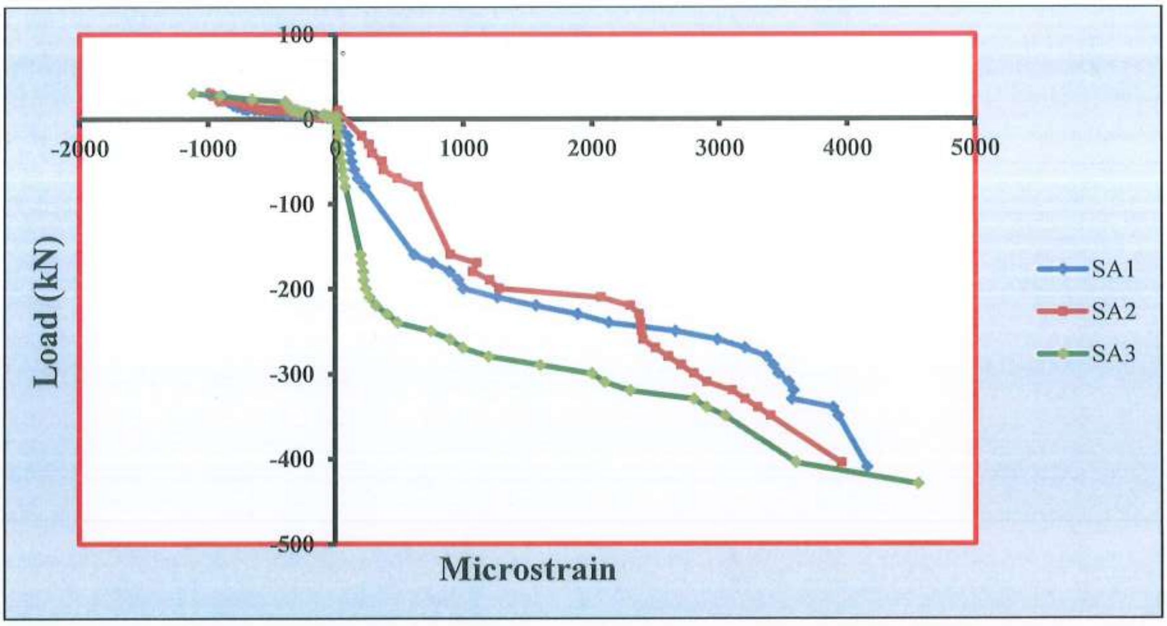

(a) Strain Distribution for SA Series

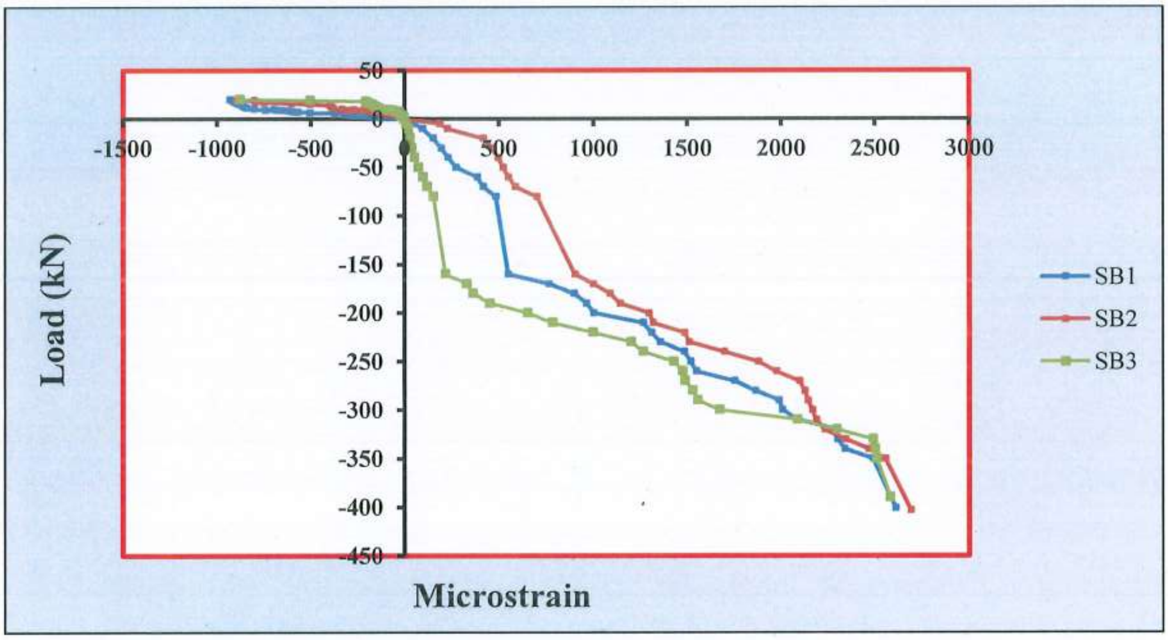

(b) Strain Distribution for SB Series

Figure 4.25 Tensile and Compressive Strain for Panels Between Top and Bottom Layers.

4.6.4 Determination of Composite Action Degree

Using equations 4.3, 4.5, and 4.6 [15, 22], Table 4.12 presents the full-composite action of experimental panels by K_1, where the forces were efficiently transferred between the wythes until failure. For experimental EPS panels, the cracking moment of inertia, Ict, is calculated by substituting the experimental values of flexural stiffness, K_0, and the modulus of elasticity of concrete into equation 4.6.The degree of composite action by K_2 was between 19% and 38%, less than that of K1, as a result of the structural element's resistance decreasing and stiffness decreasing brought on by the increase in stresses.

$$K_1 = \frac{P_{Exp}-P_{nc}}{P_c-P_{nc}} x100 \qquad 4.3\ [22]$$

$$K_2 = \frac{I_{Exp}-I_{nc}}{I_c-I_{nc}} x100 \qquad 4.5\ [15]$$

$$K_0 = \frac{162\ Ec\ I_{Exp}}{5L3} \qquad 4.6\ [15]$$

Where:

K_1 = Degree of composite action in terms of the ultimate strength .

K2 = Degree of composite action in terms of the stiffness.

I_{exp} =Experimental moment of inertia (mm^4).

I_c =Theoretical moment of inertia assuming fully-composite behavior (mm^4).

I_{nc} =Theoretical moment of inertia assuming non -composite behavior (mm^4).

K_0 = Flexural stiffness (kN/mm).

P_{Exp} =Ultimate load of experimental panel (kN).

P_c =Ultimate load of theoretical fully-composite panel (kN).

P_{nc} =Ultimate load of theoretical non-composite panel (kN).

Table 4.12 Degree of Composite Action.

Specimens ID	I_cx10^6 (mm^4)	I_{nc}x10^6 (mm^4)	I_{Exp}x10^6 (mm^4)	Pu(kN)			K_1 (%)	K_2 (%)
				Experimental panel	Full-composite panel	Non – composite panel		
SA1	77.4	10.4	25	410	228	119	266	21.8
SA2	77.4	10.4	23.4	405	228	119	262	19.4
SA3	77.4	10.4	24.6	430	228	119	285	21.3
SB1	77.4	10.4	35.8	401	228	119	258	38
SB2	77.4	10.4	32.8	403	228	119	260	33.4
SB3	77.4	10.4	32	390	228	119	248	32.2

4.7 Data Normalization for Panels

With a rectangle shear connector and for improving data quality and subsequently the performance of panels, the impact of the data normalization on the classification model can be presented by range transformation based on the maximum and minimum values of the load capacity. All models were compared with model SA3, and the percentage difference was 3% (less than 10), which is a better result [61]. Table 4.13 with Figure 4.26 shows the normalization norm relative to SA3.

Table 4.13 Normalization Data for Panels with Rectangle Shear Connector.

Panel	Pu (kN)	Normalization data
SA3	430	1.00
SA1	410	0.95
SA2	405	0.94
SB2	403	0.94
SB1	401	0.93
SB3	390	0.91

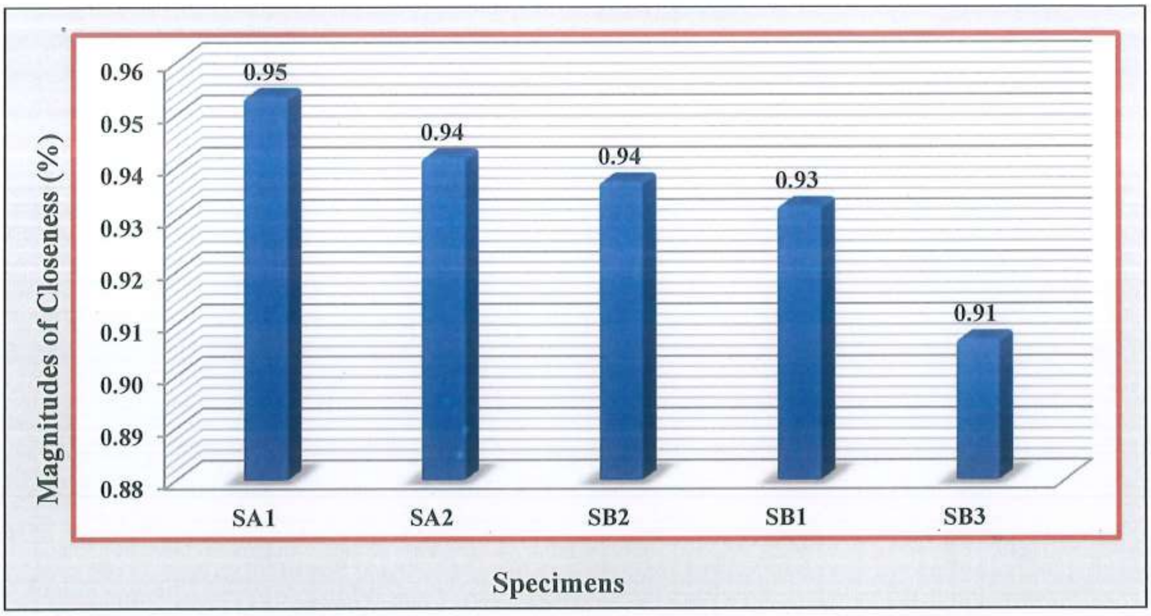

Figure 4.26 Normalization Norm with Rectangle Connector Relative to SA3.

CHAPTER FIVE:CONCLUSIONS AND RECOMMENDATIONS

5.1 General

The most significant findings from the experimental program results are reviewed in this chapter, along with some recommendations and suggestions for further research.

5.2 Conclusions

Based on three phases and the variables of the composite elements (beams and panels) that were investigated in this research, different conclusion points are drawn:

1-The rate of compressive strength of the HSSCC in the cubes was observed to be faster at the age of 3 days, up to 71.5% of 28 days, while it developed by 4% at 56 days.

2-For flexural and splitting tensile strength at 28 days, HSSCC recorded 10% and 19.8% of compressive strength, respectively.

3-The concrete achieved the advanced category of classification for which it was designed through its high flowability and spreading ability.

4-Casting in one stage, beams with a rectangular connector AR excelled in the averages of maximum load, maximum deflection, and energy absorption, while beams with an I-shaped connector AI excelled in the averages of initial stiffness and ductility index.

5-Casting in two stages, beams with a rectangular connector (BR) excelled in the averages of maximum load, ductility index, and energy absorption, while beams with an I-shaped connector (BI) excelled in the averages of initial stiffness and beams with Z-shaped (BZ) excelled in the average maximum deflection.

6-All beams with rectangular shear connectors and I-shaped and Z-shaped shear connectors failed in shear.

7-All beams with truss-shaped shear connectors failed in flexural.

8-Single-stage cast panels had higher rates of maximum load, maximum displacement, first crack load, deflection at first crack load, energy absorption, and ductility than two-stage cast plates by 4%, 30%, 3.6%, 15%, 34%, and 17%, respectively.

9-Panels cast in two stages (group B) were able to resist loads at an early stage by initial stiffness 27% higher than that cast in one stage(group A).

10-Degree of composite action for all panels was more than 100% in terms of maximum loads and between 19% and 38% in terms of stiffness.

11-All the composite panels failed due to the shear in the support zones.

12-The addition of wire mesh to the low layer increasing tension stress of panel specimens

13-The presence of concrete edges reduces layer movement and prevents their separation, contributes to stability, and provides additional resistance at the points of support.

5.3Recommendations for Future Work

1-Using other types of mesh (woven or welded) with the same shapes and the same way that the connectors were made in this study.
2-Study the flexural behaviour of one –way reinforced concrete panel with I-shaped ,Z-shaped and truss connectors.
3-Using the push-out test to investigate the behavior of the panel with shear connectors.
4-Study the flexural behaviour of two-way reinforced concrete panel with the four type shear connectors.
5-Study of the effect of fires on panel samples
6-Testing composite elements with an equal volume of friction for connectors.

7-Using the same welded wire mesh and steel reinforcement in both concrete wythes in panels.

8-Using of bonding material for connect between the concrete layer.

9-Investigating the concrete sandwich panel at various boundary conditions or under various loading scenarios, dynamic, and concentrated loads

1. Yardim, Y., et al., *AAC-concrete light weight precast composite floor slab.* Construction and Building materials, 2013. **40**: p. 405-410.DOI: https://doi.org/10.1016/j.conbuildmat.2012.10.011.

2. Putra, I.M.D.P., N.K.A. Agustini, and I.G.A.P. Eryani, *Analysis of Deviation Behavior in the SMAN 2 Abiansemal Building with the SRPMK System and Flat Slab.* Journal of Infrastructure Planning and Engineering, 2025. **4**(1): p. 39-44.DOI: https://doi.org/10.22225/jipe.4.1.2025.39-44.

3. Evstratova, A., et al. *Design of prefabricated reinforced concrete structures: comparative analysis of prefabricated reinforced concrete floor slab*. in *IOP Conference Series: Materials Science and Engineering*. 2021. IOP Publishing.

4. Yang, L., et al., *Experimental Study on Bending Behaviors of Ultra-High-Performance Fiber-Reinforced Concrete Hollow-Core Slabs.* Buildings, 2025. **15**(5): p. 812.DOI: https://doi.org/10.3390/buildings15050812.

5. Thienel, K.-C., T. Haller, and N. Beuntner, *Lightweight concrete—From basics to innovations.* Materials, 2020. **13**(5): p. 1120.DOI: http://dx.doi.org/10.3390/ma13051120.

6. Mohi-Ud-Din, M.M., et al., *Exploring the potential of rigid polyurethane foam waste in structural lightweight concrete.* Next Materials, 2025. **6**: p. 100399.DOI: https://doi.org/10.1016/j.nxmate.2024.100399.

7. Choi, K.-B., et al., *In-plane shear behavior of insulated precast concrete sandwich panels reinforced with corrugated GFRP shear connectors.* Composites Part B: Engineering, 2015. **79**: p. 419-429.DOI: http://dx.doi.org/10.1016/j.compositesb.2015.04.056.

8. Moura, B., et al., *Eco-Efficiency of Concrete Sandwich Panels with Different Insulation Core Materials.* Sustainability, 2025. **17**(4): p. 1687.DOI: https://doi.org/10.3390/su17041687.

9. Tawil, H., et al., *Mechanical and thermal properties of composite precast concrete sandwich panels: A Review.* Buildings, 2022. **12**(9): p. 1429.DOI: https://doi.org/10.3390/buildings12091429.

10. Kandil, M.A.E.-N., et al., *Effect of changing properties of wythes in precast structural sandwich panels.* Civil Engineering Journal, 2020. **6**(9): p. 1765-1778.DOI: http://dx.doi.org/10.28991/cej-2020-03091581.

11. Joseph, J.D.R., J. Prabakar, and P. Alagusundaramoorthy, *Experimental studies on through-thickness shear behavior of EPS based precast concrete sandwich panels with truss shear connectors.* Composites Part B: Engineering, 2019. **166**: p. 446-456.DOI: https://doi.org/10.1016/j.compositesb.2019.02.030.

12. Benayoune, A., et al., *Flexural behaviour of pre-cast concrete sandwich composite panel–experimental and theoretical investigations.* Construction and Building Materials, 2008. **22**(4): p. 580-592.DOI: doi:10.1016/ j. conbuildmat .2006.11.023.

13. O'Hegarty, R. and O. Kinnane, *Review of precast concrete sandwich panels and their innovations.* Construction and building materials, 2020. **233**: p. 117145.DOI: https://doi.org/10.1016/j.conbuildmat.2019.117145.

14. Joseph, J.D.R., J. Prabakar, and P. Alagusundaramoorthy, *Precast concrete sandwich one-way slabs under flexural loading.* Engineering Structures, 2017. **138**: p. 447-457.DOI: http://dx.doi.org/10.1016/j.engstruct.2017.02.033.

15. Guerrero, N., et al., *Experimental and numerical investigation on the behavior of concrete sandwich slab panel for a structural system.* Journal of Building Engineering, 2024. **86**: p. 108930.DOI: https://doi.org/ 10.1016/j.jobe .2024.108930.

16. Jacquier, N. and U.A. Girhammar. *Tests on shear connections in prefabricated composite cross-laminated-timber and concrete elements*. in *World Conference on Timber Engineering: 15/07/2012-19/07/2012*. 2012. New Zealand Timber Design Society.

17. Zende, A.A., et al., *Mechanical Properties of High-Strength Self-Compacting Concrete.* ACS Omega, 2023. **8**(20): p. 18000-18008.DOI: https://doi.org/10.1021/acsomega.3c01204?urlappend=%3Fref%3DPDF&jav=VoR&rel=cite-as.

18. Aditto, F.S., et al., *Fresh, mechanical and microstructural behaviour of high-strength self-compacting concrete using supplementary cementitious materials.* Case Studies in Construction Materials, 2023. **19**: p. e02395.DOI: https://doi.org/10.1016/j.cscm.2023.e02395.

19. Azare, A.A., et al., *Mechanical and Microstructural Characteristics of High-Strength Self-Compacting Concrete (HSSCC) with Optimal Silica Fume and Fly Ash Cement Replacement.* International Journal of Sustainable Construction Engineering and Technology, 2024. **15**(4): p. 81-99.DOI: https://doi.org/ 10. 30880/ijscet.2024.15.04.007.

20. Chilwesa, M., et al., *Evaluating the shear bond strength between old and new concrete through a new test method.* Magazine of Concrete Research, 2017. **69**(9): p. 425-435.DOI: http://dx.doi.org/10.1680/jmacr.16.00327.

21. Halicka, A., *Influence new-to-old concrete interface qualities on the behaviour of support zones of composite concrete beams.* Construction and

Building Materials, 2011. **25**(10): p. 4072-4078.DOI: http://dx.doi.org/ 10. 1016 /j.conbuildmat.2011.04.045.

22. Tomlinson, D. and A. Fam, *Flexural behavior of precast concrete sandwich wall panels with basalt FRP and steel reinforcement.* PCI journal, 2015.

23. Mahdi, S., et al., *Experimental investigation into the structural behaviour of ultra-high performance fibre-reinforced concrete box-celled composite panels.* Composites Part C: Open Access, 2022. **9**: p. 100329.DOI: https://doi.org/10 .1016/j.jcomc.2022.100329.

24. Lee, J.-H., et al., *Structural behavior of durable composite sandwich panels with high performance expanded polystyrene concrete.* International Journal of Concrete Structures and Materials, 2018. **12**: p. 1-13.

25. Richard, O., et al., *Composite behaviour of fibre-reinforced concrete sandwich panels with FRP shear connectors.* Engineering Structures, 2019. **198**: p. 109475.

26. Wang, Y., et al., *Flexural Behavior of Insulated Concrete Sandwich Panels using FRP-Jacketed Steel-Composite Connectors.* Advances in Materials Science and Engineering, 2022. **2022**(1): p. 6160841.

27. Toghroli, A., et al., *Prediction of shear capacity of channel shear connectors using the ANFIS model.* Steel Compos Struct, 2014. **17**(5): p. 623-639.

28. Titoum, M., et al., *Experimental study and finite element modelling of push-out tests on a new shear connector of I-shape.* Advanced Steel Construction, 2016. **12**(4): p. 487-506.

29. Mohammed, M.H., *Behavior of Steel Fiber Reinforced Self Compacting Concrete Slabs under One-way Bending*. 2015, Eng. & Tech. Journal.

30. Fares, A.E.-R., H. Hassan, and M. Arab, *Flexural behavior of high strength self-compacted concrete slabs containing treated and untreated geogrid reinforcement.* Fibers, 2020. **8**(4): p. 23.

31. Shaheen, Y.B. and E.A. Eltehawy, *Structural behaviour of ferrocement channels slabs for low cost housing.* Concrete Research Letters, 2017. **8**(2).DOI: https://doi.org/10.20528/cjcrl.2017.02.002.

32. M Erfan, A., et al., *Behavior of Self Compacted Concrete Ferrocement Beams.* Journal of Engineering Research and Reports, 2021. **21**(1): p. 1-14.DOI: 10.9734/JERR/2021/v21i117434.

33. El-Dehemy, H., et al., *Shear behavior of RC beams with multiple web openings having no shear reinforcement internally reinforced with expanded metal meshes.* Case Studies in Construction Materials, 2025: p. e05655.

34. *Iraqi Standard No. 5 /2019*, in *Portland cement Central Organization for Standardization and Quality Control Iraq*. 2019.

35. ASTM/C150, *Standard Specification forPortland Cement.* 2007.

36. *Iraqi Standard No. 45/1984* in *Requirements of the used fine and coarse aggregate in the concrete mixes*. 1984.

37. ASTM/C33, *Standard Specification for Concrete Aggregates.* , 2008.

38. ASTM/C1240, *Standard Specification forSilica Fume Used in Cementitious Mixtures.* 2003.

39. *Physical and mechanical properties of Silica Fume . Available from:* www.conmix.com.

40. ASTM/C494, *Standard Specification forChemical Admixtures for Concrete.* 2005.

41. *Superplasticizer Technical Characteristics. Available from: irq.sika.com*.

42. ASTM/A615, *Standard Specification forDeformed and Plain Carbon-Steel Bars for ConcreteReinforcement.* 2012.

43. de Felice, G., et al., *Guide to Design and Construction of Externally Bonded Fabric-Reinforced Cementitious Matrix (FRCM) and Steel-Reinforced Grout (SRG) Systems for Repair and Strengthening Masonry Structures*, in *ACI 549.6 R-20*. 2020, American Concrete Institute. p. 1-159.

44. ASTM(A1064/A1064M), *Standard Specification for Carbon-Steel Wire and Welded Wire Reinforcement, Plain and Deformed, for Concrete.* 2012.

45. *Properties of InsulFoam Flat EPS .Available from: www.carlislesyntec .com*.

46. ASTM/A370, *Standard Test Methods and Definitions forMechanical Testing of Steel Products* 2007.

47. IS10262, Indian standard. *Concrete mix propotioning* 2019.

48. BS12350-8, *Testing fresh concrete: Self-compacting concrete — Slump flow test.* 2010.

49. BS12350-12, *Testing fresh concrete: Self-compacting concrete — J-ring test.* 2010.

50. BS12350-9, *Testing fresh concrete: Self-compacting concrete — V-funnel test.* 2010.

51. BS EN 12390-3, *Standard Test Method forCompressive Strength of cubic Concrete Specimens.* 2019.

52. ASTM/C78, *Standard Test Method forFlexural Strength of Concrete (Using Simple Beam withThird-Point Loading.* 2018.

53. ASTM/C496, *Standard Test Method forSplitting Tensile Strength of Cylindrical ConcreteSpecimens.* 2006.

54. ACI318-14, *Building Code Requirements for Structural ConcreteOne way slab* . 2014.

55. ANSI/AISC, *Specification for structural steel buildings.* 2005. **36010**.

56. ALMULLA, J., *Precast Insulated Sandwich Panels Using Self Consolidating Lightweight Pumice Concrete* 2014: New Zealand

57. Sococol, I., P. Mihai, and I. Olteanu-Donţov, *Ductility–concept for improving the seismic response for structural reinforced concrete frame systems.* Buletinul Institutului Politehnic din Iasi. Sectia Constructii, Arhitectura, 2019. **65**(1): p. 17-30.

58. Abdulraheem, M.S., *Experimental investigation of fire effects on ductility and stiffness of reinforced reactive powder concrete columns under axial compression.* Journal of Building Engineering, 2018. **20**: p. 750-761.DOI: /10.1016/j.jobe.2018.07.028

59. Sullivan, T., G. Calvi, and M. Priestley. *Initial stiffness versus secant stiffness in displacement based design.* in *13th World Conference of Earthquake Engineering (WCEE).* 2004.

60. Myers, J.J. and R.L. Carrasquillo, *Influence of hydration temperature on durability and mechanical property performance of prestressed and precast high-performance concrete beams.* Transportation research record, 2000. **1696**(1): p. 131-142.

61. Milani, A., et al., *The effect of normalization norms in multiple attribute decision making models: a case study in gear material selection.* Structural and multidisciplinary optimization, 2005. **29**: p. 312-318.

Appendix A

High-strength self-compacting concrete mix design

- Concrete grade M70
- Calculations of mix design according to (IS 10262): 2019

1-Target strength f'_{ck} $=70 + 1.65 \times 6$

$=79.9$ MPa

or f'_{ck} $=70+8$

$= 78$ MPa , use79.9 MPa

S = 6 standard deviation, in N\ mm^2

X = 8 factor based on the grade of concrete

2- W/C = 0.32 (Table 7 and Table 8)

Water content per cubic meter of concrete for nominal maximum sizes of aggregate 10 mm = 200kg and for slump (760-850)mm ,water content will increase:

$$W_{cx} = W_c50+\frac{(x-50)}{25} \times 0.03 \times W_{50}$$

$$W_{cx} =200+\frac{(760-50)}{25} \times 0.03 \times 200$$

$$= 370.4\text{kg}$$

Using superplasticizer (third generation) reduces water content by 30%:

$$Wc = 370.4 \times 0.7$$

$$= 259.28\text{kg}$$

$$\text{Volume} = \frac{Mass}{specific\ gravity} x \frac{1}{1000}$$

$$= \frac{259.28}{1} x \frac{1}{1000}$$

$$= 0.2593 \text{ m}^3$$

3- Cementitious content $= \frac{Wc}{W\backslash C \text{ ratio}}$

$$= \frac{259.28}{0.32}$$

$$= 810.25\text{kg}$$

Increasing the cementitious by 10% =1.1 x 810.25

=891.27kg

$W_c = \frac{259.28}{891.27}$

= 0.291

Dosage of silica content 10% = 89.12 kg

Volume $= \frac{89.12}{2.2} \times \frac{1}{1000}$

$= 0.0405 m^3$

Cement content = 891.27- 89.12

= 802.15kg

Volume $= 0.2538 m^3$

4-The dosage of superplasticizer =2%

Volume $= \frac{891.2 \times 0.02}{1.08} \times \frac{1}{1000}$

$= 0.0165 m^3$

5-From Table 10, volume of coarse aggregate per unit volume of total aggregate for zone II=0.54, air content as percentage of the volume of concrete=0.01(Table6), reduces water content by 30%,Wc=0.291

Volume of coarse aggregate per unit volume of total aggregate $= 0.54 + (\frac{0.3-0.291}{0.01}) \times 0.01$

= 0.55

Volume of fine aggregate =1-0.55

= 0.45

Total volume of coarse aggregate =0.2593+0.2538+0.0405+0.0165

= 0.5701

Mass of coarse aggregate =0.5701x0.55x2.75x1000

$= 862.3 kg/m^3$

Mass of fine aggregate = 0.5701x0.45x2.65x1000

$= 679.8 kg/m^3$

6-The water ratio has been redacted to 24.5% for high results ,so the material quantities of concrete mix are:

(cement: sand: gravel) =1:0.91:1.06

cement = 802.14 kg/m^3

sand =726.9 kg/m^3

gravel =851.3 kg/m^3

water =219.48 L

SP =17.8 L (2%)

SF =89.12 kg/m^3 (10%)

Appendix B

The theoretical beam designed according to ACI 318-14 Code.

All beams with the same cross-section , compressive strength, and similar reinforcement.

Cross-section(hxb) =(200x200mm)
$f_y = 464.3$ MPa ,f'_c=57.76 MPa

1- Area of steel

To assess the performance of the connector, it was tested using the lowest percentage of reinforcing steel through the beam. The ACI 318 proposed the following equation for calculating the minimum reinforcement:

$$As_{min} = \frac{0.25\sqrt{fc'}}{fy} \, bw \, d$$

$$= 139 \text{ mm}^2 \qquad \text{(use 2Ø10mm)}$$

d=170mm(cover=25mm)

$$\rho = \frac{AS}{bd}$$

$$= 4.088 \times 10^{-3}$$

$$\rho b = 0.85\beta 1 \left(\frac{fc'}{fy}\right)\left(\frac{600}{600+fy}\right)$$

$$= 0.04 \qquad ,(\rho b > \rho)$$

$$\rho max = 0.85 \left(\frac{fc'}{fy}\right)\left(\frac{\varepsilon cu}{\varepsilon cu + 0.004}\right)$$

$$= 0.045$$

2-Uncracked section

The flexural member's stiffness is determined by both the modulus of elasticity and the moment of inertia. the beam's deflection based on a homogenous, uncracked area at loads lower than the cracking load.

$$fr = 0.62\sqrt{fc'} \qquad ,n=Es/Ec \ (n=6)$$

$$= 4.661 \text{ MPa}$$

$$\bar{y} = \frac{\Sigma A.y}{\Sigma A} \text{ or } h/2$$

$$= 100\text{mm}$$

$$I_{ut} = \frac{bh^3}{12}$$

$$=133.5\ x10^6\ mm^4$$

$$M_{cr} = fr.\ \frac{I_{ut}}{h-\bar{y}}$$,P_{cr}=37.8kN

$$=6.3\ kN.m$$

$$\Delta_{cr} = \frac{23Pcr.L3}{648EIut}$$ (For two point loads and a=L/3)

$$=0.28mm$$

3-Cracked section

The theoretical ultimate load and maximum deflection are obtained by the moment under a two-point load, where the effective moment of inertia varies considerably along the span. Only the transformed cracked sections are useful in assessing the member's stiffness at the cracked area; hence,

$$K = (\sqrt{n}\ \rho^2 + 2n\ \rho) - 2n\ \rho$$

$$=0.172$$

$$M_y = A_s f_y (d - \frac{kd}{3})$$,P_y=61.8kN

$$=10.3kN.m$$

$$I_{ct} = \frac{b.c^3}{3} + nAs(d-kd)^2$$

The position of the neutral axis is:

$$\Sigma M_{N.A=0}$$

$$\frac{200x^2}{2} = nAs(d-x)$$

$$x^2 + 8.34x - 1417.8 = 0$$

$$x = 33.7mm$$

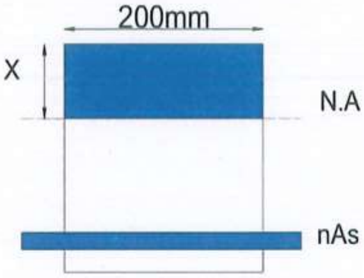

$$I_{ct} = 19.18x10^4 mm^4$$

$$I_{eff} = (\frac{Mcr}{Ma})^3 I_{ut} + (1 - (\frac{Mcr}{Ma})^3) I_{ct}$$ ($I_{eff} \leq I_{ut}$)

$$a = \frac{AS\ fy}{0.85fc'\ b}$$

6.5mm

$$M_u = A_S f_y\ (\ d - \frac{a}{2})$$,P_u=64.2kN

$=10.7\text{kN.m}$

$I_{eff} = 51\text{x}10^4\text{mm}^4$

$\Delta_y = 1.21\text{mm}$

$\Delta_{max} = 1.3\text{mm}$

Appendix C

State of the high-strength self- compacting composite concrete beams cast in one stage and two stages with rectangular, I-shaped, Z-shaped, and truss-shaped connectors

In this study, a thin metal layer of 3 mm thickness of expanded mesh is used in composite beams as shear connectors, divided into two groups. The first group was cast as a reference group in one stage to compare with the second group, which was cast in two stages. The type of casting (one or two) was investigated, as well as the type of shear connectors. The load-deflection curve of four pairs of points (zero, the first crack load and its deflection, the yield load and its deflection, and the ultimate load and the maximum deflection), used to know the characteristics of the theatrical beam model sampled CB (Appendix B). In general, all groups showed linear-elastic behavior before the first flexural cracking appeared. After that, the deflection increased as the load scaled to the ultimate load. The ultimate loads of all beams were higher than that of the theoretical specimen CB. The large increase in applied loads for all samples compared to the calculated beam CB is actually due to the presence of shear connectors in addition to the steel reinforcement (Appendix C Table 2). As for the type of connector and the casting method, their effect appears in the difference in values between groups A and B. Since the initial stiffness is defined as the ratio of the load to the deflection at the yield point, specimen CB has a lower deflection at the yield load and consequently exhibits higher initial stiffness. This indicates that model CB can develop resistance to early loads without significant deflection, and the reason is the stiffness of the section or the grade of concrete used.

Appendix C Table 1 The Properties of the Theoretical Beam CB.

Properties	Calculated value	Properties	Calculated value
P_{cr} (kN)	37.8	Δ_{cr}(mm)	0.28
P_y(kN)	61.8	Δ_y(mm)	1.21
P_u(kN)	64.2	Δ_{max}(mm)	1.3
Ductility Index	1.07		
Initial stiffness (kN/mm)	51		
Energy Absorption (kN.mm)	52		

All the tested beams reached a deflection level higher than in model CB before failure, indicating their resistance to plastic deformation rather than brittle failure. This was demonstrated by the high ductility index and energy absorption of the experimental models.

Appendix C Table 2 Comparison Between Theoretical and Experimental beam in Ultimate load and Maximum Deflection.

Specimens	Ultimate load P_u (kN)	Difference in Ultimate-load in relation to CB (%)	Δmax (mm)	Difference in Δmax in relation to CB (%)
CB	64.2	0	1.3	0
AR1	264	-355.2	15.28	-1075.4
AR2	230	-296.6	14.62	-1024.6
AR3	246	-324.1	16.34	-1156.9
BR1	219	-277.6	9.5	-630.8
BR2	205	-253.4	8.12	-524.6
BR3	212	-265.5	8.72	-570.8
AI1	216	-272.4	7.22	-455.4
AI2	195	-236.2	7.42	-470.8
AI3	235	-305.2	9.64	-641.5
BI1	190	-227.6	7.31	-462.3
BI2	207	-256.9	8.21	-531.5
BI3	190	-227.6	7.53	-479.2
AZ1	175	-201.7	8.94	-587.7
AZ2	151	-160.3	7.95	-511.5
AZ3	181	-212.1	9.12	-601.5
BZ1	164	-182.8	8.01	-516.2
BZ2	174	-200	9.83	-656.2
BZ3	187	-222.4	8.65	-565.4
AT1	131	-125.9	7.86	-504.6
AT2	135	-132.8	7.989	-514.5
AT3	136	-134.5	7.95	-511.5
BT1	130	-124.1	6.73	-417.7
BT2	123	-112.1	5.21	-300.8
BT3	128	-120.7	5.98	-360

Appendix C Table 3 Comparison Between Theoretical and Experimental beam in Ductility Index, Initial stiffness, and Energy Absorption.

Specimens	Difference in the ductility index in relation to CB (%)	Difference in initial stiffness as compare with CB (%)	Difference in energy absorption as compare with CB (%)
Theoretical beam CB	0	0	0
AR1	-16.8	66.1	-4196.1
AR2	-91.6	69.2	-3663.3
AR3	-122.4	70.5	-4097.2
BR1	-120.6	54.8	-2233.2
BR2	-175.7	50.6	-1818
BR3	-164.5	52.3	-2065.7
AI1	-89.7	41.4	-1386.3
AI2	-132.7	48.5	-1342.9
AI3	-120.6	52.2	-1993.7
BI1	-119.6	49.1	-1406.6
BI2	-81.3	50.6	-1694.8
BI3	-88.8	50.5	-1486.2
AZ1	-90.7	61.6	-1433.6
AZ2	-117.8	62.8	-1102.8
AZ3	-57.9	61.1	-1510.4
BZ1	-77.6	59.9	-1251
BZ2	-68.2	65.3	-1704.2
BZ3	-89.7	57.6	-1482.6
AT1	-106.5	67.3	-262
AT2	-62.6	66.9	-292.7
AT3	-131.8	66.5	-293.9
BT1	-88.8	62.2	-225.6
BT2	-78.5	53.7	-120.6
BT3	-33.6	58	-173.5

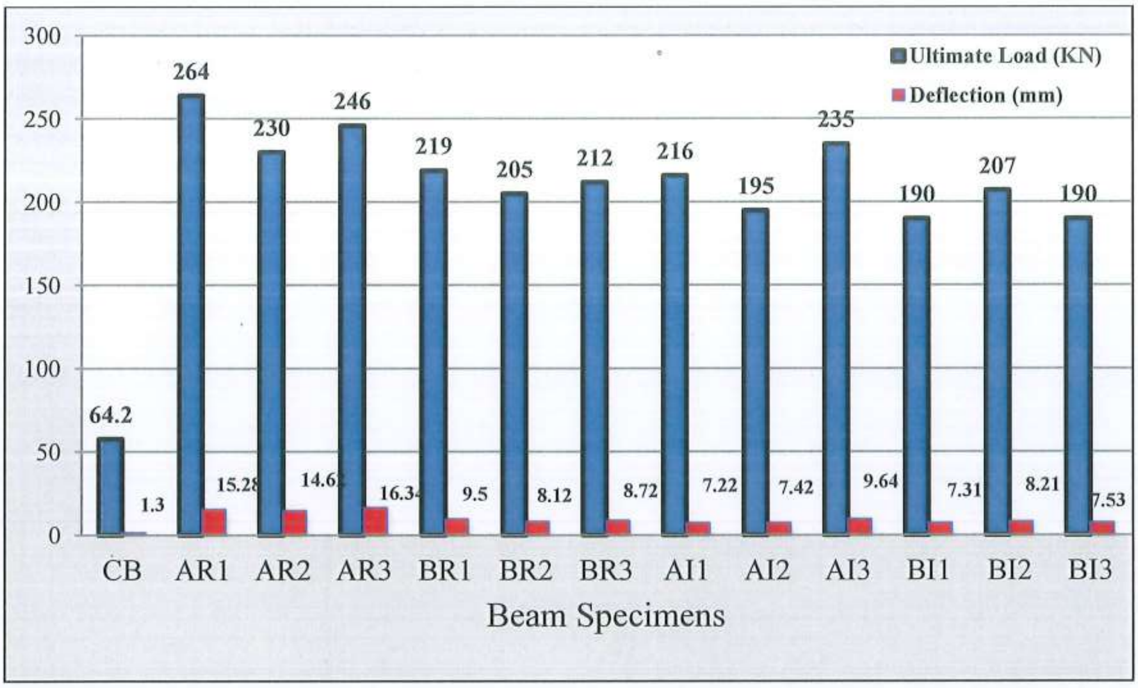

Appendix C Figure 1 Comparison Between Theoretical Specimen CB and Beams (AR, BR, AI, BI) in Ultimate Load and Maximum Deflection.

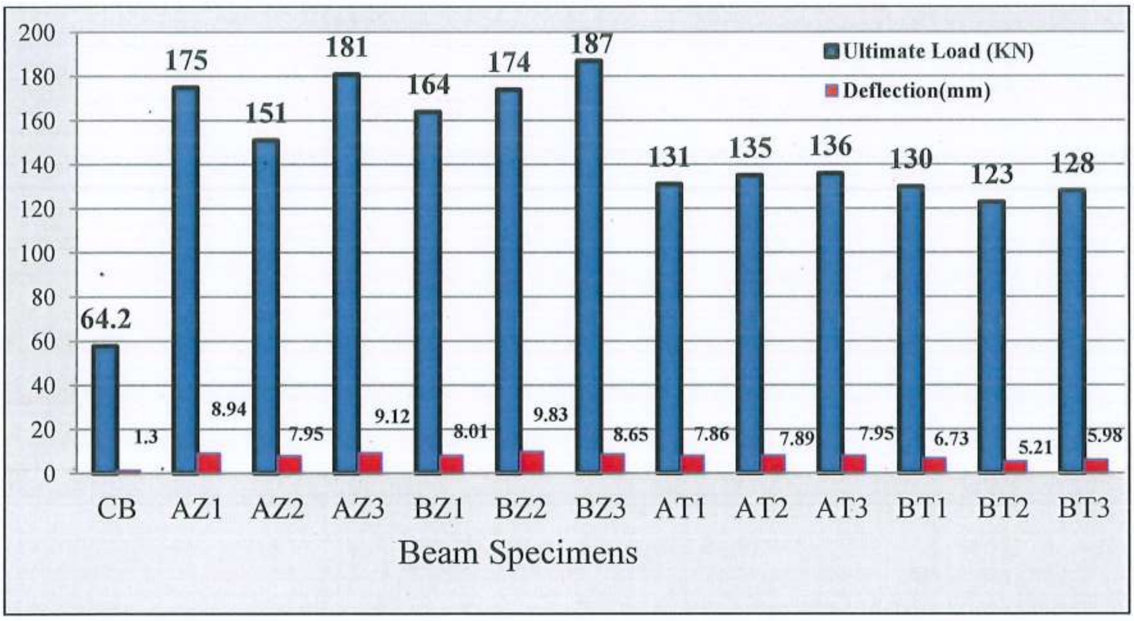

Appendix C Figure 2 Comparison Between Theoretical Specimen CB and Beams (AZ, BZ, AT, BT) in Ultimate Load and Maximum Deflection.

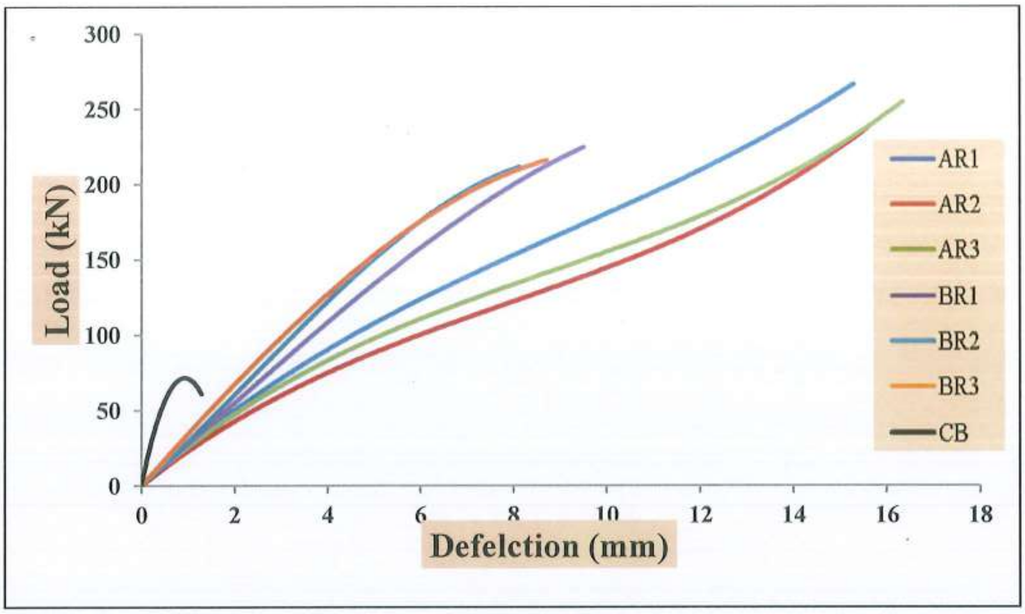

Appendix C Figure 3 Load-Deflection Relationship for Series AR, BR Beams, and CB Beam.

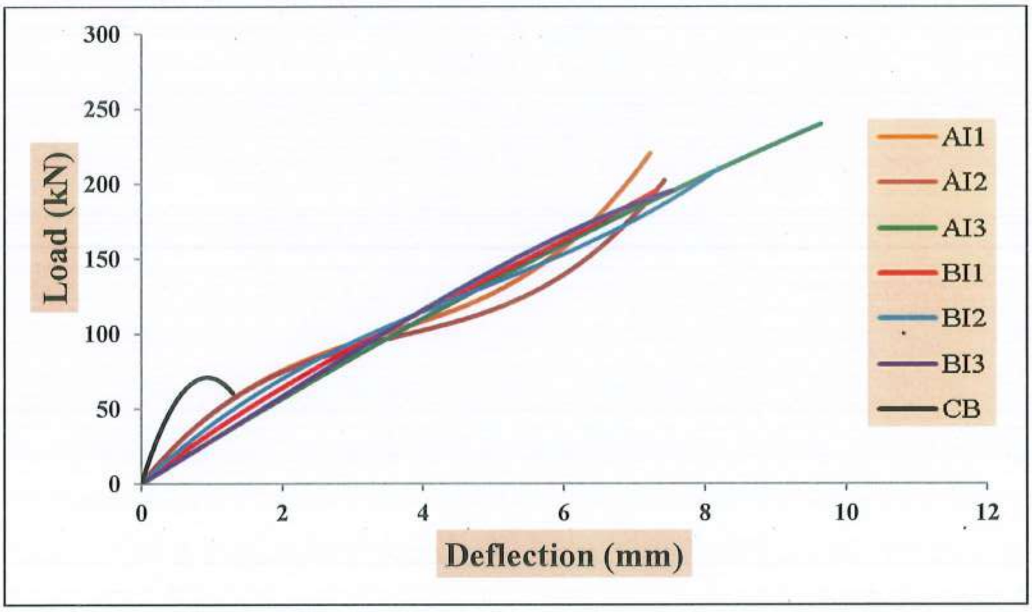

Appendix C Figure 4 Load-Deflection Relationship for Series AI, BI Beams, and CB Beam.

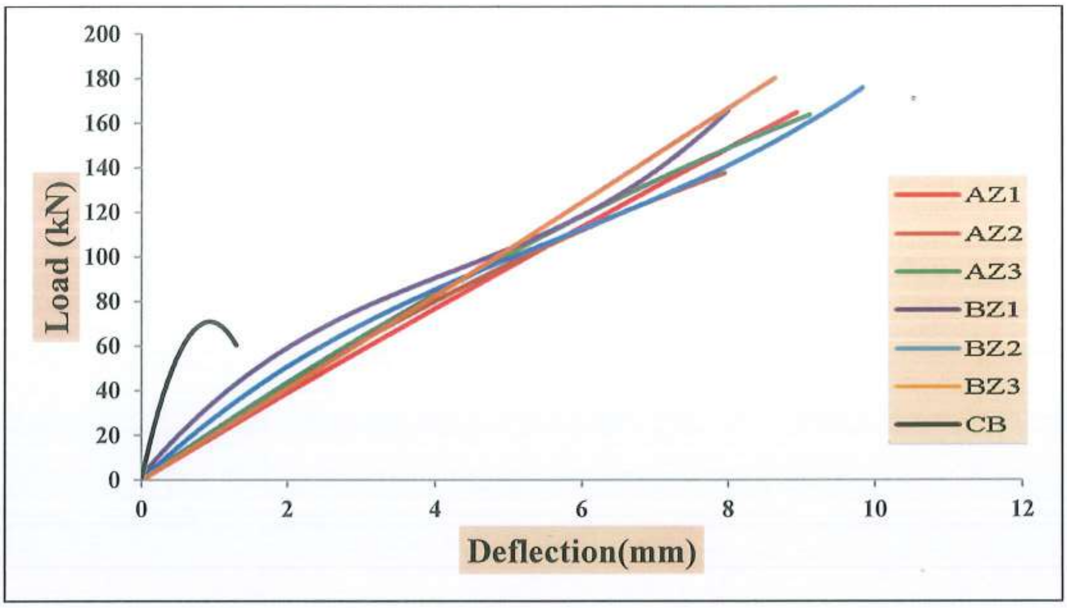

Appendix C Figure 5 Load-Deflection Relationship for Series AZ, BZ Beams, and CB Beam.

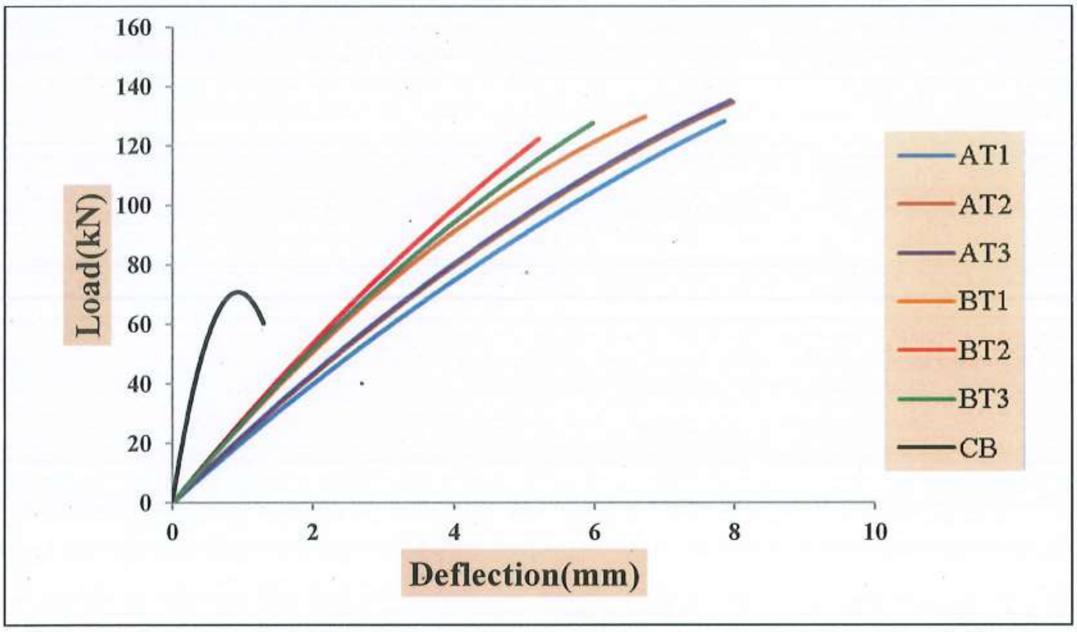

Appendix C Figure 6 Load and Deflection Relationship for Series AT, BT Beams, and CB Beam.

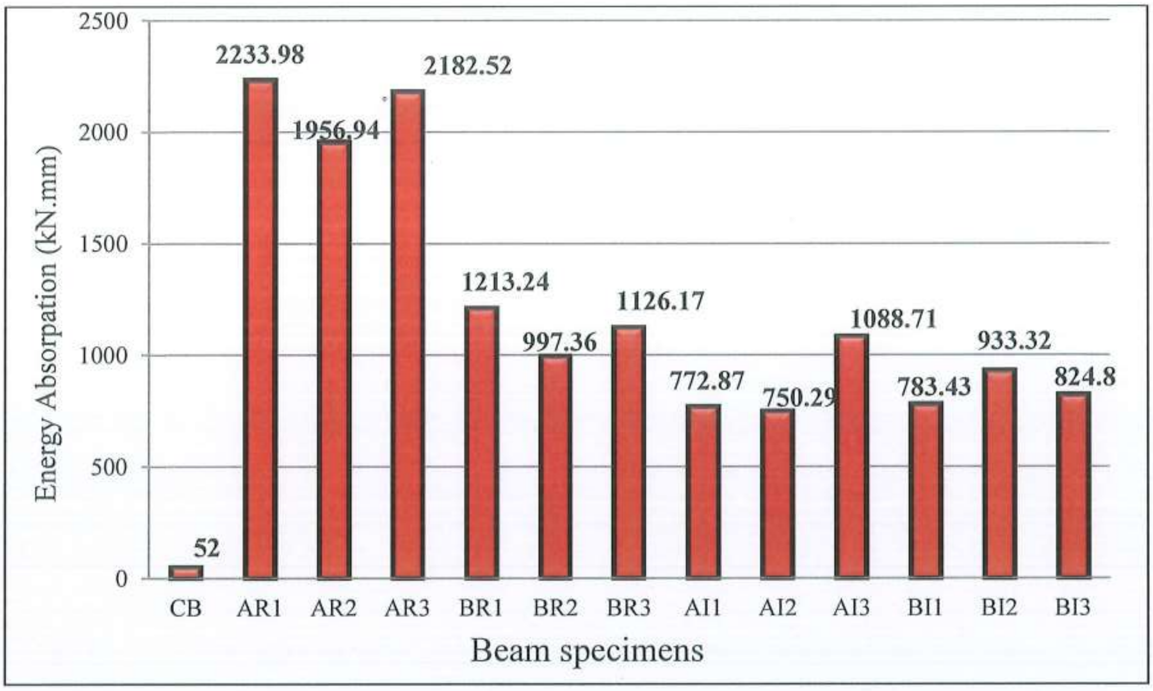

Appendix C Figure 7 Comparison Between Theoretical Specimen CB and Beams (AR, BR, AI, BI) in Energy Absorption.

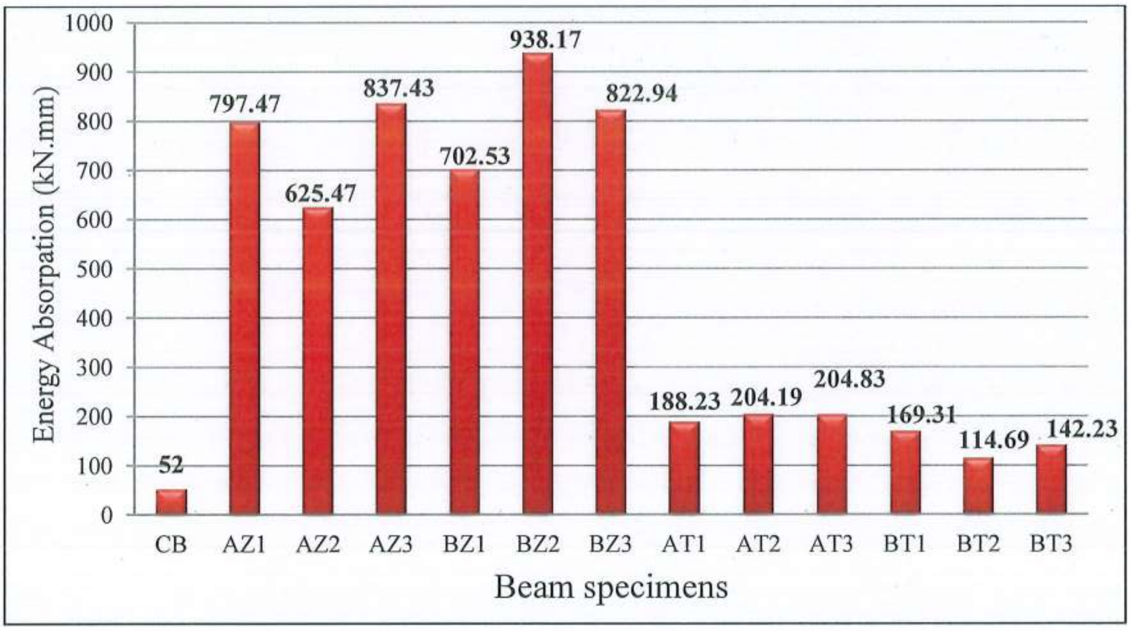

Appendix C Figure 8 Comparison Between Theoretical Specimen CB and Beams (AZ, BZ, AT, BT) in Energy Absorption.

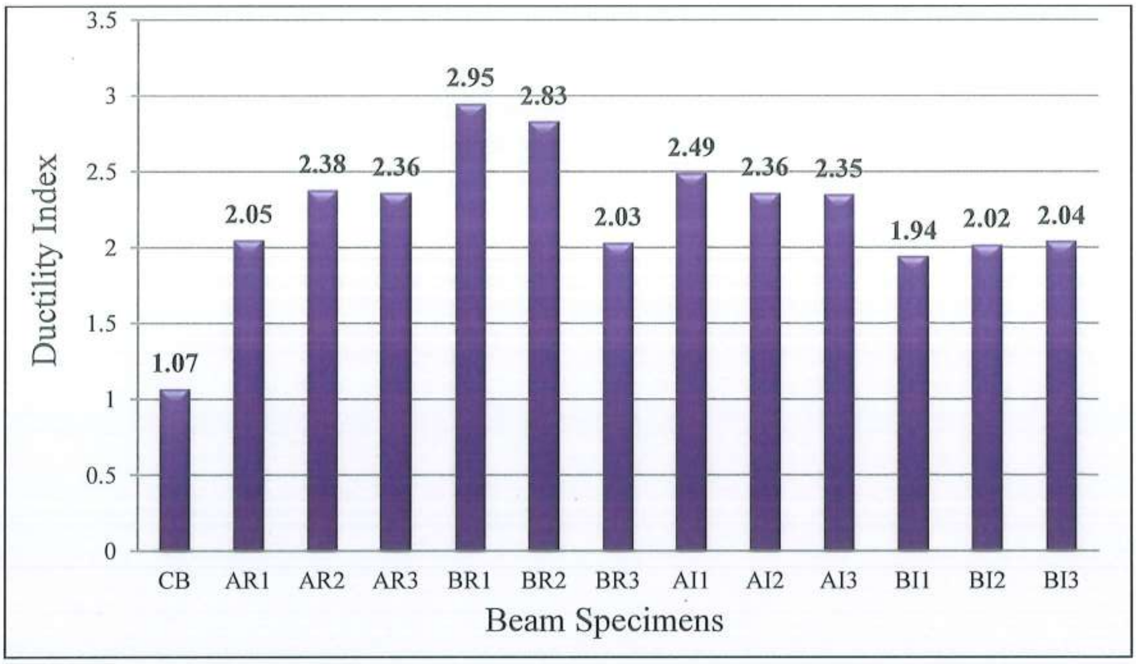

Appendix C Figure 9 Comparison Between Theoretical Specimen CB and Beams (AR, BR, AI, BI) in Ductility Index.

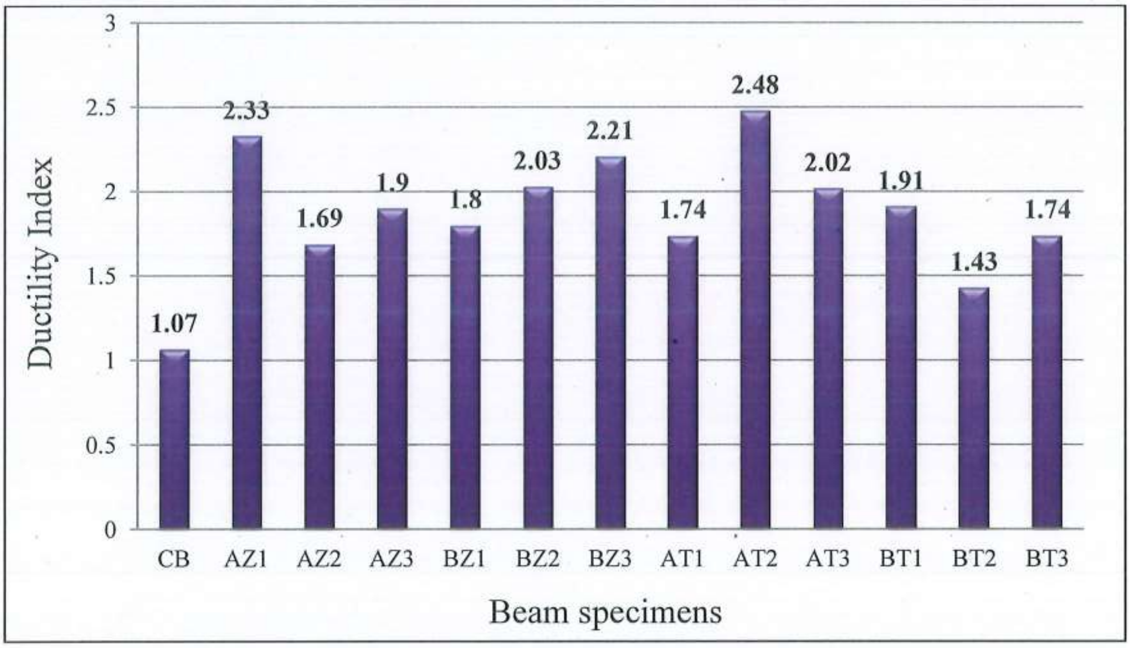

Appendix C Figure10 Comparison Between Theoretical Specimen CB and Beams (AZ, BZ, AT, BT) in Ductility Index.

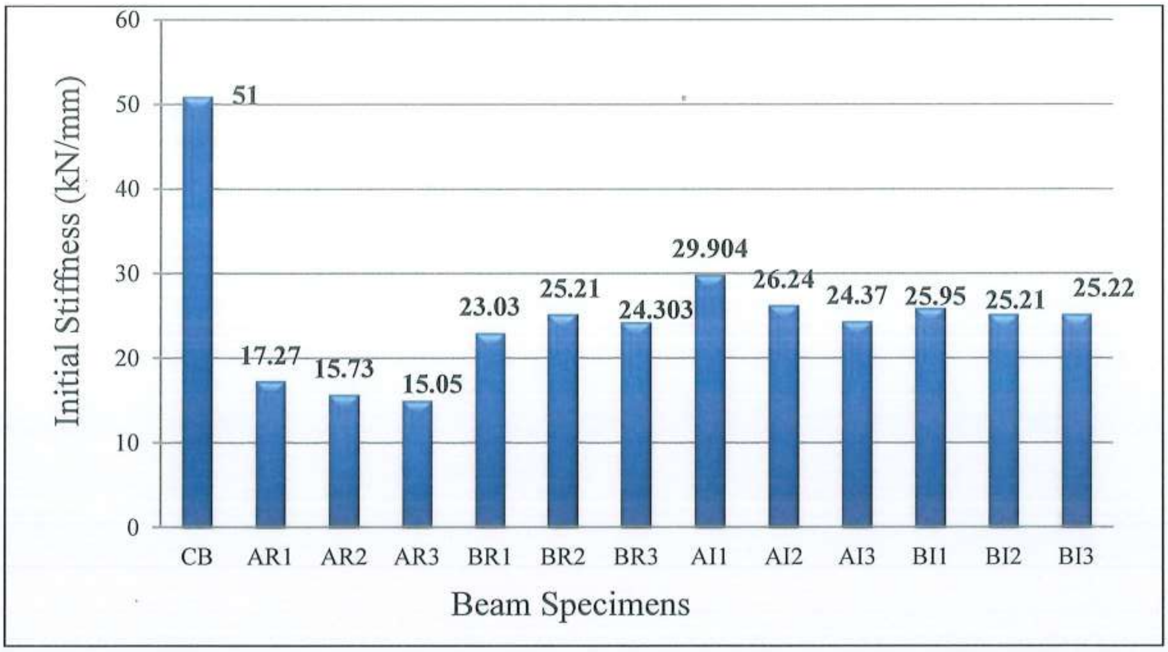

Appendix C Figure11 Comparison Between Theoretical Specimen CB and Beams (AR, BR, AI, BI) in Initial Stiffness.

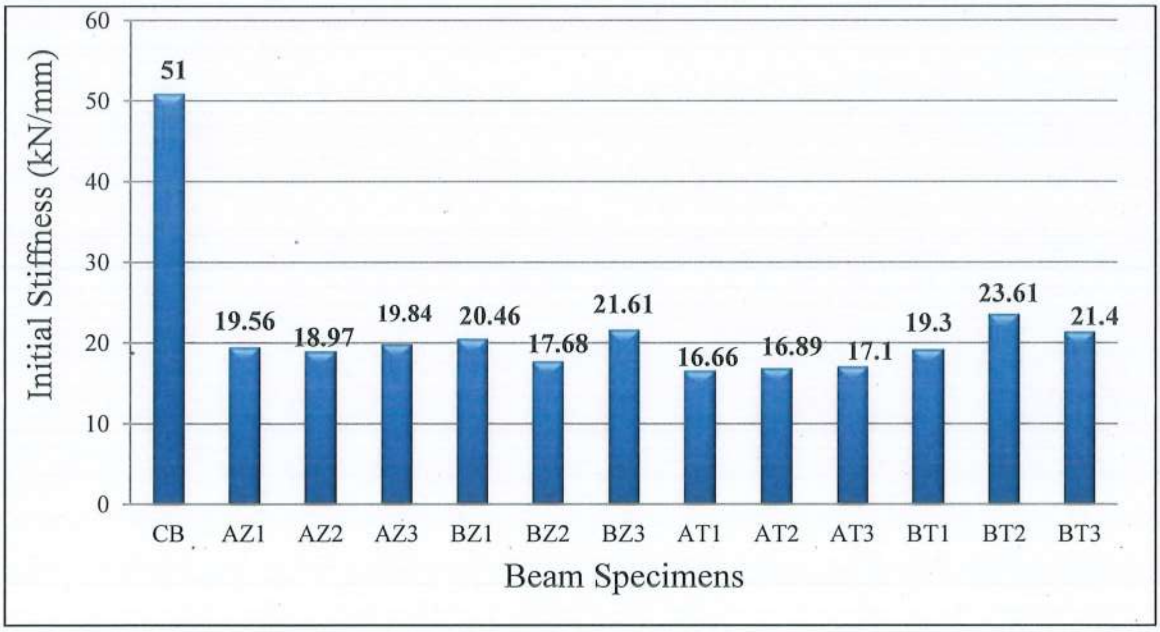

Appendix C Figure12 Comparison Between Theoretical Specimen CB and Beams(AZ, BZ, AT, BT) in Initial Stiffness.

Appendix D

The theoretical panel designed according to AC I318-14 Code

1-Panel cross- section

For the composite panels in the third phase, all the specimens are designed as solid panels with the same cross-section, compressive strength, and similar reinforcement.

f_y =464.3 MPa , f'_c=57.76 MPa

slab dimension(Lxb) =(1220x610)mm

d= h-cover-Ø/2 ,Ø =10mm ,cover = 15mm

$h=\frac{L}{20}$ (simply support) =61mm (61x1.06 for f_y >420MPa)

=64.8mm (use180 mm)

This height corresponds to the height of the rectangular shear connector (140 mm) used in the beams in the second stage and the reinforcing steel with the concrete cover.

d=160 mm

$$As= \frac{A_{bar}}{s} x1000 \qquad (s=150\ mm)$$

$$=523.3\ mm^2$$

$$\rho =5.36x10^{-3}$$

$$As_{min} =0.0018x1000x150 \qquad (ACI\text{-}Code7.6.1.1)$$

$$=270\ mm^2$$

$$\rho_{min} =\frac{As_{min}}{bd}$$

$$=2.7x10^{-3}$$

$$\rho_{b}= \frac{\beta 1}{m} \left(\frac{600}{600+fy} \right)(dt/d)$$

,dt/d=1 (For one layer reinforcement)

,ß1 =0.65 (f'c>55MPa)

$$,m = \frac{fy}{0.85\,fc'}$$

$$=9.45$$

$$\rho b \;=0.037$$

$$\rho_{max} \;=\rho b\left(\frac{0.003+fy/ES}{(0.003+0.004)}\right)$$

$$=0.028$$

$$\rho_{min} < \rho < \rho_{max}$$

2-Fully -composite section

In this section, all layers act as a single unit in resisting bending.

The modulus of rupture (f_r) $= 0.62\sqrt{fc'}$

$=4.661$ MPa

The moment of inertia of the un cracked section(I_{ut})

$$=\frac{bh^3}{12}$$

$$=\frac{610x180^3}{12}$$

$$=296.5x10^6\ mm^4$$

$$M_{cr} = \frac{f_r.I_{ut}}{yt}$$

,y_t = The distance from the neutral axis to the tension face (90mm)

$$=15.35kN.m$$

$$P_{cr} = 92.1\ kN$$

$$\Delta_{cr} = \frac{23Pcr.L3}{648EIut}$$

(For two point loads and a=L/3)

$$=0.3mm$$

The moment M_y calculated from the balanced force C with T, such

$K =(\sqrt{n}\ \rho^2 +2n\ \rho)-2n\ \rho$,n =Es/Ec ,$Ec=4700\sqrt{fc'}$

$\rho =5.36x10^{-3}$,n=6 ,Ec=35720MPa

$K = 0.189$

$M'_y = Asf_y(d-\frac{kd}{3})$ $,P_y = 218.4kN$

$= 36.4kN.m$

By taking the moment of area about the neutral axis, the depth of the neutral axis of the cracked portion was determined

$\Sigma M_{N.A} = 0$

$\frac{610x^2}{2} = nAs(d-X)$

$X^2+10.29X-1647.1=0$

$X^2 = 35.76mm$

$I_{ct} = (\frac{b.c^3}{3} + nAs(d-kd)^2)$

$= 62.35x10^6 mm^4$

$I_{eff} = (\frac{Mcr}{Ma})^3 I_{ut} + (1-(\frac{Mcr}{Ma})^3) I_{ct}$

$M_u = As\ f_y(d-\frac{a}{2})$ $,P_u = 228kN$

$= 38kN.m$

$I_{eff} = 77.4x10^6 mm^4$

$\Delta_y = 2.3mm$

$\Delta_{max} = 3\ mm$

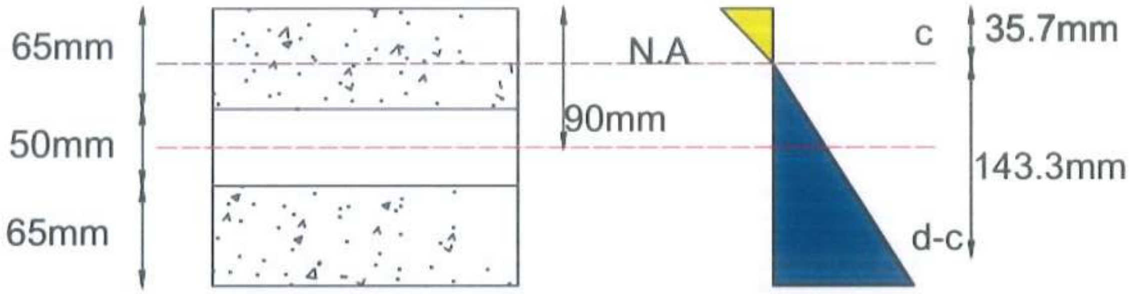

Appendix D Figure 1 Neutral Axis of Full-Composite Cracked Section.

3-Non -composite section

For non-composite action , the wythes are treated as individual sections

f_r =4.661 MPa

I_{ut} $=I_{ut1}+I_{ut2}$

$=2[\frac{bh^3}{12}]$

$=27.9\text{x}10^6\text{mm}^4$

For uncracked section

M_{cr} $=\frac{f_r.I_{ut}}{yt}$,y_t=32.5mm

=4kN.m

P_{cr} =24kN

Δ_{cr} =0.85mm

For cracked section

K =0.189 C=16.7mm ,d=45mm (65-cover-Ø/2)

I_{ct} $=2[\frac{b.c^3}{3}+nAs(d\text{-}kd)^{\ 2}]$

$=10.25\text{x}10^{6}\ \text{mm}^{4}$

$M_y\ = 2Asf_y(d-\frac{kd}{3})$,P_y=64.2kN

$=10.7\text{kN.m}$

$M_u\ = 2As\ f_y(d\text{-}\frac{a}{3})$,P_u=119kN

$=19.92\text{mm}$

$I_{eff}\ =10.4\text{x}10^{6}\text{mm}^{4}$

$\Delta_y\ =6.1\text{mm}$

$\Delta_{max}\ =11.4\text{mm}$

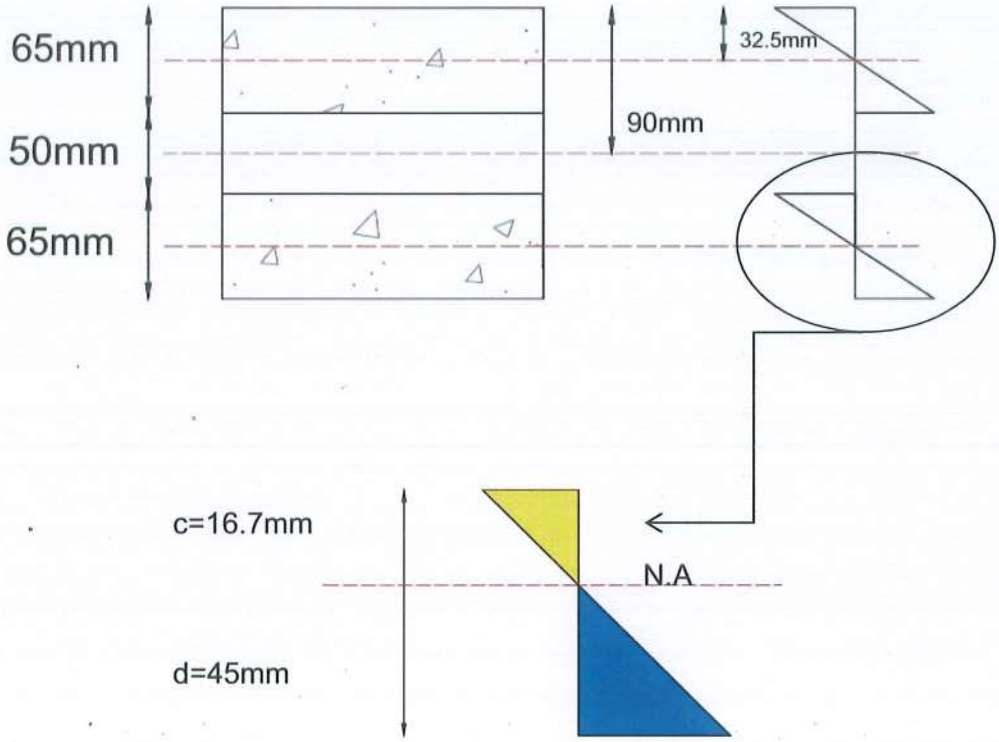

Appendix D Figure 2 Neutral Axis of Non-Composite Cracked Section.

Appendix E

State of the one-way high-strength self-compacting composite concrete panels cast in one stage and two stages with rectangular-shaped connectors.

Another composite element was investigated in this study as a panel cast in one stage (groups SA), and two stages (groups SB). The results obtained from testing the element in this state were compared with the theoretical models (C.S$_1$ and C.S$_2$) in Table 2, and Table1 summarizes their characteristics. Despite the variations in loads and stiffness between the groups SA and SB, the ductility of all panels subjected to a 2-point load is larger than the calculated theoretical panel. This could be because of cross- sectional properties; panels with a rectangular shear connector, an insulation layer, and mesh reinforcement with bar reinforcement given higher results in averages of ultimate load ,maximum deflection, energy absorption.

The load-displacement relationship from the numerical analysis is compared with the experimental results was represented by their properties at the first crack point, the yield point, and the failure point. The non-composite section bends significantly under lower maximum loads than those in practical models, due to the individual section's load resistance and the lower stiffness of the section (EI_{eff}). The model C.S1 develops high early resistance to the loads with less deflection than the experimental models and also less than model C.S2; this could be attributed to the highly effective stiffness of C.S1 or the high compressive concrete, which affects the calculated composite action for panels SA and SB.

Appendix E Table 1 The Properties of The Theoretical Fully-Composite and Non-Composite Panel.

Properties	Fully-composite panel	Non-composite panel
P_{cr}(kN)	92.1	24
Δ_{cr}(mm)	0.3	0.85
P_y(kN)	218.4	64.2
Δ_y(mm)	2.3	6.1
P_u(kN)	228	119
Δ_{max}(mm)	3	11.4
Ductility Index	1.3	1.87
Initial stiffness (kN/mm)	95	10.5
Energy Absorption (kN.mm)	466.2	718.3

Experimental results showed that all panels, whether cast in one or two stages, could absorb and dissipate energy with noticeable warning cracks instead of collapsing brittlely.

Appendix E Table 2 Comparison Between Theoretical Panel C.S$_1$and Experimental Panels.

Specimens	Variation in ultimate-load in comparison to C.S$_1$ (%)	Variation in ductility index in comparison to C.S$_1$ (%)	Difference in initial stiffness as compare with C.S$_1$ (%)	Difference in Energy absorption as compare with C.S$_1$ (%)
C.S$_1$	0.0	0.0	0.0	0.0
SA1	-79.8	-286.2	71.2	-612.3
SA2	-77.6	-365.4	73.1	-716.2
SA3	-88.6	-323.1	71.7	-746.6
SB1	-75.9	-230.8	58.9	-373.3
SB2	-76.8	-281.5	62.4	-466.0
SB3	-71.1	-240.0	63.3	-427.9

Appendix E Table 3 Comparison Between Theoretical Panel C.$_{S2}$and Experimental Panels.

Specimens	Variation in ultimate-load in comparison to C.S$_2$ (%)	Variation in ductility index in comparison to C.S$_2$ (%)	Difference in initial stiffness as compare with C.S$_2$ (%)	Difference in Energy absorption as compare with C.S$_2$ (%)
C.S$_2$	0.0	0.0	0.0	0.0
SA1	-244.5	-168.4	-160.3	-362.5
SA2	-240.3	-223.5	-143.0	-430.0
SA3	-261.3	-194.1	-156.1	-449.7
SB1	-237.0	-129.9	-272.3	-207.3
SB2	-238.7	-165.2	-240.3	-267.5
SB3	-227.7	-136.4	-232.2	-242.7

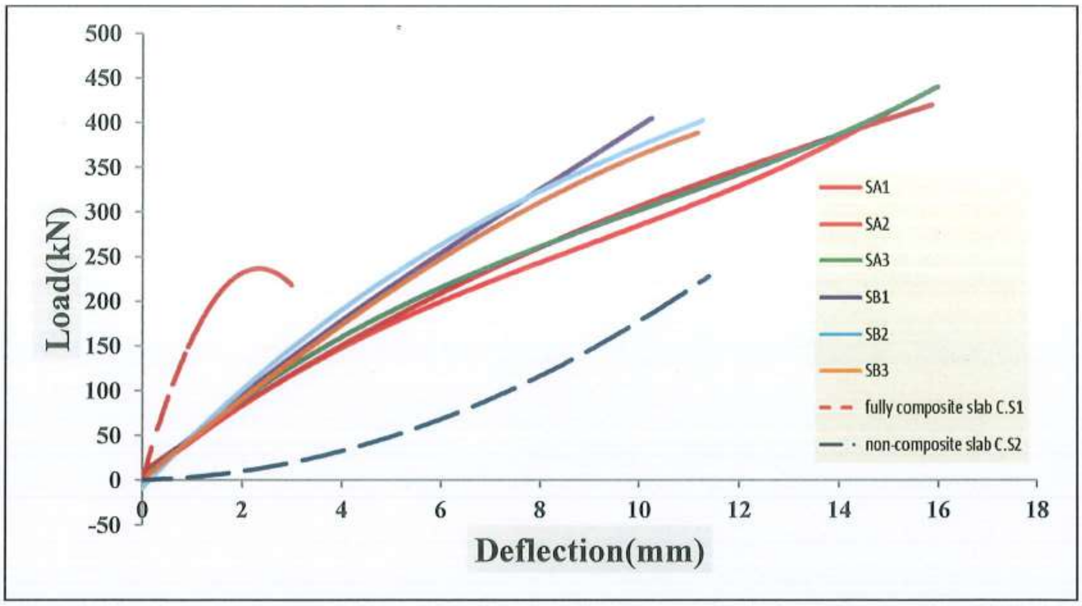

Appendix E Figure 1 Load-Deflection Relationship for Panels.

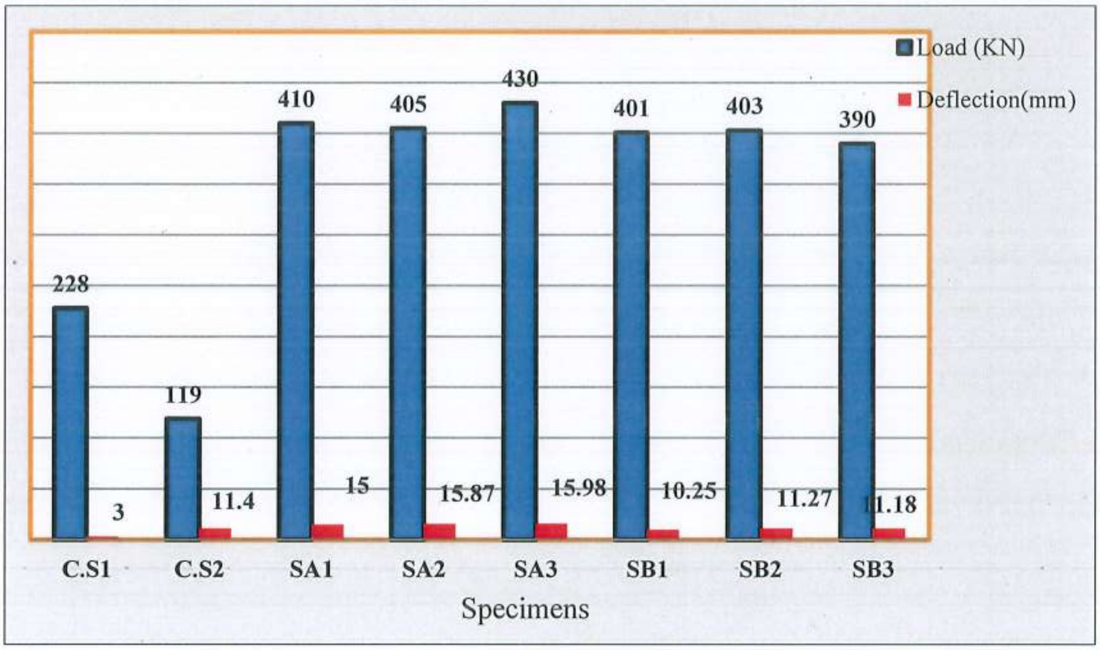

Appendix E Figure 2 Comparison Between Theoretical and Experimental Panel in Ultimate Load and Maximum Deflection.

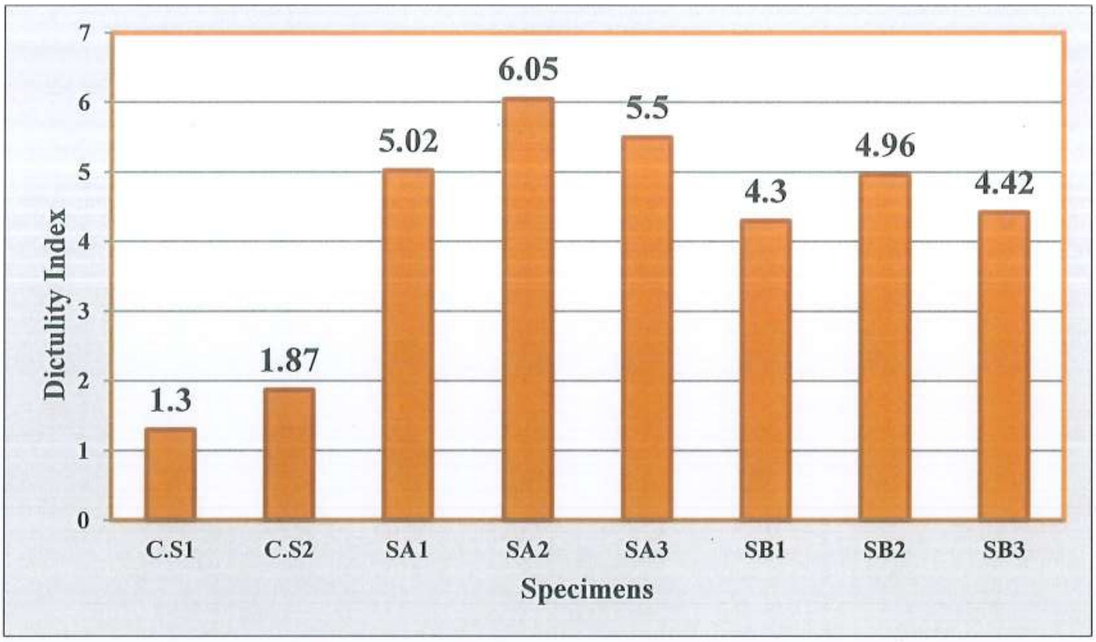

Appendix E Figure 3 Comparison Between Theoretical and Experimental Panel in Ductility Index.

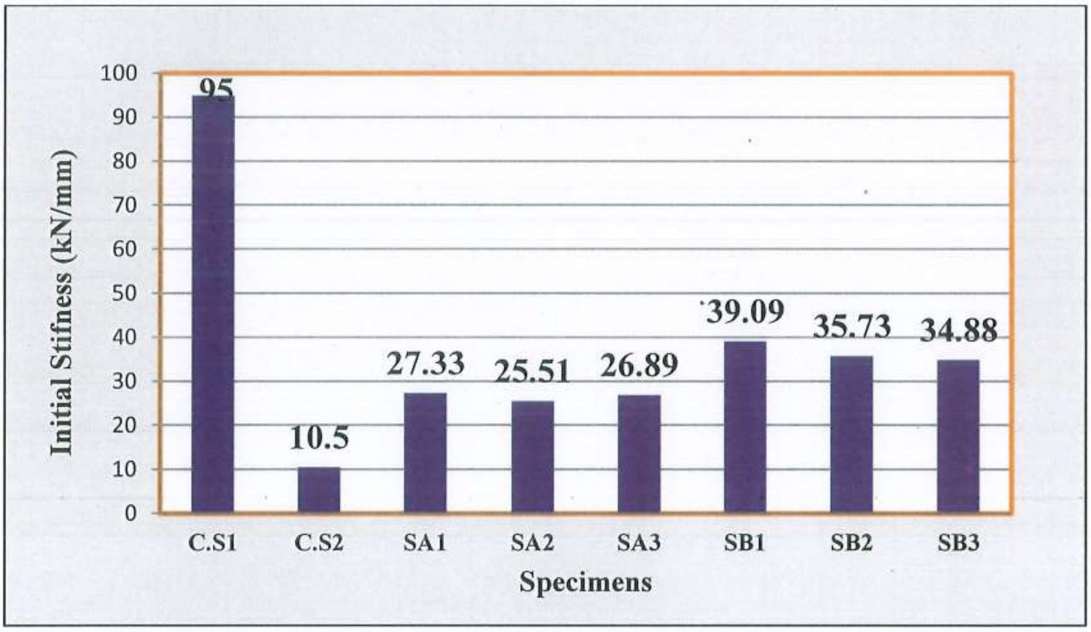

Appendix E Figure 4 Comparison Between Theoretical and Experimental Panel in Initial Stiffness.

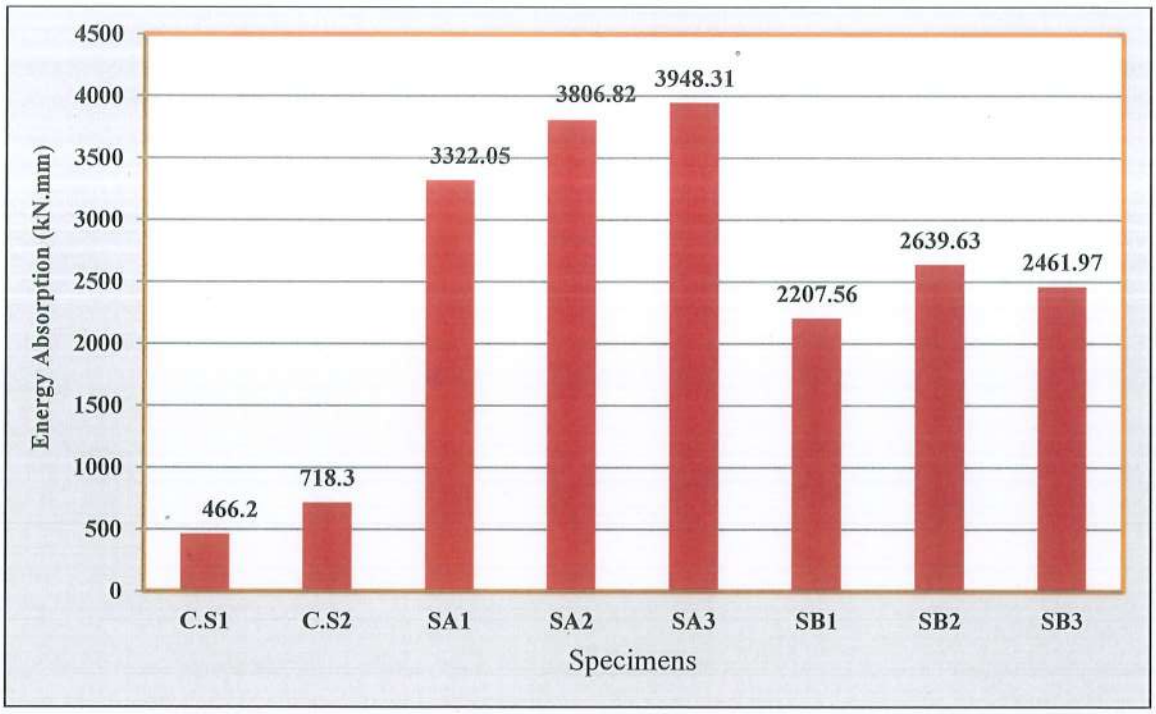

Appendix E Figure 5 Comparison Between Theoretical and Experimental Panel in Energy Absorption.

وزارة التعليم العالي والبحث العلمي

جامعة ميسان / كلية الهندسة

قسم الهندسة المدنية

الاداء الإنشائي لعناصر خرسانية مركبة عالية المقاومة ذاتية الدمك

من قبل

زينب إبراهيم سعيد

الرسالة مقدمة كجزء من متطلبات الحصول على درجة الماجستير في علوم الهندسة المدنية/الانشاءات

الى كلية الهندسة /جامعة ميسان

كانون الاول 2025

بأشراف : أ.م. د. مرتضى عباس عبدعلي

الخلاصة

يُعدّ استخدام الالواح المركبة من طبقتين من الخرسانة مع طبقة البوليسترين الموسّع (EPS) أفضل طريقة بناء مركبة تجمع بين خفة الوزن والأداء الفعال. تتأثر الألواح الهيكلية الخرسانية المركبة بنسبة وزنها إلى قوتها، وقدرة موصلات القص على نقل الأحمال وتحقيق العمل المركب. الهدف من هذه الدراسة هو تطوير عناصر خرسانية مركبة عالية المقاومة ذاتية الدمك ومزودة بموصلات قص مصنوعة من شبكة معدنية موسّعة (expanded metal mesh). يتألف البرنامج المختبري من ثلاث مراحل ومتغيرين هما: نوع موصلات القص وصب الطبقات الخرسانية على مرحلة واحدة وعلى مرحلتين. تركز المرحلة الأولى على تحديد وتحقيق الخصائص المطلوبة للخرسانة عالية المقاومة ذاتية الدمك. في المرحلة الثانية تم فحص أربعة اشكال مختلفة لموصلات القص تحت تأثير حمل الانحناء: (1) موصل مستطيل الشكل، (2) موصل على شكل حرف I، (3) موصل على شكل حرف Z، و(4) موصل على شكل مسنم. تم اقتراح استخدام 24 عتبة خرسانية مسلحة بأبعاد (1200 × 200 × 200) ملم موزعة على 4 مجموعات حيث تتكون كل مجموعة من ست نماذج. تم صب 12 عتبة في مرحلة واحدة. ثم صُبّت 12 عتبة أخرى على مرحلتين يفصل بينهما 24 ساعة من الوقت. أُجريت المرحلة المختبرية الثالثة لدراسة سلوك الانحناء لستة ألواح خرسانية أحادية الاتجاه مركبة مع طبقة البوليسترين الموسع(EPS) بأبعاد (1220 × 610 × 180) ملم مزودة بوصلات قص مستطيلة الشكل. قُسّمت الألواح إلى مجموعتين كل مجموعة تضم ثلاث عينات صُبّت بنفس طريقة صب العتبات في المرحلة الثانية. دُرست نتائج حمل الشق الأول والحمل الأقصى والانحراف وخصائص الإجهاد ونمط الفشل للعتبات والألواح المركبة. في المرحلة الأولى أظهر الخلطة الخرسانة مقاومة انضغاط عالية في المرحلة المبكرة بالإضافة إلى مقاومة عالية بعد عمر28 يوم حيث بلغت 72.3ميكاباسكال.حققت الخرسانة الطرية بسبب تجانسها وتماسكها تدفق عالي تحت تأثير وزنها مما سهّل عملية نقلها وصبّها والوصول إلى داخل اجزاء موصلات القص والتسليح المستخدم وملئ القالب في النماذج للمرحلتين الثانية والثالثة. في المرحلة الثانية، حققت العوارض ذات موصلات القص المستطيلة الشكل المصبوبة في مرحلة واحدة، نتائج عالية في معدلات الحمل الأقصى والانحراف الأقصى بالإضافة إلى امتصاص الطاقة (246.66 كيلو نيوتن، 15.41 ملم، و2124.48 كيلو نيوتن .ملم على التوالي) مقارنةً بأنواع موصلات القص الأخرى. كما حققت العوارض ذات موصلات القص على شكل حرف I والمصبوبة في مرحلة واحدة ايضا، نتائج عالية في معدلات الصلابة الأولية ومؤشر اللدونة (26.83 كيلو نيوتن/ملم و2.4% على التوالي). فشلت جميع العوارض المركبة نتيجةً للقص، بينما فشلت العوارض ذات موصلات القص المسنمة نتيجةً للانحناء. وبناءً على الإجهادات القصوى، يمكن ترتيب أنواع موصلات القص تنازليًا من المستطيل، ثم I، ثم Z، وأخيرًا الشكل المسنم. في المرحلة الثالثة، فشلت جميع الألواح المركبة ذات موصلات القص المستطيلة تحت تأثير القص عند حمل أقصى ،بلغ متوسطه 415 كيلو نيوتن للألواح المصبوبة على مرحلة واحدة، و398 كيلو نيوتن للمجموعة الثانية المصبوبة على مرحلتين. أظهرت الألواح المصبوبة بالكامل زيادة في متوسط حمل الشق الأولي، والحمل الأقصى، ومؤشر اللدونة، وامتصاص الطاقة بنسبة 3.6%، و4.09 %، و14%، و34% على التوالي. حققت الألواح المصبوبة على مرحلتين صلابة أولية عالية، تزيد بنسبة 27% عن تلك المصبوبة على مرحلة واحدة. انخفضت قيمة العمل المركب المحسوبة لجميع الألواح نتيجة لانخفاض صلابة المقطع، والتي تراوحت بين 19% و38%، بينما تم تحقيق قيم عالية تتجاوز 100% بناءً على حمل الانهيار.